ENGINEERING RESEARCH INSTITUTE
THE UNIVERSITY OF MICHIGAN
ANN ARBOR

A STUDY AND DEVELOPMENT OF PARAVANES OF THE HIGH LIFT-DRAG RATIO TYPE AND THE HIGH-LIFT TYPE

Russell A. Dodge
Department of Engineering Mechanics

Hadley J. Smith
George Sonnemann
Engineering Research Institute

Project 2036

BUREAU OF SHIPS
U.S. NAVY DEPARTMENT
CONTRACT NObs-55574

July 1955

en M

UMP0630

PREFACE

This is a report of a study and development of paravanes conducted under U.S. Navy Department Contract NObs-55574 and administered by the Bureau of Ships Code 520, with Mr. Mark Kurtz acting as Project Engineer. Particular credit is due to Mr. Kurtz for the guidance which he gave the personnel and the project throughout its progress.

The project was supervised by Russell A. Dodge and the full-time staff consisted of Dr. Kurt P. H. Frey, Hadley J. Smith, and Dr. George Sonnemann. Messrs. Smith and Sonnemann were present throughout the project, but at the time this report was being prepared the latter was available only as a consultant. Mr. Smith is still at the University and is fully conversant with all phases of the project.

It was especially fortunate to have the services of Dr. Kurt P. H. Frey who was also present during the term of the project. He has a long record of experience in fields involving fluid flow and it so happens that he is one of the few who have had actual design experience with paravane-like devices. Although his services were not available for this report, he deserves great credit for many of the ideas incorporated in it.

Numerous other people were engaged from time to time for special assignments. These include W. W. Hagerty, H. M. Hansen, L. G. Clark, F. C. Michelsen, Wm. Samborski, F. H. Westervelt, M. El-Saden, and T. J. Banwell. Professors Hansen and Clark studied the problem of stability control early in the project. Mr. Michelsen made the final detailed drawings of both paravanes. Mr. Westervelt assisted in the study, design, and detailing of the control mechanism. Professor Hagerty is familiar with the entire project since he participated in the planning and in the group conferences and made many valuable suggestions. William Samborski carried out many of the technical details throughout the course of the project and is thoroughly acquainted with every aspect of it.

A large part of the experimental work was done in the towing tank of the Department of Naval Architecture and Marine Engineering. The project is indebted to Professor L. A. Baier, Chairman of that Department, not only for the facilities but also for many valuable suggestions which were made possible by his long experience with ships and shipping. Mr. P. A. Snell of the same Department constructed all the towing models for the experimental work and often assisted in the conducting of the experiments.

TABLE OF CONTENTS

TABLE OF CONTENTS (cont.)

TABLE OF CONTENTS (cont.)

SUMMARY

The primary objective of the project was to develop a compact paravane having a high lift-drag ratio. After investigating a variety of designs capable of supplying the desired lift, the tailless biplane with end vanes appeared to provide the best combination of high lift-drag ratio, stability, ruggedness, and compactness.

A full-scale prototype was designed which should equal or approach the desired lift-drag ratio of ten. This estimate is based on the performance of models and a reasonable allowance for the beneficial effect of the much higher Reynolds numbers of the prototype. If the paravane and any towed body together do not produce a small enough sweepback angle of the tow cable, this angle may be improved substantially by a small increase in the lift of the paravane.

The prototype design is such that the bridling, the angular positions of the lift vanes and trim surfaces, and the location of the center of gravity can be readily varied for trial at sea. These adjustments permit changes in the angle of attack and the roll of the lift vanes so as to obtain, respectively, the maximum lift-drag ratio and the desired equilibrium depth.

The prototype contains a depth control for countering depth disturbances and maintaining a preselected depth in the range of 30 to 50 ft when the paravane is towed at an outboard distance of about 200 ft. The depth-control mechanism is entirely mechanical and is actuated by depth and the vertical acceleration of the paravane. It can be adapted to operate control surfaces other than those shown in the drawings of the prototype.

The proposed design has excellent launching characteristics and readily assumes an outboard position. At one stage in its travel to the outboard position, a very large force develops in the tow cable when the latter is of a fixed length. This condition can be counteracted by proper handling of the cable during launching.

As an added task, it was required to design a very compact paravane having high lift. The lift-drag ratio could be fairly low, if necessary. This paravane was to operate in connection with a float which, when under tow, is slightly below the water surface.

In model tests of high-lift paravanes, the tailless biplane exhibited very favorable performance, and this design was selected for the full-scale prototype. Each of the two lift vanes were made up of six elementary vanes, giving a slotted-vane effect. Lift coefficients of 2.3 to 3.3 were obtained in models tested at low Reynolds number. For the adopted design, a value of 2.86 is required and should be readily obtained with the full-scale prototype.

It was concluded that the tailless biplane with end vanes is a promising configuration for both the high lift-drag ratio and the high-lift paravane. As discussed in detail in this report, this conclusion was influenced by the specifications for several characteristics besides the lift-drag ratio and lift. Therefore, the designs developed in this investigation will not necessarily be desirable for all applications of high lift-drag or high-lift paravanes.

It was also concluded that, of the design details of the high lift-drag ratio biplane which were not made adjustable in the prototype, the most important items are the aspect ratio and stagger of the lift vanes, the chord of the end vanes, and the location and type of the depth-control surfaces. Also important are the hinge moments and the detailed nature of the control action produced by the depth-control mechanism.

It is recommended that full-scale tests of both paravanes be conducted at sea. The need for such trials is clearly indicated by the fact that the largest models tested were about one-third scale, based on the chord of the lift vanes, and the fact that the maximum towing speeds were about one-half the minimum at sea. Furthermore, realistic disturbances could not be simulated in model tests.

CHAPTER 1

GENERAL INTRODUCTION

A glossary and a nomenclature are contained in Appendix A of this report.

1.1 DESCRIPTION OF THE PROBLEM

The task, as originally specified, consisted of theoretical and experimental work to be conducted in three phases, the primary requirements of which are summarized as follows:

I. Research to establish basic facts pertaining to the theory of high lift-drag ratio paravanes.

II. Investigation and development of high lift-drag ratio paravanes by means of small-scale models.

III. Construction of large-scale and/or full-scale prototypes of high lift-drag ratio paravanes for evaluation under operational conditions.

Subsequently, Phase III was revised to require only the design of a full-scale prototype of a high lift-drag ratio paravane. Also, a requirement was added which specified the development and full-scale design of a prototype high lift paravane for use with a float.

In addition, the contractor was furnished with certain advisory specifications giving detailed characteristics which it was desired to realize in the prototype paravanes. These details are summarized in the first section of Parts A and B of this report.

Because it was desired that the contractor conduct independent research uninhibited by earlier work, results of other paravane investigations aimed at the attainment of a high lift-drag ratio were not made available except where prior independent study under this project led logically to consultation of specific phases of other work.

1.2 THE NATURE AND COURSE OF THE WORK

In order to meet the requirements described in the preceding section, several major lines of investigation and numerous detailed studies were conducted during the course of the project. Those programs which received special emphasis were as follows:

a. A general theoretical and experimental study of the hydrodynamic aspects of high lift-drag ratio paravanes followed by an investigation of the influence of details of the hydrodynamic design. Some experimental work with depth-control surfaces was then conducted, followed by the design of a full-scale prototype.

b. A preliminary theoretical study of the stability of paravane-like devices, consisting primarily of an investigation of the possibility of using a stability-control mechanism, if needed, which would be completely contained within the interior of the paravane. The mechanism was considered also as a potential source of energy which might be required by the depth-control mechanism mentioned in Program c.

c. A study of mechanisms to control automatically the depth of a high lift-drag ratio paravane followed by theoretical analysis and tests to determine the depth-control characteristics of a model system employing a high lift-drag ratio paravane evolving from Program a. A full-scale prototype was designed and a study was made of more refined designs which full-scale tests might show to be required. The depth-control mechanisms considered were intended to control the average depth and such excessive oscillations of depth as could not be eliminated in Programs a or b.

d. A theoretical and experimental study of high-lift paravanes for use with a float in a manner similar to the "O" Type, Kite-Otter, Mine Sweep Paravane. A full-scale prototype was designed.

At the outset of Program a, it appeared that the desired combination of a very high lift-drag ratio, fairly high lift, and limited size might necessitate a radical hydrodynamic design which could tend to be unstable. This consideration led to the initiation of Program b early in the course of the project. However, Program a produced models which not only were quite stable, but also contained insufficient space to house both stability and depth-control mechanisms. Also, Program c indicated the possibility of obtaining depth-control mechanisms not requiring an auxiliary power supply. As a result, Program b was discontinued after a preliminary study of stability control.

Program a produced relatively compact paravane models having high lift-drag ratios and surprisingly favorable stability under test conditions. Since much of the work on control surfaces necessarily followed the full

development of the paravane itself, both funds and time for this phase of the work were somewhat restricted. Consequently, this report contains recommendations for modification of the full-scale prototype should difficulties arise in the performance of the combined paravane and depth-control mechanism.

Program d, the development of a high lift paravane, was authorized during the latter portion of the project. A promising model was developed in a short time, followed by the design of a full-scale prototype.

Programs a and c are described in Part A of this report and Program d is contained in Part B. Program b is summarized in Appendix E. Drawings of the prototype paravanes are contained in Appendices F and G. The other appendices describe some of the methods and details of the investigation.

PART A

HIGH LIFT-DRAG RATIO PARAVANE

CHAPTER 2

PROTOTYPE DESIGN OF HIGH LIFT-DRAG RATIO PARAVANE

2.1 INTRODUCTION

It was desired to design a paravane which would produce a lift of 20,000 lb at 16 knots and have a lift-drag ratio of 10. The design was to be such that the entire paravane could be contained in a 10-ft cube. The tow point was to be about 30 ft above the water. The paravane was to be controlled closely to any desired depth in the range of 30 to 50 ft and was to operate at an outboard distance of about 200 ft. In addition the paravane was to be capable of towing an added body from a point on the cable. It was also required that the control of depth be accomplished without transmitting power to the paravane from the ship and without the use of devices such as propellers which might be noisy. Stability, dependability, and ruggedness were important considerations and the buoyant force was to exceed the weight.

A few preliminary computations showed that a lift-drag ratio of 10 was about the ultimate that could be expected from any conventional lifting device and at first it was thought that this paravane would have to be something of the flying-wing type which is known to be difficult to control.

From the specifications the lift, L, per unit dynamic pressure, $\rho V^2/2$, at 16 knots is

$$L/q = \frac{20{,}000}{730} = 27.4 = C_L \times S .$$

Assuming the coefficient of lift, C_L, to have a value of 0.5, the lifting surface must have an area, S, of 54.8 sq ft.

After experiments with numerous small-scale models, efforts were concentrated on the most promising design, namely, the tailless biplane configuration with end vanes. Early experiments on somewhat larger models of two different scales indicated that the requirements might be met with an aspect ratio of 2, a span of 7.16 ft, and a chord of 3.6 ft and again suggested that the tailless biplane configuration was the most promising of all basic types. More recent experiments indicate that the H configuration with small, thin end vanes might be somewhat better, especially with respect to the effectiveness of depth-control surfaces.

Several test runs, some of which were witnessed by a representative of the Bureau of Ships, indicated a very satisfactory lift-drag ratio. When operating at its best, the conditions are somewhat critical and it has not always been possible to attain the extremely small sweepback angles which were witnessed.

2.2 PROTOTYPE PARAVANE

The drawings of the full-scale prototype paravane are reproduced in small size in Appendix F and are referred to in the following discussion.

In the original tests, using aspect ratios from 1 to 3, it appeared that the paravane was more stable, and therefore more easily controlled, with an aspect ratio of 1. Consequently, it was decided to propose an initial design with aspect ratio 1-1/2, as shown on the drawings. This concession to controllability was made in the belief that much more can be learned by successful experiments on the proposed stable prototype than by unsuccessful experiments on a more radical and less controllable design. The towing studies showed the importance of the decalage of the lift vanes. The prototype has been designed so that the decalage can be varied, if desired, by chipping off the weld and reorienting one or both lifting surfaces.

Also, provision has been made for changing the position of the bridling connections. These connections have been placed in the lift vanes for the purpose of reducing the structural load. The bridling system consists of four lines running from the connections on the lift vanes and converging at the outboard end of the tow cable.

It is expected that the space within the lifting vanes and end vanes will be filled with styrofoam or some similar light-weight filler in order to give the flat surfaces additional strength under hydrostatic pressure. A few spaces at the outboard end of the lower end vane are provided for the purpose of adding weight and thereby controlling to some extent the position of the

center of gravity. Another adjustment is provided by the presence of trim tabs on the lower end vane. These can be locked in any desired position, and they might be particularly important in adjusting the paravane to widely differing operating depths.

The control surfaces of the prototype are located on the upper end vane. The surfaces are a modification of a balanced type shown in the literature [17, 18].* They have been moved outward toward the end-vane tips, in comparison to the position used in models (Fig. 4-15), so as to increase their effect on roll.

The profile of the lift vanes is not a standard section, but rather is one designed for ease of manufacture while retaining good hydrodynamic characteristics similar to those of the Göttingen No. 385 profile [15, vol 1, p. 89]. For both sections, the high-pressure side is flat. Number 385 has a leading edge of small radius and a thickness ratio of about 0.1. In the selected profile, the radius of the leading edge was increased for ease of construction. Also, a thickness ratio of .088 was chosen and was a compromise to obtain a minimum weight while maintaining structural strength.

In the absence of end plates, the characteristics of the selected profile are similar to those of Fig. 3-6 which is based on Göttingen profile No. 389. The latter has a thickness ratio of 0.1 and is similar to No. 385, the primary difference being a slight concavity of the high-pressure side of No. 389.

Some characteristics of the full-scale design follow.

Lift-vane area	54.5 ft^2
Lift per unit area at 16 knots	375 lb/ft^2
Lift-vane span	6 ft - 4-1/2 in.
chord	4 ft - 3-1/4 in.
aspect ratio	1.5
thickness ratio	.088
gap, percent of chord, approximate	86%
Decalage of the lift vanes	plus 2°
Orientation of the lift vanes with respect to leading edge of end vane	
outboard vane	35°
inboard vane	37°

*Numbers in brackets refer to the bibliography at the end of this report.

Angle of stagger of lift vanes	
aerodynamic angle of stagger, nominal	45°
geometric angle of stagger with reference to chord of inboard vane, approximate	53°
Overall height including control housing	7 ft - 11-1/8 in.
Overall width	6 ft - 4 in.
Overall length	10 ft - 2 in.
Displacement	2060 lb
Approximate weight in aluminum without load in the compartments and without control mechanism	2000 lb

2.3 PROTOTYPE DEPTH CONTROL

The depth-control device which evolved from the considerations to be discussed in this section is shown in Appendix F.

The types of control equipment which could be considered for this problem were limited considerably by the operating conditions. The latter were especially restrictive in the case of two components, namely, the transducers for detecting the depth error and the source of the energy required for the control action. Also, it was required that the equipment be non-electrical, thus requiring components employing hydraulic, pneumatic, and solid members.

Transducers.—A pressure-sensitive component, such as a diaphragm or bellows, may be used to measure the depth error by responding to the pressure in the wake of the paravane. However, if the paravane oscillates in resonance with the sub-surface waves, it follows a path where the pressure is unrepresentative of depth error and an additional indication of the error is required. Transducers sensitive to the first derivative of the error, that is, the vertical velocity of the paravane, were not feasible. Consequently, a seismic device was selected which provides sensitivity to the second derivative of the error, namely, the vertical component of the acceleration of the paravane.

Energy Source.—It was required to do without any continuous supply of energy from the ship. The storage of energy on the paravane would require periodic replenishment which was unacceptable from an operating viewpoint. Moreover, energy storage appeared to involve equipment of excessive bulk. As the paravane design evolved into an assembly of relatively flat vanes, the bulk factor also ruled out equipment for converting the kinetic energy of the

paravane into pneumatic or hydraulic pressure for operating conventional control equipment. The possibility of energy conversion was also limited by the desire to avoid moving parts such as a turbine rotor, especially when exposed to sea water.

If the mechanism were to be of the error-actuated type, it appeared that the diaphragm and seismic devices might assume the double roles of transducers and energy suppliers. This approach required that these elements be made large enough to manipulate the control surfaces directly.

Pressure-Seismic, Error-Actuated Control Mechanism.—The prototype design is a depth-control mechanism deriving its energy from diaphragm and seismic transducers. The air pressure on the interior of the diaphragm is made sufficient to hold the mechanism in midposition when the paravane is at the correct depth. The seismic masses are counterpoised to permit response only to vertical accelerations of the paravane. In either a prototype or a final design, the special diaphragm may be conveniently replaced by a Titeflex Monel Bellows which has unusually good properties for this application.

When connected to the diaphragm as shown, the seismic masses will assist the relatively large diaphragm in manipulating the control surfaces when the vertical acceleration of the paravane is in a direction opposite that of the depth error. This is the condition encountered in depth variation of the oscillatory type. When the error in depth is large, such as during launching, the decreased pressure on the diaphragm results in the seismic masses resting against a stop and thus being inactive.

During a steady-state oscillation of the depth, the amplitude of the seismic force increases as the square of the frequency of the oscillation. For a given wave pattern, this frequency increases in proportion to the first power of the towing speed. Thus, the seismic unit contributes to the output of the mechanism a force which increases as the square of the towing speed. This characteristic is desirable since the resisting hydrodynamic moment of the control surface increases in the same manner.

No damping or spring elements are included in the mechanism since the proposed control surfaces add damping and spring actions estimated to be adequate. The version of the mechanism shown in the drawing will provide the greatest hinge moments to the control surface and an essentially proportional control action. The addition of a slightly restrictive orifice at the entry to the diaphragm water chamber will permit integrating action at very low frequencies.

An alternate version of the control mechanism, not shown in the drawing, may be obtained by reversing the connection between the seismic and diaphragm units so that the former aids the latter when the depth error and acceleration are in the same direction. In this case, the control surface may

be made to lead the depth error at the frequencies of disturbances due to waves. At lower frequencies, the surface will lag the error and have an amplitude proportional to the error in the depth below the average water surface. This arrangement would be desirable, but it decreases the hinge moment which the mechanism can produce. It is therefore feasible only by utilizing flow spoilers or control surfaces which are more easily manipulated than those now proposed. The alternate arrangement would also be feasible in servomechanism equipment, such as that illustrated at the end of Chapter 5, where the seismic and diaphragm transducers would be required to drive only a very small load.

The advantages of the error-actuated mechanism in simplicity and potential compactness appeared substantial. Furthermore, this device comprises a step in the development of a servomechanism control, if the latter should prove necessary. These considerations, plus the fact that the nature of the required control action can be determined in detail only under full-scale conditions, indicated that the error-actuated type should be selected for the first full-scale tests.

CHAPTER 3

HYDRODYNAMIC DESIGN. THEORETICAL CONSIDERATIONS

3.1 INTRODUCTION. REYNOLDS NUMBER. CAVITATION

The problem is illustrated schematically in Fig. 3-1 which defines X, Y, and Z axes, the cable sweepback angle, σ, and other quantities which are used to describe the position of the paravane. The paravane is represented by three force components acting at the bridling point A, those in the Y and X directions being, respectively, the lift and drag forces of the paravane. The Q-axis is an auxiliary axis useful in analyzing the depth-control problem. The cable is shown as a straight line in this figure.

The major physical components of the problem are the water, the ship, the winch or other equipment at the tow point, the tow cable, the bridling system of the paravane, the paravane, and any added drag attached to the tow cable. The present task essentially involves only the bridle and paravane, so the other parts will be considered only to the extent that they affect the performance of these two elements.

The principal specifications for the paravane, given in section 2.1, are taken up in the succeeding sections of this Chapter under the headings of lift, lift-drag ratio, control, and structure. The equilibrium position of the paravane-cable system is also discussed, since it places certain requirements on the design of the paravane.

It is desirable to obtain the lift hydrodynamically rather than by special propulsion or other means. Devices capable of developing such a hydrodynamic force may be roughly classified according to their lift coefficient, C_L, which is a measure of their ability to produce lift. Some approximate values are as follows:

a. C_L = 1.0 or less
Conventional lift vanes, that is, vanes with profiled cross-section but without special lift-increasing features such as slots or other openings in their external surface.

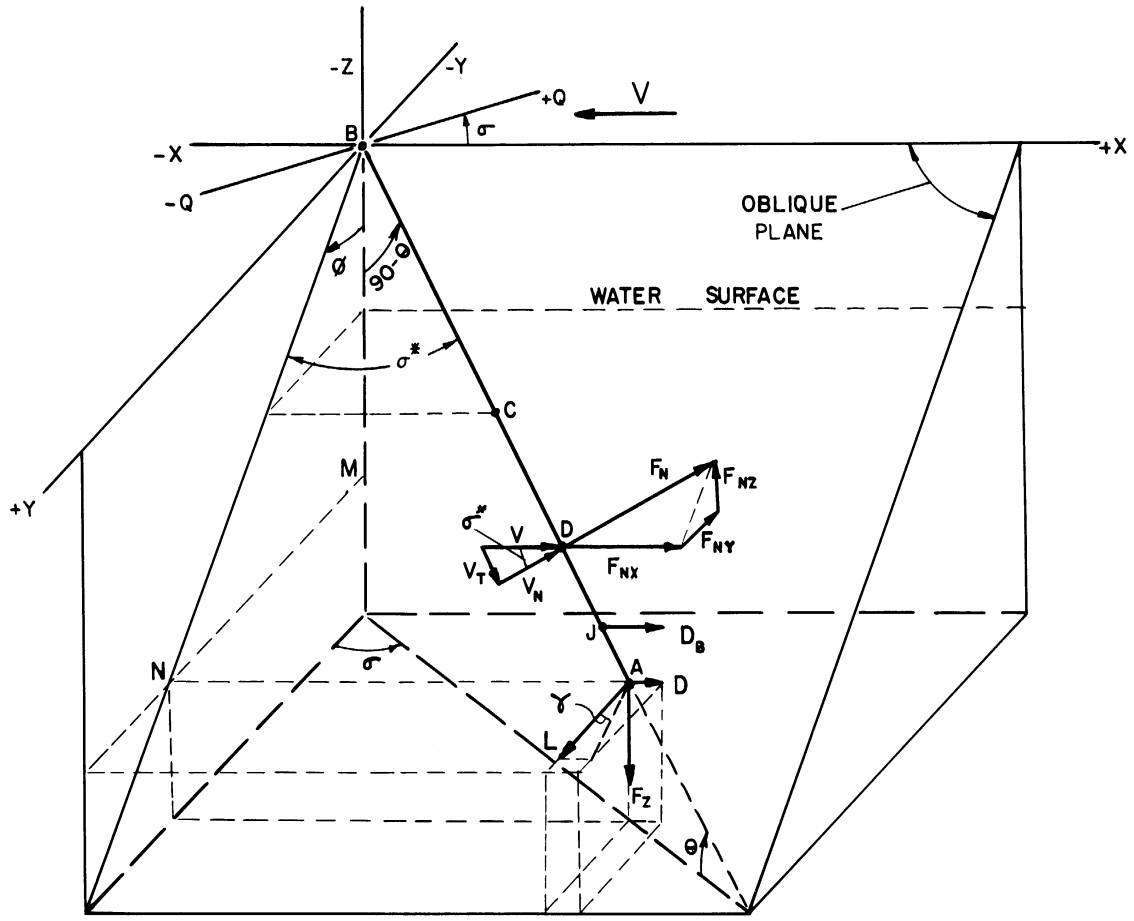

L_C = BJA = length of tow cable
L_{Cy} = MN = outboard distance
L_p = JA = paravane pendant
h = BM = equilibrium depth below tow point
z = BM = instantaneous depth below tow point
V = velocity of ship or relative velocity of fluid

A = bridling point
B = tow point
C = point of cable entry into water
D = application point of the resultant of the drag exerted directly on the cable
J = junction of paravane and added extra drag pendants

Fig. 3-1. Paravane tow-cable BJA and the components of the hydrodynamic forces applied to it by the paravane at A, by an added drag at J, and by the drag exerted directly on the cable with resultant at D. Not shown are the gravitational and hydrostatic forces on the cable and paravane and the reactions at B.

b. C_L = 1.0 to 3.0 and higher
High lift vanes utilizing slots, suction, or other means of controlling the boundary layer.

c. C_L = 10
Power-driven, rotating cylinders producing lift by the Magnus effect.

When drag is also considered, the requirement for a high lift-drag ratio clearly dictates the use of conventional lift vanes.

Reynolds Number. Cavitation.—The decision to use conventional lift vanes makes it possible to proceed with the task of determining the major factors influencing the design of the paravane. Two such factors are the effect of Reynolds number on the hydrodynamic properties of vanes and the need to avoid cavitation. They prove to be of secondary importance in the present task and, except for occasional references, have been deleted from the analysis in the following sections of this Chapter. However, a discussion of them is presented in Appendix B.

3.2 LIFT

The lift and drag of a profiled vane are

$$L = qSC_L \ , \tag{3.1}$$

$$D = qSC_D \ , \tag{3.2}$$

where

$$q = \rho V^2/2 \ . \tag{3.3}$$

Here, ρ is the mass density of the fluid, q is the dynamic pressure, S is the reference area of the vane, and C_L and C_D are respectively its lift and drag coefficients. The latter coefficients are determined experimentally at various angles of attack of the approach velocity, V, of the fluid. Their variation with Reynolds number will be neglected for reasons discussed in Appendix B.

The lift equation (3.1) can be written

$$\frac{L}{q} = SC_L \ , \tag{3.4}$$

where the left side is determined by the specifications of section 2.1 and the right side involves the design factors S and C_L, the values of which are subject to selection so long as their product satisfies (3.4). The value of L/q may be determined from Fig. 3-2 when the lift, L, is specified at a given towing speed, V. If a value of C_L is selected on the basis of factors yet to be discussed, this value and that of L/q from Fig. 3-2 may be used in Fig. 3-3 to determine the area S. Since they have the common axis L/q, Figs. 3-2 and 3-3 can be combined into one diagram, Fig. 3-4, which is convenient for design purposes.

In order to apply Fig. 3-4 to the present problem, it is evidently necessary to stipulate a value for C_L. A lift coefficient of 0.5 is a conservative average for conventional vanes which generally will provide this value at a suitable angle of attack. A suitable angle of attack is one which is fairly well centered between the high angle corresponding to stall and the low or negative angle at which the lift begins to reverse in direction. Then for a lift of 20,000 lb at 16 knots and a lift coefficient of 0.5, Fig. 3-4 indicates L/q to be 27.4 and the required area to be 54.8 sq ft.

A smaller area would have been sufficient if a larger lift coefficient had been assumed. For example, Fig. 3-4 indicates an area of only 10.96 sq ft for C_L equal to 2.5. This smaller area would be desirable from the standpoint of meeting the size limitation of section 2.1, but a high lift device, such as a slotted vane, would be required to obtain the higher value of C_L. In such a device the danger of cavitation is greatly increased and in any case the lift-drag ratio would be adversely affected.

In the case of a single vane, the required area can be had by various combinations of the span and chord of each vane. For a rectangular vane, the area is

$$S = bc \quad , \tag{3.5}$$

where b is the span and c the chord of the vane. Another important quantity defined by a combination of b and c is the aspect ratio, which is

$$AR = b/c \quad , \tag{3.6}$$

and by (3.5) may also be written,

$$AR = S/c^2 \quad . \tag{3.7}$$

Equations (3.6) and (3.7) may be represented on one diagram as shown in Fig. 3-5 which indicates the combination of b and c corresponding to a given area and various aspect ratios. It is seen that several factors bear on the final selection of b and c which now is tantamount to selecting the aspect ratio, since S has been determined. These factors will now be considered in some detail.

VELOCITY V (IN KNOTS)
18 17 16 15 14 13 12 11 10 9 8 7 6
LIFT L (IN POUNDS)
50000
40000
30000
20000
15000
10000
9000
8000
7000
6000
5000
4000
3000
2500
2000
1500
DYNAMIC PRESSURE q x 10⁻² (IN POUNDS / SQUARE FEET)
10 9 8 7 6 5 4 3 2.5 2 1.5 1
LIFT PER UNIT DYNAMIC PRESSURE L/q (IN SQUARE FEET) X 10⁻¹
1 1.5 2 2.5 3 4 5 6 7 8 9 10

Fig. 3-2.

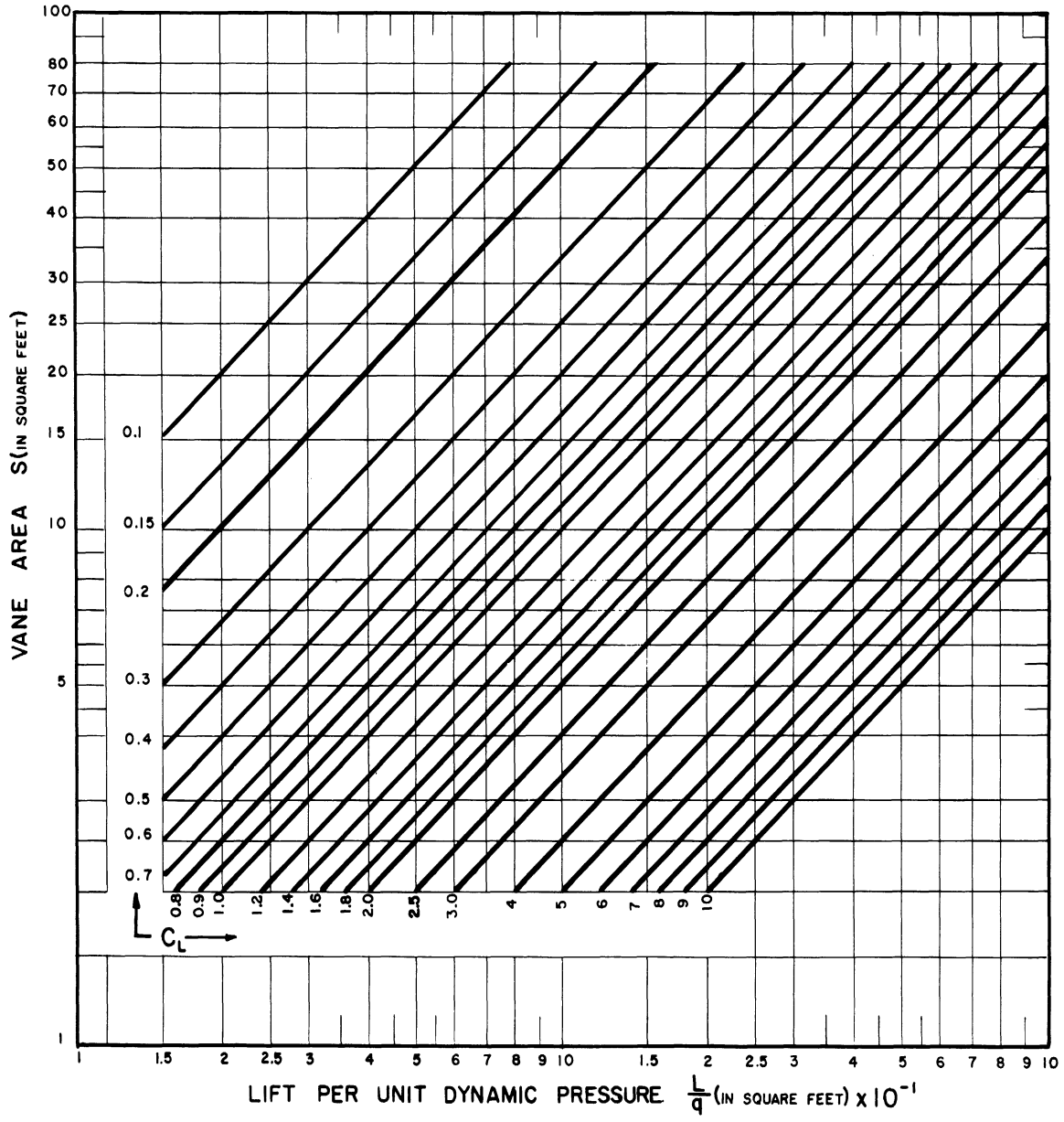
VANE AREA S(IN SQUARE FEET)
100
80
70
60
50
40
30
25
20
15
10
5
1
0.1
0.15
0.2
0.3
0.4
0.5
0.6
0.7
0.8
0.9
1.0
1.2
1.4
1.6
1.8
2.0
2.5
3.0
4
5
6
7
8
9
10
C_L
1
1.5
2
2.5
3
4
5
6
7
8
9
10
1.5
2
2.5
3
4
5
6
7
8
9
10
LIFT PER UNIT DYNAMIC PRESSURE $\frac{L}{q}$(IN SQUARE FEET) X 10^{-1}

Fig. 3-3.

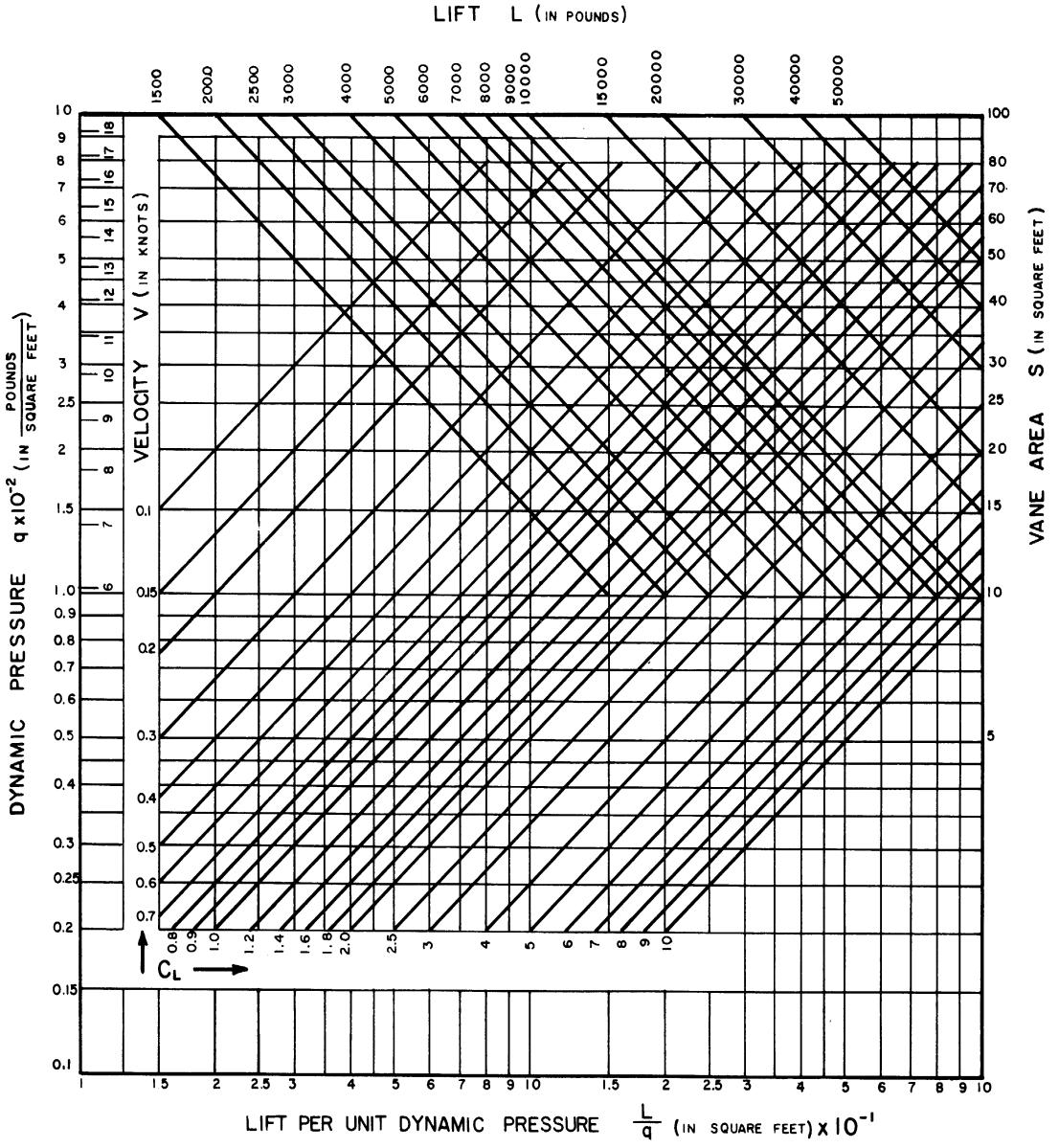
LIFT L (IN POUNDS)
1500
2000
2500
3000
4000
5000
6000
7000
8000
9000
10000
15000
20000
30000
40000
50000
DYNAMIC PRESSURE q x10⁻² (IN POUNDS/SQUARE FEET)
VELOCITY V (IN KNOTS)
VANE AREA S (IN SQUARE FEET)
CL
LIFT PER UNIT DYNAMIC PRESSURE L/q (IN SQUARE FEET) x 10⁻¹

Fig. 3-4.

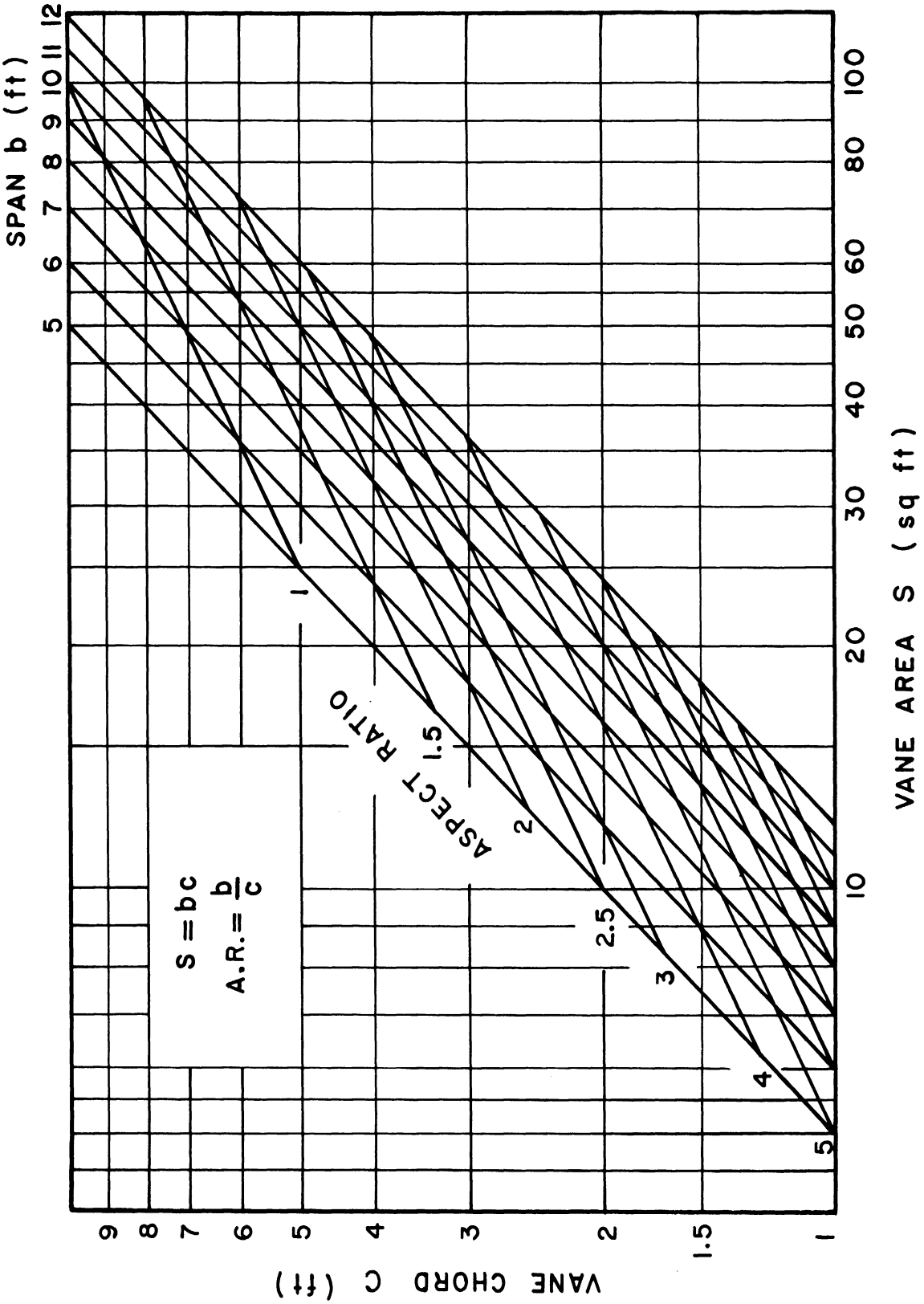
SPAN b (ft)
5 6 7 8 9 10 11 12
VANE CHORD C (ft)
9 8 7 6 5 4 3 2 1.5 1
VANE AREA S (sq ft)
10 20 30 40 50 60 80 100
ASPECT RATIO
1
1.5
2
2.5
3
4
5
S = bc
A.R. = b/c

Fig. 3-5.

For the present, the assumption of a monoplane design will not limit the generality of any conclusions reached if the possibility of multivane designs is considered before discarding a particular combination of b and c. The span and chord are limited by the specification that the maximum dimension be 10 ft. The variation, with depth, of the magnitude and direction of the fluid velocity due to ocean waves indicates the smallest possible span to be desirable. This conclusion stems from the fact that the span line of a paravane lift vane is essentially vertical so that a small span would assist in achieving a lift distribution unaltered by wave motion. The aspect ratio is important primarily for its effect on the lift-drag ratio which is discussed in the following section.

3.3 LIFT-DRAG RATIO

The significance of the aspect ratio can be seen by introducing the expression for that part of the total drag of a vane known as the induced drag. The latter quantity, D_i, is due to the vortex which forms at each tip of a lift vane and is defined as [14]

$$D_i = qSC_{Di} = \frac{L^2}{\pi q b^2} \quad . \tag{3.8}$$

From Equations (3.1) and (3.8), the induced-drag coefficient for a single rectangular vane is

$$C_{Di} = \frac{C_L^2}{\pi(AR)} \quad . \tag{3.9}$$

If L is divided by D_i from Equation (3.8), there results

$$\frac{L}{D_i} = \frac{\pi b^2}{L/q} = \frac{\pi S(AR)}{(L/q)} \quad , \tag{3.10}$$

in which only AR can be varied since the other quantities have been fixed by previous considerations. If no means such as end plates are used to increase the effective span, if AR is made a maximum by making b equal to the maximum of 10 ft, and if L/q is 27.4 and S is 54.8, as before, then

$$\frac{L}{D_i} = 11.4 \quad . \tag{3.11}$$

Equation (3.10) suggest that the ratio of lift to induced drag may be increased by enlarging the span when L/q is held constant or by increasing the aspect ratio when L/q and S are fixed. Moreover, Equation (3.11) indicates that the maximum possible lift-drag ratio for a suitable single vane is less than 11.4, since the parasite drag has been neglected and only the induced component of the total drag has been considered. A multivane design would improve this situation since then the required lifting area could be achieved by several vanes of smaller area, each having higher aspect ratio. This conclusion assumes that the spacing of the vanes would not have to be so great as to exceed the limiting dimension of 10 ft. End plates, which are discussed later, would improve L/D_i by reducing the tip vortices. When end plates are used, the geometric value of AR in (3.10) must be replaced by a so-called effective value based on experiment.

The effect of aspect ratio on the actual lift-drag ratio of a typical conventional vane without end vanes, such as Göttingen profile No. 389, is shown in Fig. 3-6 [15, vol 1, p. 50-53, 76, 90; vol 2, p. 28]. A value of 0.5 for C_L is seen to correspond to an angle of attack near the maximum lift-drag ratio. Moreover, this angle is above the point of lift-reversal and sufficiently below the stall point where C_L is a maximum. An increase in the aspect ratio increases the angle of attack at which L/D is a maximum and also increases L/D. If the lift-drag ratio is to be 10 or more, it is seen that the aspect ratio would have to be at least 2. An increase in aspect ratio also provides a less rapid change of the L/D with angle of attack, especially for angles near the maximum of L/D. A low rate of change is desirable in order that the high lift-drag ratio may not depend too critically on the angle of attack.

The factors influencing the overall lift-drag ratio, such as the experimental values of L/D in Fig. 3-6, are dependent on the total drag. Consequently both the induced and parasite drags must be considered. The total drag may be written

$$D = D_\pi + Di \quad , \tag{3.12}$$

where the new term D_π is referred to as the parasite drag. The parasite drag coefficient, $C_{D\pi}$, is defined by

$$D_\pi = qSC_{D\pi} \quad . \tag{3.13}$$

By substituting in (3.12) expressions in C, q, and S, there results

$$C_D = C_{D\pi} + C_{Di} \quad , \tag{3.14}$$

which by (3.9) becomes

$$C_D = C_{D\pi} + \frac{C_L^2}{\pi(AR)} \quad . \tag{3.15}$$

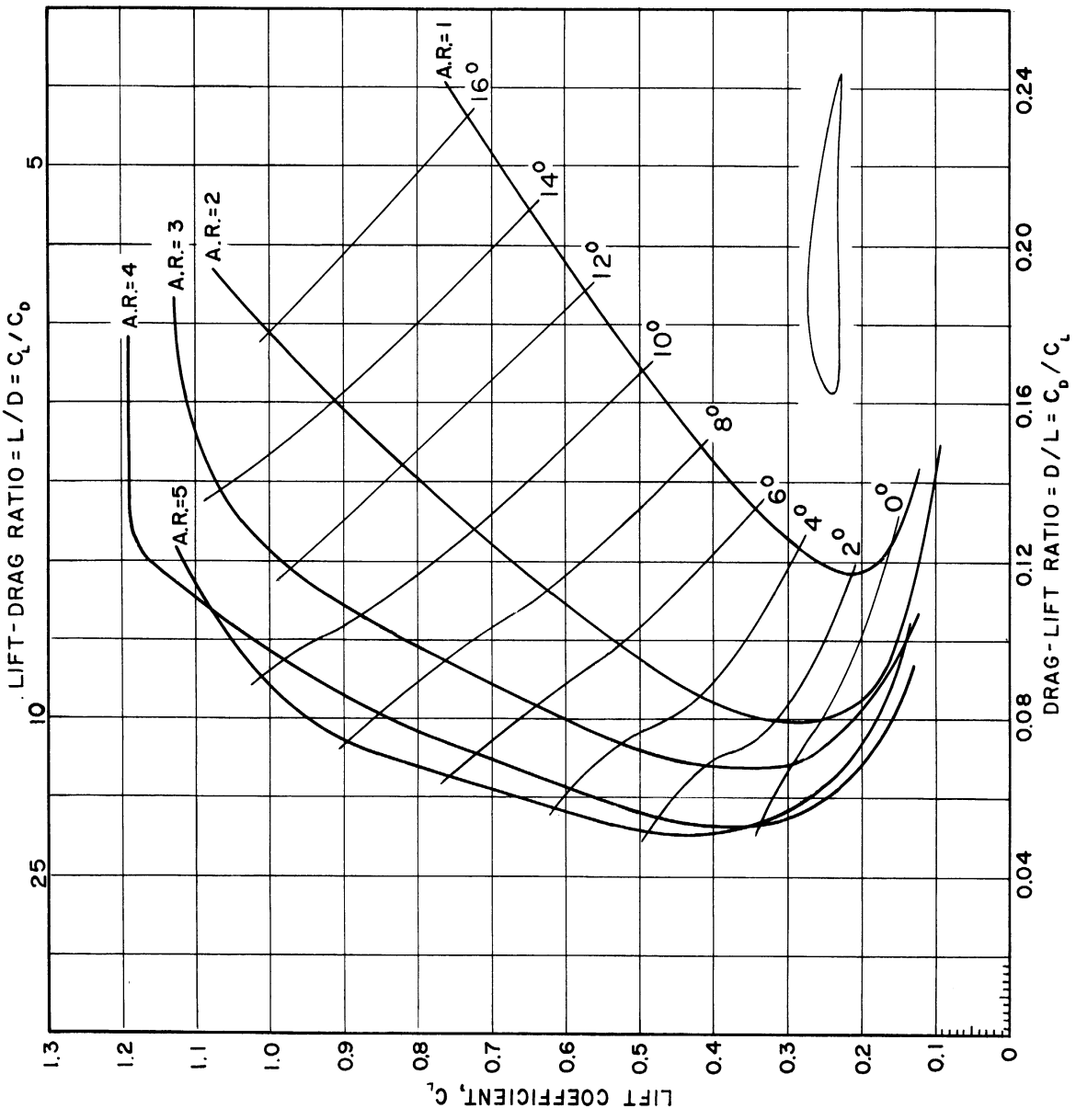
A.R.=1
A.R.=2
A.R.=3
A.R.=4
A.R.=5
16°
14°
12°
10°
8°
6°
4°
2°
0°
LIFT-DRAG RATIO = L/D = C_L/C_D
DRAG-LIFT RATIO = D/L = C_D/C_L
LIFT COEFFICIENT, C_L
5
10
25
0.24
0.20
0.16
0.12
0.08
0.04
1.3
1.2
1.1
1.0
0.9
0.8
0.7
0.6
0.5
0.4
0.3
0.2
0.1
0

Fig. 3-6.

Similarly, the lift-drag ratio may be expressed as

$$\frac{L}{D} = L/(D_\pi + D_i) \quad , \tag{3.16}$$

or

$$\frac{L}{D} = \frac{C_L}{C_D} = \frac{1}{\frac{C_{D\pi}}{C_L} + \frac{C_L}{\pi(AR)}} \quad , \tag{3.17}$$

in which either D_π or $C_{D\pi}$ have yet to be discussed. An important part of the parasite drag is the profile drag, D_o, with the corresponding coefficient written C_{Do}. Figures 3-7 and 3-8 are plots of (3.17). They indicate, for several aspect ratios, the values of C_L and $C_{D\pi}$ at which the lift-drag ratio is a maximum. These curves assume that no end plates are used. In general, reductions of $C_{D\pi}$ increase the lift-drag ratio although the gain requires a closer control of the angle of attack, especially near the maximum of L/D. Means to reduce the value of $C_{D\pi}$ would be of interest. Practically, these are limited to reducing C_{Do} by giving the vane a hydraulically smooth surface and selecting a profile which yields a high value of L/D over a suitable range of C_L and range of angle of attack.

The advantage of using end plates has been inferred previously. Fig. 3-9, which applies to a monoplane design [16], indicates the improvement that end plates produce in the lift-drag ratio of a vane at each of two aspect ratios. At angles of attack in a range for which the lift-drag ratio is near its maximum, a substantial gain in the value of L/D is realized by the addition of end plates and is about the same for both aspect ratios shown. Furthermore, lift-drag ratios of 10 or higher are seen to be possible with an aspect ratio of only 1.315 and for a wide range of angle of attack. In this range other beneficial effects of end plates are seen to be an increase in the value of C_L and a decrease in the rate of change of lift-drag ratio with respect to angle of attack. However, in the case of the latter item, increases in aspect ratio are more effective than end plates.

3.4 EQUILIBRIUM POSITION OF THE PARAVANE-CABLE SYSTEM

This subject has a bearing on the hydrodynamic design of the paravane and has an effect on the dynamic characteristics of the system which are important in depth control. At this point its effect on the hydrodynamic design is of interest. In analyzing the equilibrium of the system, the angular

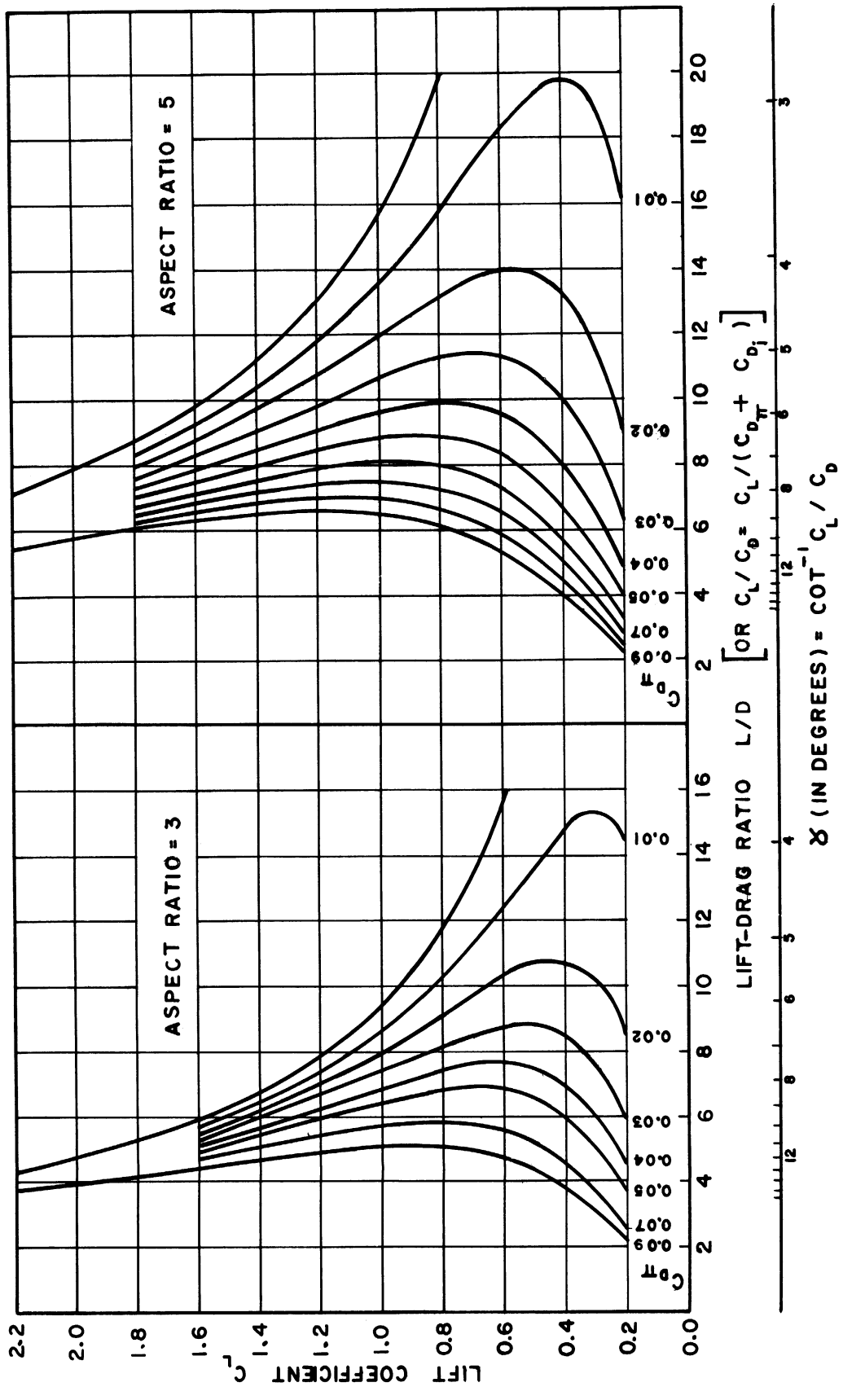
ASPECT RATIO = 5
ASPECT RATIO = 3
C_{D_T}
0.01
0.02
0.03
0.04
0.05
0.07
0.09
LIFT COEFFICIENT C_L
2.2
2.0
1.8
1.6
1.4
1.2
1.0
0.8
0.6
0.4
0.2
0.0
LIFT-DRAG RATIO L/D [OR $C_L/C_D = C_L/(C_{D_T} + C_{D_i})$]
α (IN DEGREES) = $\cot^{-1} C_L / C_D$

Fig. 3-7.

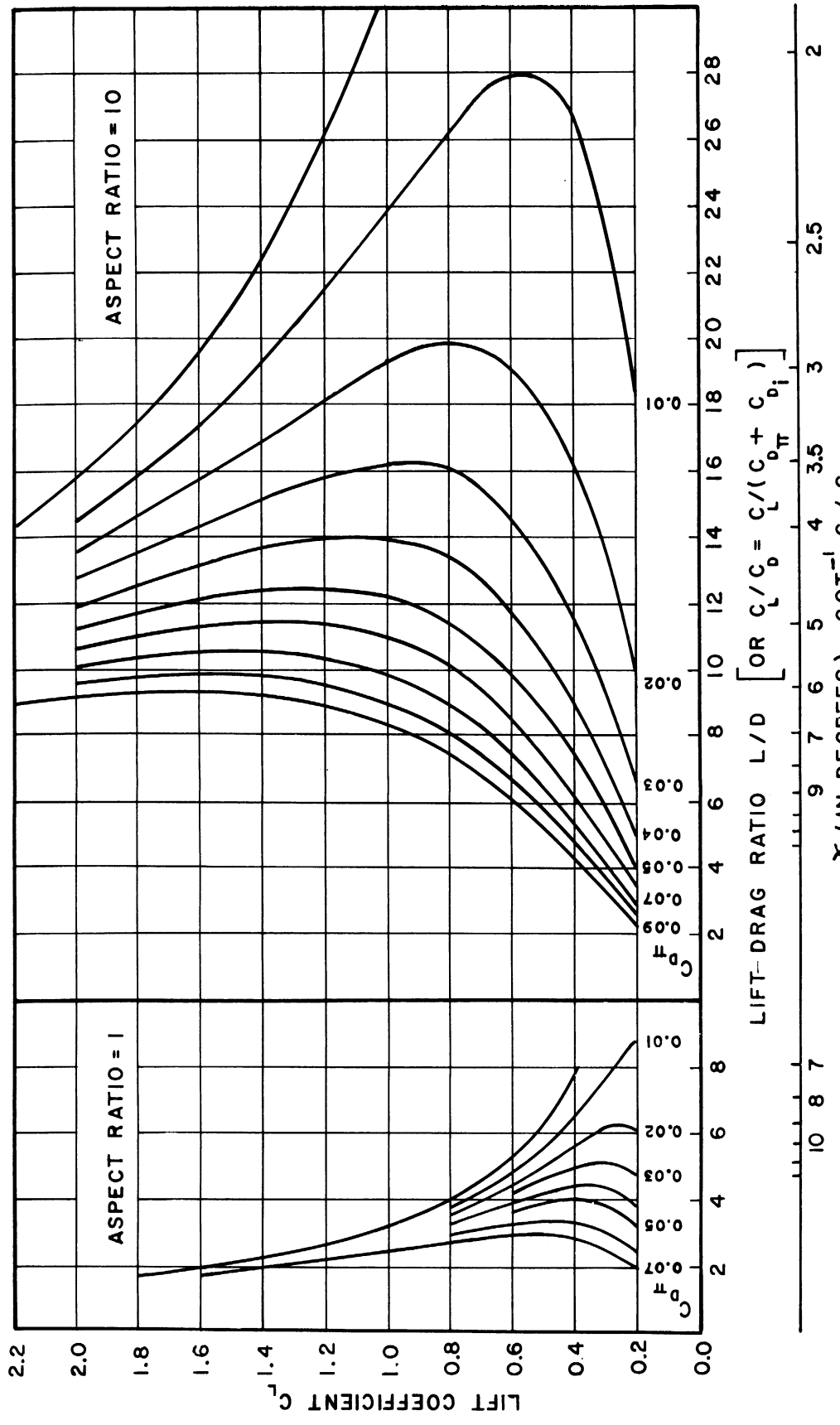
ASPECT RATIO = 10
ASPECT RATIO = 1
C_{D_T}
0.01
0.02
0.03
0.04
0.05
0.07
0.09
LIFT COEFFICIENT C_L
2.2
2.0
1.8
1.6
1.4
1.2
1.0
0.8
0.6
0.4
0.2
0.0
LIFT-DRAG RATIO L/D [OR $C_L/C_D = C_L/(C_{D_T} + C_{D_i})$]
2
2.5
3
3.5
4
5
6
7
8
9
10
28
26
24
22
20
18
16
14
12
10
γ (IN DEGREES) = $\cot^{-1} C_L/C_D$

Fig. 3-8.

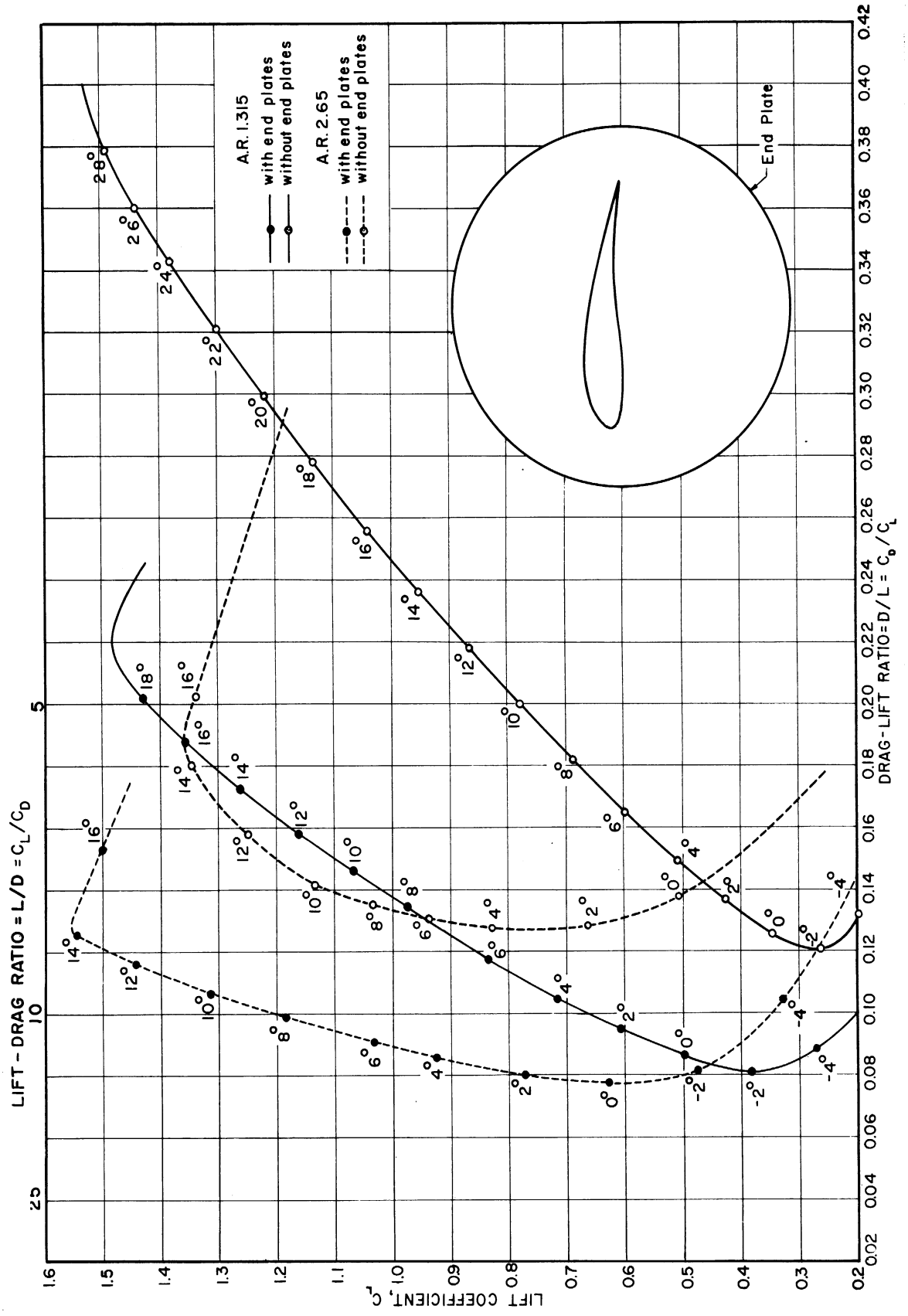
A.R. 1.315
with end plates
without end plates
A.R. 2.65
with end plates
without end plates
End Plate
LIFT - DRAG RATIO = L/D = C_L/C_D
DRAG-LIFT RATIO = D/L = C_D/C_L
LIFT COEFFICIENT, C_L

Fig. 3-9.

orientation of the paravane will be assumed to be constant and the force D_B to be always parallel to the X-axis of Fig. 3-1. The cable is assumed to be straight. This condition will be examined later.

The position of the system is thus defined by that of the paravane. The latter may be described by three space coordinates such as σ, L_{Cy}, and h, or σ, L_C, and h of Fig. 3-1. The cable declination angle, θ, is an alternate coordinate for h, these two quantities having the relations

$$h = L_{Cy} \frac{\tan \theta}{\cos \sigma}$$

and

$$h = L_C \sin \theta \quad .$$

If the equilibrium values of the outboard distance and the depth of the paravane are fixed at the values specified in section 2.1, then L_{Cy} and h are determined and σ is the only unknown space coordinate. The specifications of section 2.1 and data available regarding F_N and D_B of Fig. 3-1 leave only one other unknown quantity entering into the equilibrium of the system, that is, F_Z, the vertical component of the force which the paravane must develop. In order to determine σ and F_Z, it is necessary to derive two independent equations based on the assumption that the system is in equilibrium. One of these equations proves to be sufficient to determine σ to a good approximation and this equation will be obtained at first.

Equilibrium Value of the Cable Sweepback Angle.—Referring to Fig. 3-1, and equating to zero the sum of the moments about the Z-axis, the following equation is obtained

$$L(L_{Cy} \tan \sigma) - D(L_{Cy}) - D_B(0.9\, L_{Cy}) - F_N(0.75\, L_{Cy}/\cos \sigma) = 0 \,, \quad (3.18)$$

where counter-clockwise moments are positive by convention. Also, the outboard distance of point J has been assumed to equal $0.9\, L_{Cy}$. The outboard distance of point D has been taken as $0.75\, L_{Cy}$ because the straight cable is half submerged. F_N has been assumed to be horizontal, which introduces very little error when taking moments about the Z-axis. This fact is due to the slight declination of the cable dictated by the data of section 2.1, the angle θ being only about 16° in this problem.

The cable drag is defined as

$$F_N = \frac{1}{2}\rho V_N^2 C_{NC} S_C = \frac{1}{2}\rho V^2(\cos^2\sigma^*) C_{NC} (0.5 L_C d)$$

$$= q(\cos^2\sigma^*) C_{NC}[0.5\, dL_{Cy}/(\cos\sigma)(\cos\theta)]$$

$$= (0.5)q\, C_{NC}\, dL_{Cy} \cos\sigma \ , \qquad (3.19)$$

where use has been made of the approximate relations

$$\cos\sigma^* = \cos\sigma$$
$$\cos\theta = 1 \ .$$

The validity of these approximations is a consequence of the fact that the cable has small declination. In writing (3.19), S_C has been taken as $0.5\, L_C d$ since one-half the cable is submerged.

Equation (3.18) may be written

$$\tan\sigma = \frac{D}{L} + 0.9\frac{D_B}{L} + \frac{0.75}{\cos\sigma}\frac{F_N}{L} \ . \qquad (3.20)$$

Substituting (3.19) in (3.20), and rearranging, yields

$$\tan\sigma = \frac{1}{L/D} + 0.9\frac{1}{L/D_B} + (.75)(.5)\, C_{NC} d\, L_{Cy}\frac{1}{L/q} \ . \qquad (3.21)$$

Equation (3.20) indicates the contribution of the various drag forces to the cable sweepback angle, σ. Equation (3.21) relates σ to the specified quantities L_{Cy}, L/D, and L/q, as well as the ratio L/D_B of the lift to any extra drag and the tow-cable properties C_{NC} and d.

Equations (3.20) and (3.21) are based on the assumption that the tow cable is straight when the system is in equilibrium. Static relations show that, if the cable is reasonably flexible, the deviation from a straight line will be small for the relatively short and small diameter cable involved in the present case. This condition will exist because the tendency toward curvature, due to the gravitional and hydrostatic forces on the cable (in a vertical plane) and the hydrodynamic drag on the cable (essentially in the oblique plane of Fig. 3-1), is much less than the straightening effect of the

very high tensile force applied to the cable as a result of the large lift force developed by the paravane.

If K is defined as

$$K = 0.9 \frac{1}{L/D_B} + (0.75)(.5)\, C_{NCd}\, L_{Cy} \frac{1}{L/q} , \qquad (3.22)$$

then Equation (3.21) becomes

$$\tan \sigma = \frac{1}{L/D} + K . \qquad (3.23)$$

This equation is plotted in Fig. 3-10. Using the following representative values,

$L/q = 27.4$ sq ft $d = 1$ in.

$L_{Cy} = 200$ ft $C_{NC} = 0.4$

where the low value of C_{NC} is taken to represent the use of a faired cable, and letting L/D_B equal 6.67,

$$K = .135 + .091 = 0.226 . \qquad (3.24)$$

Also, K is .091 when D_B is zero and K is zero when both D_B and F_N are zero. Fig. 3-10 then yields the following results:

Drag	Paravane L/D	K	σ	Change in σ due to decrease in L/D, percent
D (paravane only)	10	0.	5.7°	
	7	0.	8.1°	+ 42
D and F_N	10	0.091	10.8°	
	7	0.091	13.0°	+ 20
D, F_N, and D_B	10	0.0226	18.1°	
	7	0.0226	20.1°	+ 12

The change in the lift-drag ratio, L/D, of the paravane itself is seen to be of diminishing importance percentagewise as the total drag of the

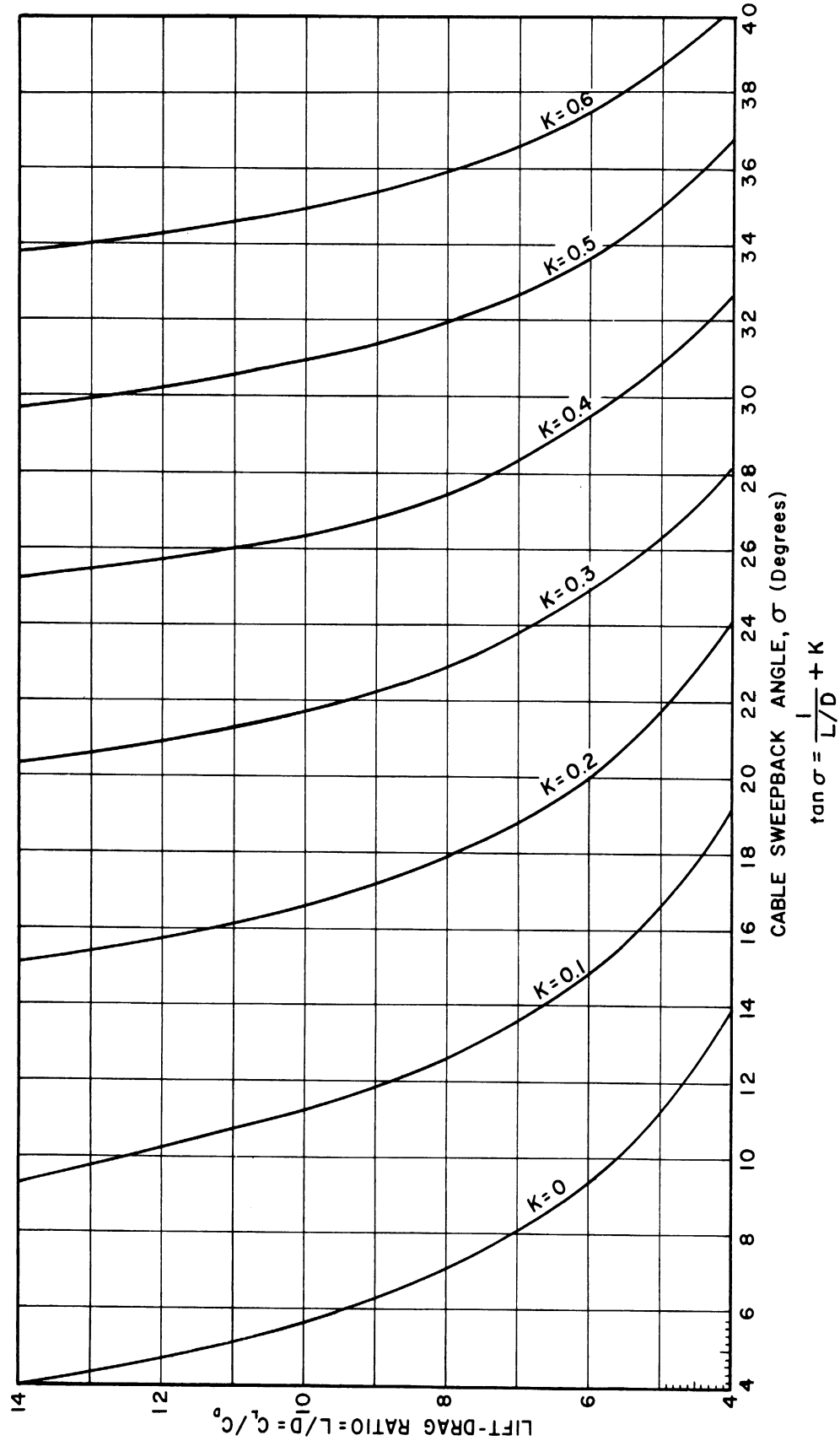
K=0.6
K=0.5
K=0.4
K=0.3
K=0.2
K=0.1
K=0
CABLE SWEEPBACK ANGLE, σ (Degrees)
tan σ = 1/(L/D) + K
LIFT-DRAG RATIO = L/D = C_L/C_D
40
38
36
34
32
30
28
26
24
22
20
18
16
14
12
10
8
6
4
14
12
10
8
6
4

Fig. 3-10.

system increases. Moreover, the 30% decrease in L/D causes an average increase of 2.2°, whereas the various drag forces account for an increase of 6° on the average. The effect of cable drag, about 5°, is seen to be considerable despite the assumption of fairing.

As a consequence of the small effect on σ of the 30% change in the lift-drag ratio of the paravane, it may be expected that small reductions of L/D below a value of 10 will have little effect on the equilibrium position when the complete system is considered. For example,

Drag	L/D	K	σ	Change in σ
D, F_N, and D_B	10	.226	18.1°	
	9	.226	18.6°	+2.8%

The distance by which the paravane is aft of the tow point is

$$X = L_{Cy} (\tan \sigma)$$

so that the change in the aft distance for a reduction of L/D from 10 to 9 is

$$\Delta X = X_{final} - X_{initial} = 200(\tan 18.6) - 200(\tan 18.1°) = +2.2 \text{ ft} .$$

The increase in σ and X due to the assumed 10% decrease in L/D can be readily offset by an increase of less than 10% in the lift, L. Fig. 3-9 indicates that such an increase in L may be accomplished by very small increase in the angle of attack while avoiding significant further decrease in L/D. Alternately, L may be increased by a small increase in S. For example, when L/D is 10, Equation (3.20) yields

$$\tan \sigma = \frac{1}{L/D} + 0.9 \left(\frac{1}{L/D_B}\right) + (.75)(.5)\, C_{NCd}\, L_{Cy} \left(\frac{1}{L/q}\right)$$

$$= 0.1 + 0.135 + .091 = .326 , \qquad (3.25)$$

and when L/D is decreased by 10% to a value of 9,

$$\tan \sigma = 0.111 + 0.135 + .091 = .337 .$$

The effect of increasing L by 5% when L/D is 9, can be determined by replacing L by (1.05 L) and d by $(1.05)^{1/2}$d in (3.21) whence

$$\tan \sigma = \frac{.111}{1.05} + \frac{.135}{1.05} + \frac{(1.05)^{1/2}}{1.05}(.091)$$

$$= .105 + .128 + .089 = .322 ,$$

where the quantity $(1.05)^{1/2}d$ is introduced because the cable diameter must be increased by this factor in order to maintain the same stress factor of safety as existed before increasing the lift by 5%. The small increase in L, when L/D equals 9, is seen to reduce σ to a value less than that existing when L/D is 10.

Generation of the Downward Component of Force.—The lift and drag components of the resultant hydrodynamic force on the paravane have been discussed in some detail. The vertical component, shown as F_Z in Fig. 3-1, must also be considered. In particular, it is desired to determine the magnitude and direction which F_Z must have when the paravane-cable system is in static equilibrium. This step can be accomplished by again writing equations expressing the equilibrium of the moments of the external forces on the paravane-cable system. The equation expressing the equilibrium of moments about the Z-axis has already been used and it yielded an equation which determined σ. F_Z being the only remaining unknown, it will be sufficient to sum the moments about one axis other than Z, such as the X-, Y-, or Q-axes, all of which are perpendicular to the Z-axis and will therefore yield an equation independent of that already obtained. A summation of moments about the X-axis provides the simplest equation.

Assuming that F_Z is downward as shown in Fig. 3-1, a summation of moments about the X-axis yields

$$-L(h) + F_z(L_{Cy}) + W_C(0.5\, L_{Cy}) - B_C(0.75\, L_{Cy}) + (W - B)\, L_{Cy} = 0 , \qquad (3.26)$$

where F_N does not appear since it intersects the X-axis. W_C and B_C are the gravitational and hydrostatic forces on the cable while W and B are those on the paravane. The factors (0.5) and (0.75) appear because the cable is half submerged. Then, from (3.26),

$$F_Z = \frac{h}{L_{Cy}}(L) - 0.5(W_C) + 0.75\, B_C + (B - W) , \qquad (3.27)$$

where F_z is expressed in terms of known quantities and h is given the specified value of 60 ft corresponding to a paravane depth of 30 ft. For a paravane lift-drag ratio of 10, σ was found above to be 18° and cos σ is 0.951. If L_{Cy} equals 200 ft, then

$$\tan \Theta = \frac{h}{L_{Cy}} \cos \sigma = 0.285$$

so that

$$\Theta = 15.9^\circ \text{ and } \sin \Theta = 0.274 ,$$

from which

$$L_C = h/\sin \Theta = 219 \text{ ft} .$$

Thus for a stranded steel cable having a specific weight of

$$\gamma_C = 320 \text{ lb/ft}^3$$

in sea water of specific weight

$$\gamma_\omega = 64 \text{ lb/ft}^3 ,$$

it is found that

$$W_C = 382 \text{ lb and } B_C = 38.2 \text{ lb} .$$

Assuming also that

$$B - W = 60 \text{ lb and } L = 20{,}000 \text{ lb} ,$$

then at a depth of 30 ft (h = 60) , Equation (3.27) yields

$$F_z = 6{,}000 - 191 + 29 + 60 = 5{,}898 \text{ lb} . \qquad (3.28)$$

Considering only the change in the first term of (3.28), a depth of 50 ft (h = 80) requires

$$F_z = 8{,}000 - 191 + 29 + 60 = 7{,}898 \text{ lb} .$$

Since Equation (3.27) yields positive values of F_z, equilibrium requires that the latter be directed downward as assumed initially.

Comparing (3.27) and (3.28), the term $L(h/L_{Cy})$ is seen to contribute

over 98% to the required value of F_z, which is therefore given quite accurately by the equation

$$F_z = \frac{h}{L_{Cy}} (L) \quad . \tag{3.29}$$

The horizontal lift, L, is required to have a value of 20,000 lb at 16 knots (27 ft/sec). Also, since the variation in C_L with speed is being neglected for reasons given in Appendix B, Equation (3.1) indicates that L may be expected to vary as V^2. Consequently, the required value of L at any speed is

$$L = 20{,}000 \left(\frac{V}{27}\right)^2 \quad , \tag{3.30}$$

where V is expressed in ft/sec. Then if h and L_{Cy} are constant at the specified values of 60 and 200 ft, respectively, Equation (3.29) indicates that the required value of F_z must also vary as V^2, that is, for a depth of 30 ft

$$F_z = 5{,}898 \left(\frac{V}{27}\right)^2 \text{ lb} \quad . \tag{3.31}$$

The requirement that F_z vary as V^2 suggests that it be produced hydrodynamically. This step may be accomplished, for example, by a constant roll of the paravane through an angle ϵ about an axis parallel to the direction of motion. The lift vector will then have a downward component. The horizontal component, L, of the lift must continue to have the value given by Equation (3.30). Thus the required value of ϵ is determined by substituting (3.30) and (3.31) into the equation

$$\tan \epsilon = \frac{F_z}{L}$$

to obtain

$$\tan \epsilon = \frac{F_z}{L} = \frac{5{,}898}{20{,}000} = .2949 \quad , \tag{3.32}$$

whence

$$\epsilon = 16.4° \quad ,$$

which is a constant for all towing speeds. The resultant lift is required to be

$$L_R = \frac{L}{\cos \epsilon} = 20{,}000 \left(\frac{V}{27}\right)^2 \left(\frac{1}{.9591}\right) = 20{,}853 \left(\frac{V}{27}\right)^2 \text{ lb} \quad .$$

Thus L_R must exceed the required horizontal lift of Equation (3.30) by only 4% and ϵ need by only 16.4° in order to produce the large value of F_Z required to obtain an equilibrium depth of 30 ft at all speeds. Other points bearing on the desirability of producing F_Z by a roll of the paravane are discussed in the next section in connection with the consideration of the depth controllability of the design.

3.5 CONTROL. ORIENTATION, LAUNCHING, AND DEPTH

The necessity that the paravane be controllable points to a number of additional design factors.

Orientation Control.—A superior hydrodynamic design would be of little avail if the intended angles of attack, roll, and yaw of the lift vanes were not maintained reasonably well. In the range of orientation for which the bridling lines remain taut, the equilibrium values of these angles are determined by the moments, about a set of axes through the bridling point, of forces acting on the paravane. These paravane axes will be assumed to consist of a pitch axis which is vertical, a roll axis parallel to the direction of motion, and a yaw axis which is horizontal and perpendicular to the direction of motion. The paravane axes therefore have an origin at the bridling point A of Fig. 3-1 and, respectively, have the directions of the vectors F_Z, D, and L of that figure. Control of orientation requires that, at the desired constant angles of roll, pitch and yaw, and over the range of towing speed, the design of the paravane and bridling system achieve equilibrium of the moments of the gravitational, hydrostatic, and hydrodynamic forces acting on the various components of the paravane.

Maintaining a constant orientation over the range of speed requires that the moments, about the paravane axes, of forces which do not depend on towing speed (weight and static buoyancy) must be equilibrated independently of the moments of the hydrodynamic forces on the paravane. A constant angular position is seen later in this section to be especially important to the depth controllability of the paravane. At that point the control of orientation is considered further.

In general, the control of orientation requires attention to the bridling system, to the relative location of the various components of the paravane, and to the location of the centers of gravity and buoyancy and the hydrodynamic centers of the vanes. In practice, these factors were considered in a general way in designing models and refinements were made in the course of the test program.

Launching Control.—The control of the paravane during launching was studied experimentally by comparing and refining the launching behavior of various models the original designs of which were based primarily on other

factors. The principal requirements that could be anticipated were that the model be self-righting in the water when not under tow, have a large range of angle of attack between the stall and lift-reversal points, and have a configuration which avoids interference, that is, prevents the wake or wash of various components from seriously interfering with the flow about the lift vanes, especially if a rapid outward sweep should occur during launching.

The requirement that the paravane be self-righting in the water, when not under tow, dictates that its center of gravity lie below its center of buoyancy when it is upright. When the paravane is not upright, the weight and buoyancy should produce a large enough couple to right it quickly.

Proper launching behavior also requires that the action of the depth control shall not produce an excessive rate of descent, especially at the beginning of launching when a large error in depth would be detected by the control mechanism.

A brief survey showed that an analytical study of launching was not worthwhile due to the complex and highly nonlinear differential equations involved.

Depth Control.—An important factor in the design of the paravane is that the automatic depth control to counter the action of disturbances be obtainable with a mechanism which is reasonably simple and has moderate size and power. This consideration points to several factors influencing the hydrodynamic design and will now be discussed under the subjects of the manipulated element and the natural depth.

Manipulated Element

A component of the hydrodynamic design which is intended to supply the depth-correcting influence to counter disturbances may be termed a manipulated element since it must be actuated by the control mechanism. Examples of such elements are flow spoilers and also control surfaces such as ailerons, flaps, elevators, and rudders. A manipulated element may also be a movable, internal mass capable of reorienting the paravane when its position is changed. It is desirable that the hydrodynamic design be such that the depth of the paravane will be effectively governed by the actuation of the manipulated element selected and that this actuation will not require excessively large forces.

A given type of manipulated element may influence depth in any of a number of simple ways, or some combination of them. For example, the paravane depth may be controlled by producing sufficient vertical force to offset that of any disturbance, such as by reorienting the paravane. If the paravane is equipped with end vanes, these will be approximately horizontal. If an end vane is equipped with control surfaces on its trailing edge, the deflection of

such surfaces may develop a vertical force. If the control surfaces are deflected in unison as flaps, the force is obtained directly by changing the effective camber of the end vane. If the control surfaces are deflected in opposite directions as ailerons, the vertical force may be developed indirectly by causing a roll of the paravane.

Instead of meeting the disturbance with an opposing force, the role of the manipulated elements may be to reduce the force which the disturbance is capable of exerting on the paravane. For example, the vertical motion of waves produces a disturbance by the varying angle at which the water attacks any horizontal surfaces such as end vanes. The manipulated element may attempt to vary the orientation of the paravane about its yaw axis so that the oscillating flow would have a minimum angle of incidence with respect to the horizontal surfaces and so limit the depth-disturbing force exerted on the paravane.

Manipulated elements, such as flaps, which develop a depth-corrective force directly by producing a lift over their stabilizer surface can provide the quickest control action. Manipulated elements which develop a depth-corrective influence indirectly by reorienting the paravane can probably produce the largest forces. For example, variations of the roll of the paravane determine the size of the vertical component of the lift, the latter being the largest component of force acting on the paravane. However, manipulated elements of this type have the disadvantage that the generation of the depth-corrective influence is delayed by the time required to change the angular position of the paravane. Moreover, the depth disturbance may interfere with control action of this kind by affecting the orientation of the paravane as well as its depth. Also, it may be necessary to limit the righting couple of the weight and buoyancy of the paravane in order that the element might effectively vary the orientation.

The minimization of the hinge moments which the control mechanism must supply to actuate the manipulated element will depend on the moments about the hinge axis of the gravitational, buoyant, hydrodynamic, damping, and inertial forces acting on the manipulated element. In general, it is most important to minimize the hydrodynamic moment and inertial moment since these are greatest. Also, they vary, respectively, as the square of the towing speed and the square of the frequency of manipulation and therefore place a varying requirement on the output of the mechanism. Manipulated elements of the control-surface type will experience a zero hydrodynamic moment and a minimum inertial moment if the center of force and the center of mass of the control surface lie on the hinge axis.

The moments due to the weight and buoyancy of a control surface do not vary with speed or frequency and therefore are readily compensated by the control mechanism. These moments can be reduced to zero if the centers of gravity and buoyancy lie on the hinge axis. The damping moments vary approxi-

mately as the first power of the frequency of manipulation and will generally be small for the disturbance frequencies experienced by paravanes. In the above statements of the conditions under which the moments of certain forces will be zero, neglect has been made of the small effect which those forces have on the friction in the bearings of the hinge shaft of the control surface.

A number of designs of stabilizer-control surface combinations have been developed to realize special characteristics such as minimization of hinge moments [17, 18]. These designs should be considered for the paravane.

Natural Depth

The depth controllability of the paravane also involves the relation between the desired depth which the control equipment seeks to maintain and the equilibrium depth naturally assumed by the paravane. Ideally, the natural depth should be the same as the desired depth so that the depth-control equipment is required at most to achieve an efficient approach to the proper depth and thereafter to counter disturbances tending to create an error in depth. In this way the deflection of the manipulated element to either side of its mid-position will have an average value of zero over the period of an oscillating disturbance. This requirement is especially important in a high lift-drag ratio paravane since an appreciable difference between the desired and natural depths would cause the average deflection of the manipulated element to be significantly different than zero. This condition will usually have an unfavorable effect on the lift-drag ratio by causing an increase in the drag of the paravane.

Another difficulty arises by virtue of the fact that the depth-corrective force which the manipulated element must provide quickly becomes excessive with deviation of the natural equilibrium depth from that desired. To appreciate this fact, moments will again be summed with respect to the X-axis of Fig. 3-1 in order to determine the depth-rate-of-change of F_z as the equilibrium depth changes. The resulting value will be a conservative estimate of the required depth-corrective force since it considers only the static forces which must be overcome and ignores the force due to any disturbance present. In considering deviations of the system from the equilibrium depth, it is appropriate to hold L_C constant instead of L_{Cy}. From Fig. 3-1 the relation between L_C and L_{Cy} is

$$L_{Cy} = (L_C^2 - h^2)^{1/2} \cos \sigma \ .$$

This expression may be substituted in Equation (3.29) to obtain

$$F_z = \frac{h}{(L_C^2 - h^2)^{1/2}} \left(\frac{L}{\cos \sigma}\right) \ , \qquad (3.33)$$

and the rate of change of F_z with h is

$$\frac{dF_z}{dh} = \frac{L_c^2}{(L_c^2 - h^2)^{3/2}} \left(\frac{L}{\cos \sigma}\right) . \qquad (3.34)$$

Utilizing the representative values

$$h = 60 \text{ ft} \qquad L_c = 219 \text{ ft}$$

$$\cos \sigma = .9511 \qquad L = 20{,}000 \text{ lb}$$

Equation (3.34) yields

$$\frac{dF_z}{dh} = 107.9 \text{ lb/ft} .$$

Since by (3.34) this quantity varies as the hydrodynamic force L which has a value of 20,000 lb at 16 knots, then at any speed of V (ft/sec),

$$\frac{dF_z}{dh} = 107.9 \left(\frac{V}{27}\right)^2 \text{ lb/ft} \qquad (3.35)$$

for depths in the neighborhood of 30 ft (h = 60). Consequently, the depth-corrective force must be at least 107.9 lb for each foot by which the deviation between the natural depth and the desired depth exceeds the allowable depth error. On the other hand, if the natural depth can be made approximately equal to the desired depth, this large force will oppose disturbances tending to produce an error in depth.

The control of natural depth by roll has already been suggested and it was found that an angle of only 16.4° was adequate for a depth of 30 ft. The effect of roll will now be investigated further. Regardless of whether the natural depth is obtained by means of roll, any roll angle ϵ which happens to occur will contribute to F_z some portion, F_z', given by

$$F_z' = L (\tan \epsilon) ,$$

whence

$$\frac{dF_z'}{d\epsilon} = \frac{dF_z}{d\epsilon} = L/\cos^2 \epsilon . \qquad (3.36)$$

In Equation (3.36) the quantity $\cos^2 \epsilon$ will have a maximum value of unity so that the minimum value of $dF_z/d\epsilon$ is

$$\frac{dF_z}{d\epsilon} = L = 20{,}000 \left(\frac{V}{27}\right)^2 \text{ lb/radian} = 349 \left(\frac{V}{27}\right)^2 \text{ lb/degree} , \qquad (3.37)$$

where V is in ft/sec. The minimum rate of change of the natural depth, h, with ϵ is given by the quotient of (3.36) and (3.34), whence

$$\frac{dh}{d\epsilon} = \frac{dF_z/d\epsilon}{dF_z/dh} = \frac{(L_C^2 - h^2)^{3/2}}{L_C^2} \left(\frac{\cos \sigma}{\cos^2 \epsilon}\right)$$

$$= \frac{349}{107.9} = 3.23 \text{ ft/degree} , \qquad (3.38)$$

which is a constant for all speeds and has the value 3.23 ft per degree when the depth is near 30 ft. The equilibrium depth is seen to be very sensitive to the angle of roll which must therefore be controlled in any event. Consequently, the roll might as well be controlled at the angle corresponding to the required value of h.

As seen in Equation (3.32), ϵ must be independent of towing speed in order to obtain a constant equilibrium depth. Maintaining the roll at a constant value over a range of speeds requires independent equilibria of the moments, about the roll axis, of the velocity-independent and hydrodynamic forces acting on the paravane. This condition cannot be achieved exactly because a non-zero value is specified for the resultant of weight and buoyancy which is usually outboard from a roll axis passing the bridling point as shown, for example, in Fig. 4-9. Consequently, the resultant force will provide a roll moment. Only hydrodynamic lift is available to balance this moment with the result that the equilibrium value of the roll angle will vary with speed. However, the variation due to this reason will not be large primarily because the lift of the paravane greatly exceeds the resultant of weight and buoyancy and, to a small extent, because of the righting couple which the latter forces provide if the roll is varied from the desired value. For a change in speed from 6 to 16 knots, the above condition will cause a change in roll of about 2° which, by Equation (3.38), corresponds to a change of 6.5 ft in the equilibrium depth. This result assumes that the resultant of weight and buoyancy is 100 lb and is outboard from the roll axis by 5 ft. The effect of the righting

couple is ignored since it will be small for a roll of only 2°.

The maintenance of the desired equilibrium depth over the speed range also requires that the pitch angle of the paravane, that is the angle of attack of the lift vanes, remain constant. Otherwise, h will vary due to its dependence on L as given in Equation (3.33). The angle of pitch is determined primarily by the equilibrium of hydrodynamic moments due to the lift and drag forces on the vanes and other components of the paravane. It may be expected that the angle of pitch at which these moments are in equilibrium will vary but little with speed because the coefficient of the hydrodynamic moment of a vane is quite constant at the Reynolds numbers anticipated (Appendix B1). However, the yaw angle of the paravane, which determines the angle of attack of any horizontal surfaces of the paravane, will vary with speed. This condition exists because the yaw axis is horizontal and the angle of yaw will depend upon a balance of the velocity-independent moment of weight and buoyancy and the hydrodynamic moment of the drag of the paravane. Since the drag has been minimized, it does not greatly exceed the resultant of weight and buoyancy as did the lift. An estimate made on the same basis as that for roll, indicates that the angle of yaw may vary as much as 17° in the velocity range of 6 to 16 knots. The resulting change in the equilibrium depth will have a direction opposite that due to the accompanying change of roll.

In general, the desired equilibrium values of the pitch, roll, and yaw angles, and the particular adjustment of the design which provides those values, must be determined under full-scale conditions. Thus the prototype design will require some adjustments such as variation in the location of the center of gravity, in the bridling, and in the setting of trim surfaces. Only the last two of these could also be of appreciable assistance in reducing the change of depth with speed, should an excessive change result from the sum of the effects described in the preceding two paragraphs.

3.6 STRUCTURE. WEIGHT, BUOYANCY, AND RUGGEDNESS

In this section it is desired to discuss briefly those structural considerations which directly influence the design of the lift vanes.

The need to control the sum of the gravitational and buoyant forces on the paravane in order to obtain a small upward resultant directs attention to the average specific weight and the volume of the lift vanes. Several measures are available for varying the specific weight, since a vane may be solid, hollow, or of hollow construction with any of a number of filler materials. The volume of a vane is a function of its area, profile shape, and thickness ratio. The first two of these quantities have been shown to be largely determined by a number of factors such as the required lift, lift-drag ratio, avoidance of cavitation, and wide range of angle of attack between

the lift-reversal and stall points. Although these factors also place some limitations on the thickness ratio, some latitude remains in this regard. To determine the extent of this latitude, it is desirable to test promising models with vanes of various thickness ratios.

The need for ruggedness bears directly on the aspect ratio, thickness, and internal construction of the lift vanes. While the lift-drag ratio is improved by increasing the aspect ratio, strength considerations suggest decreasing the latter, increasing the thickness, and adopting internal bracing.

In general, therefore, the average specific weight, thickness ratio, and internal construction of the vanes are at the disposal of the structural designer. It is evident that the high lift, high lift-drag ratio, and limited size tend to require a highly stressed structure. In an extreme case, it may be necessary to adjust the weight of the paravane by means of the specific weight so that the required buoyancy is provided by braced vanes of the maximum thickness ratio which is acceptable hydrodynamically. The aspect ratio could then be a maximum and therefore made to equal the desired value or made to approach it as far as consistent with ruggedness. While the actual design process may consider these factors in a different sequence, this discussion indicates that sufficient flexibility exists to permit a suitable structural design, provided that the weight is subject to adjustment when the combination of specifications tends to require a highly stressed structure.

3.7 DESIGN IMPLICATIONS OF THEORETICAL FACTORS. GENERAL CONFIGURATION

The principal characteristics needed in the high lift-drag ratio paravane have been seen to consist of requirements on the lift per unit dynamic pressure, lift-drag ratio, size, operating depth and outboard distance, control, the resultant of buoyancy and weight, and ruggedness. These characteristics point to a number of design factors. Some of the latter conflict with each other as to their influence on the design of the paravane. The following summary is helpful in determining the overall implication of these factors on the design of the paravane.

Desired Characteristic	Design Factor
$\frac{L}{q} = 27.4$	$SC_L = 27.4$

Utilize a lift-vane profile which minimizes S by permitting a high value of C_L at a suitable angle of attack, α, well away from the stall and lift-reversal points.

$$\frac{L}{D} = 10 \qquad \frac{L}{D_i} = \frac{C_L}{C_{Di}} = \frac{\pi S(AR)}{L/q}$$

Conventional lift vanes are desirable for high L/D. For a single lift vane, AR is limited by the restriction of the span due to the effect of wave motion on the lift and due to the size limit of 10 ft. The latter requirement limits L/D_i to a maximum of 11.4. To obtain a value of 10 for L/D, a multivane design and end plates may be required so as to secure, respectively, a geometric and an effective increase in AR.

$$\frac{L}{D} = 10 \qquad \frac{L}{D} = \frac{C_L}{C_{D\pi} + C_{Di}} = \frac{1}{\frac{C_{D\pi}}{C_L} + \frac{C_L}{\pi(AR)}}$$

Minimization of $C_{D\pi}$ requires a hydraulically smooth vane surface and a low profile drag coefficient, C_{Do}, as indicated by a high overall lift-drag ratio. The latter must correspond to the suitable range of α. The rate of change of L/D with α should be small near the maximum of L/D. Experimental data indicate that the latter characteristic is improved principally by increase in aspect ratio.

Equilibrium Position $\qquad \tan\sigma = \frac{1}{L/D} + \frac{.9}{L/D_B} + \frac{(.75)(.5)}{L/F_N}$

L/D of the paravane has diminishing importance as the added drag, D_B, and the cable drag, F_N, are considered. D_B and F_N account for most of σ. A small increase in L may be obtained by a slight increase in α or S and can compensate for fairly large deficiencies in L/D.

Equilibrium Position $\qquad F_z = \frac{h}{L_{Cy}} (L)$

The large values of L require that F_z be large. A small roll angle and a small increase in the resultant lift will satisfy this requirement and maintain the desired lift in the horizontal direction.

Launching Control

Proper launching behavior dictates that the velocity-independent moments alone cause the paravane to be self-righting in the water when not under tow. The vane profile and general configuration should permit initiation and continuation of launching from a wide range of angle of attack of the lift vanes. The configuration should avoid interference effects and the depth-control equipment should not cause an excessively rapid descent. The requirement that the weight and buoyancy right the paravane dictates that the center of gravity of the paravane should lie below its center of buoyancy. The righting moment should be large enough to right the paravane quickly.

Depth Controllability $\qquad$ Manipulated Element

Published data indicates designs of the manipulated element which may permit it to influence depth effectively without requiring excessive hinge moments for its actuation. Elements generating the depth-corrective action directly provide the quickest action. Other types of elements may obtain this action by reorienting the paravane and then larger corrective forces are possible. Effectiveness of control surfaces in rolling the paravane requires that the righting moment of weight and buoyancy be limited in magnitude.

Depth and Orientation Controllability — Natural Depth

The natural equilibrium depth, h, below the tow point should equal the desired depth as nearly as possible. The rate of change of h with the roll angle, ϵ, is very large and requires that ϵ be held constant. This factor implies that F_z should be produced by means of roll. For the natural depth to be independent of speed, the roll and yaw must be independent of towing speed, thus requiring independent equilibration about the roll and yaw axes of the moments of the velocity-independent and hydrodynamic forces on the paravane. This condition cannot be realized completely. These considerations dictate that the prototype paravane permit adjustments of the bridling, the location of the center of gravity, and the setting of trim surfaces.

Structure — Maximum aspect ratio permitted by the lift, size, and strength requirements.

The specific weight, thickness ratio, and internal construction of the vanes are the variables which are primarily available for the structural design.

It is convenient to begin the consideration of the general configuration of the paravane with some remarks on stability which so far has not been considered. If the paravane orientation is constant, the paravane-cable system has a single position of stable equilibrium. The uniqueness of the position follows from the fact that the equations of equilibrium were seen to be satisfied by only one value of σ and F_z when σ is restricted to the range of zero to 90 degrees. The equilibrium in this position is a stable one because any displacement of the system from equilibrium causes the sum of the moments about each axis of the system (X, Y, and Z axes of Fig. 3-1) to deviate from zero in such a way as to oppose the displacement. The plausibility of this statement can be seen physically in Fig. 3-1 where, if L_C is constant and the other space coordinates are θ and σ, any change of either of these angles is seen to increase the moment arms of external forces opposed to the direction of the change. The proof of these statements is readily obtained by replacing L_{Cy} in the moment equations (3.18) and (3.26) by $(L_C \cos\theta \cos\sigma)$ and differentiating the summation of moments on the left-hand side of the equations with respect to σ and θ, considering L_C to be a constant. Also the various force components are taken as constants because they are largely independent of σ and θ due to the assumed constant orientation of the paravane.

Although it appears possible to obtain a design capable of maintaining the constant equilibrium orientation assumed above, the angular position of the paravane will always be subject to disturbances displacing it from its equilibrium state at least temporarily. Therefore, the existence of a unique position of stable equilibrium of the paravane-cable system also requires that the paravane itself have an equilibrium orientation, with respect to the paravane axes (pitch, roll, and yaw), which is unique and stable. Under these conditions the system possesses static stability.

The equations determining the dynamic stability of the system cannot be profitably examined here. In general, they are also written by summing moments about the axes of the system and of the paravane. However, now the system is assumed to have a general displacement from static equilibrium and also a general angular velocity and acceleration having components with respect to all axes of the system and of the paravane. Consequently, velocity and acceleration-dependent forces must also be considered. Furthermore, highly nonlinear differential equations result which cannot be conveniently solved as were the simple algebraic equations of static equilibrium. General considerations indicate that the degree of dynamic stability will decrease as the aspect ratio is increased, thus limiting the latter. However, in order to proceed with the design, a better approach consists of drawing conclusions from experience with the stability of aircraft. It is desired to consider the implications of this experience as to a stable configuration of a high lift-drag ratio paravane. The result will then be appraised as to its compatability with the design factors determined from the theoretical analysis.

The evolution of aircraft design has led from multiplane designs to the simpler monoplane and, although not always realized in particular models, adequate dynamic stability has generally been possible throughout this process. The relative simplicity and known stability of the monoplane suggests it as a starting point in developing a paravane design.

The monoplane configuration derives much of its stability from the tail surfaces. The size limitation and need for low drag in the paravane make the fuselage of a monoplane undesirable. One way to eliminate the fuselage without losing the benefit of the tail surfaces, is to increase the tail-surface area as the latter is moved closer to the wing. To remove the enlarged tail surface from the downwash wake of the wing, it should be displaced from the plane of the latter. If the translated surface is now made identical to the wing, this process leads to a simple biplane design in which stability of the angle of attack of the lift vanes can be insured by a proper angle of stagger. Mutual interference can be avoided by providing an adequate gap between the lift vanes. Then if the two lift vanes are connected by two end vanes, rather than cantilevered from a fuselage, the desired end-plate effect is achieved.

The general design suggested above appears in Fig. 4-9 and not only provides the desired multivane design and end vanes, but is also seen to be compatible with a number of the other design factors noted earlier. The end vanes serve to complete a configuration which is favorable structurally. They also provide an opportunity for installing trim surfaces and control surfaces without the degree of interference with the flow about the lift vanes which such components may cause if mounted on the lift vanes. The end vanes would lie essentially in horizontal planes with one above the other, and the lift vanes would be approximately vertical, one outboard from the other. Consequently, ample opportunity exists for adjusting the location of the center of gravity, both horizontally and vertically, by means of loading compartments in the vanes. The biplane design permits attaching bridling lines at widely spaced points on the paravane and appears to offer no particular obstacle to achieving an adjustable bridling.

CHAPTER 4

HYDRODYNAMIC DESIGN. EXPERIMENTAL WORK

4.1 INTRODUCTION

The experimental work on the hydrodynamic design of the high lift-drag ratio paravane was conducted first in a flow channel and later in the naval towing tank at the University of Michigan. The models tested represented a variety of monoplane and multiplane configurations, including the biplane design suggested by theoretical factors. Numerous versions of the biplane were investigated in order to determine the importance of various design details.

In general, the models were of three sizes based on the chord length of the lift vanes. Small models usually having a chord of about 2.75 in. were tested in the flow channel. Intermediate models of about 5.5-in. chord and large models of 15-in. chord were studied in the towing tank. A 15-in. chord is about one-third that of the full-scale prototype ultimately designed.

In the channel, the flow velocity was about 1 ft/sec when testing models for performance, and 2 to 3 in./sec when photographing their flow patterns. The towing tank permitted speeds as high as 15 ft/sec. With the larger models used in the tank, velocities in the range of 2.5 to 7.5 ft/sec provided sufficiently high Reynolds numbers. The specified full-scale velocity range of 6 to 16 knots corresponds to speeds between 10 and 27 ft/sec.

Except for a few tests with an added drag on the tow cable, all experimental work related to hydrodynamic design was conducted with a negligible drag due to sources other than the paravane. In each case the tow cable had a relatively short length and small diameter. Under these conditions, the cable sweepback angle was a fairly good indication of the lift-drag ratio of the model, the relation between these quantities being

$$\tan \sigma = D/L,$$

as can be seen in Fig. 3-1.

Some corresponding values are as follows:

L/D	γ	L/D	σ
11	5.1°	7	8.1°
10	5.7°	6	9.5°
9	6.3°	5	11.3°
8	7.1°	4	14.0°

4.2 EXPERIMENTAL WORK IN THE FLOW CHANNEL

The flow channel used in testing small models was a conventional type having a free water surface and devices to avoid entry disturbances. In order to obtain a test region of uniform velocity distribution, the depth of the test section was reduced by means of a submerged false bottom having a ramp-like approach. The channel was used to check the performance of small models on a tow line and to secure photographs of the flow about such models when held in a predetermined position. The models were constructed of Plexiglas or Lucite.

Model tests in the flow channel were necessarily conducted at low Reynolds numbers because the channel limited the models to a small size and the velocity of flow was low. Consequently, when interpreting the test results it was necessary to allow for the effects of low Reynolds number, such as an increase in drag and a resulting decrease in the lift-drag ratio. For this reason, more emphasis was placed on stability and other performance characteristics than on the value of the lift-drag ratio, although attention was paid to measures for improving the latter. The small models had the advantage of ease of construction and manipulation and, in combination with the flow channel, proved to be very useful. Many configurations were tested since there was no assurance that the biplane design suggested by theoretical considerations would meet all the design requirements.

Figure 4-1 shows the initial Plexiglas model which was constructed to test the proposed biplane design. This model had two highly polished lift vanes, each of which had a chord of 2.75 in. and an aspect ratio of one. The gap was equal to the chord length. The end vanes were profiled flat plates with the high-pressure sides facing each other. The stagger angle was 45° and the lift vanes could be rotated to vary the angle of attack. The two lift vanes were identical, unsymmetrical profiles with flat pressure sides. Figure 4-1a shows the model in perspective, while Fig. 4-1b is a top view with the upper end vane removed.

The lift vanes were adjusted so that the smallest value of the cable sweepback angle was obtained. The angle of declination of the tow

cable (θ of Fig. 3-1) was about 20°. The test results may be summarized as follows:

(a) The cable sweepback angle was about 17°, which is relatively large. This result can be attributed to the high drag at a low Reynolds number. As noted in Appendix B, the coefficient of profile drag increases a great deal when the Reynolds number is below 300,000 and for the flow-channel tests the Reynolds number was always below 100,000.

(b) The bridling system was evolved from an initial system equivalent to four separate tow lines to the single-point bridling system shown in Fig. 4-1a.

(c) During the initial test with the model, it was found that the outboard lift vane (or outboard tip of the upper end vane) had a tendency to rise. Consequently, several holes were drilled in the vanes to lighten the upper end and mercury was added to the outboard vane. This step had a two-fold effect. First, it made the outboard vane heavier and counteracted tip-rise effect when towing. Second, it lowered the center of gravity.

(d) The stability of the model was quite good. This result led to the construction of other models of similar design.

Two biplane models of larger aspect ratio were constructed and tested. In these models, Figs. 4-2 and 4-3, the outboard lift vane is assembled from two single vanes which form an angle of 192° on the high-pressure side, i.e., each vane had a dihedral angle of 6°. The gap at the plane of symmetry was about 1.5 times the chord. The span of these models was 5-3/16 in. The chord lengths of the inboard and outboard lift vanes were respectively 1-1/2 and 1-3/4 in. for Fig. 4-2, and 1-1/8 and 1-1/2 in. for Fig. 4-3. In addition, a stabilizing vane was added to the suction side of the inboard lift vane of Fig. 4-3. In the first model, the angles of attack of both lift vanes were adjustable, while in the second model only the inboard vane was adjustable.

With these models the cable sweepback angle was considerably improved but the stability was very poor. Also, it seemed inadvisable to attempt further improvements at that time since the test region of the flow channel was too shallow for such relatively large models.

The next three models were modifications of Fig. 4-1 and were constructed to determine whether recovery, stability, and structural rigidity could be improved and a depth-control housing added without substantially increasing the drag.

In the model of Fig. 4-4, a ship-shaped body representing a depth-

control housing was attached to the under side of the lower end vane at a point beneath the inboard lift vane. This addition did not increase the largest dimension of the model. The position and angle of incidence of the body could be varied. The presence of this body improved the recovery characteristics of the model when a large disturbance brought about a negative angle of attack of the lift vanes. The equilibrium value of the cable sweepback angle was not affected noticeably, but this may be attributable to the fact that this angle was already large.

Figure 4-5 shows the top view of a biplane model similar to Fig. 4-1 and to which a symmetrically profiled vane was added to serve as a vertical stabilizer. The stabilizer was located behind the outboard lift vane by a distance such that the cubical space limitation was not exceeded.

Although not shown, the ship-shaped body and the vertical stabilizer also were used together. This combination, in conjunction with the bridling system of Fig. 4-1, enabled the model to recover its equilibrium sweepback angle after a disturbance displaced the angle of attack of the lift vanes to about minus 30°. On the other hand, the model of Fig. 4-1 failed to return to its equilibrium cable sweepback angle after a disturbance of the same type. Instead, it gradually fell back to an angle of 90°.

Figure 4-6 shows a vertical fin placed in the model of Fig. 4-1 and located halfway between the lift vanes with its trailing edge in line with the trailing edges of the end vanes. The location of the vertical fin was changed during the tests by moving it from side to side and from back to front. From the standpoint of ability to recover from a disturbance causing a negative angle of attack, the best location was as shown in Fig. 4-6. The cable sweepback angle was not noticeably affected at any of the several positions tried. This may be true only when the sweepback angle is large as it was in this case. The modification was studied to observe the hydrodynamic effect of such a vane in case it should be desirable to increase the rigidity of the end vanes due to the addition of control surfaces or a housing for the control mechanism.

A number of other designs were tested. A model consisting solely of a lift vane was gradually elaborated on until a fairly complete monoplane resulted. The various alternate additions to the simple vane were a single horizontal end vane, a beam-like fuselage with a second lift surface arranged in tandem with the original vane, and a beam-like fuselage with tail assembly. In the last case the tail surfaces were mounted both in the plane of the lift vane and above that plane. The last two models provided a fairly high lift-drag ratio but had poor stability. The other arrangements were even more unstable.

Tests were made of box-kite-like designs in various orientations

with respect to the flow and with both flat plates and profiled surfaces as lift and end vanes. Several extensions and refinements of the design were tried. None of these models approached the original biplane design in performance.

The biplane design of Fig. 4-1 provided the best overall performance of the models tested in the flow channel. Other designs, which were not practical in the flow channel, or grew out of later tests, were investigated in the towing tank, as will be seen.

4.3 EXPERIMENTAL WORK IN THE TOWING TANK

This section contains some of the results from tests of the biplane models in the towing tank. The tank itself, additional tests of the biplane design, and the study of other configurations are described in Appendix C.

The towing tank permitted more extensive and quantitative tests of the biplane design of Fig. 4-1. The models were constructed of wood. The location of the center of gravity and the weight were controlled by means of lead sheet inlaid in one or more of the vanes. In the photographs the location of the inlays is indicated by rectangular areas having a different grain structure than the adjacent wood.

The various model sizes are illustrated in Fig. 4-7, the smallest being a Plexiglas model used only in the flow channel and having lift vanes of 2.75-in. chord. The other models have 5.5-in. and 15-in. chords and are representative of sizes tested in the towing tank.

The largest model of Fig. 4-7 is equipped with a later version of the bridling system, namely, the four-line system converging at the bridling point which is at the outboard end of the tow cable. It was previously mentioned that the bridle which evolved during the flow-channel tests consisted of a single vertical line. This system was also used in the initial towing-tank experiments. Figure 4-8 shows a rigid but adjustable bridle of this type mounted on a 5.5-in. chord biplane model. The rigid bridle had the advantage that the location of the bridling point was determined exactly and could be readily changed. Some of the experimental results with this system will be discussed later.

In the initial towing tests the outboard equilibrium position of the paravane usually was as shown in Fig. 4-9. It is observed that the tip-rise effect was present since the outboard tip of the model was tilted upward, a condition which is not desirable since a roll in the opposite direction is necessary to maintain the desired depth. Fairing of the end vanes, as in Fig. 4-8, reduced the drag of the end vanes but the tip-rise effect was essen-

tially unaltered. Tests were conducted with models in which the stagger of the lift vanes was reduced to zero. The tip rise diminished. However, the stability in pitch was considerably less and other complications arose, such as the fact that two equilibrium values of the cable sweepback angle were possible because the design no longer provided a unique equilibrium orientation of the towed paravane. Reducing the chord of the end vanes by 50 percent, and making them from a thin strip, eliminated the second equilibrium position. However, it also reduced the damping of vertical oscillations when towing in quiet water. It was concluded that some reduction of the stagger and the end-vane chord were possible with a net gain. The model having zero stagger exhibited satisfactory performance as long as the chords of the end vanes were not too large. An intermediate stagger angle may be a better compromise. However, other means were developed for avoiding tip rise and which could also be used to maintain the desired roll and depth. Consequently, the 45° stagger and the end vanes of full chord were retained in later models.

The other means for controlling tip rise will now be considered. Four different ways of adjusting the hydrodynamic moments affecting roll are shown in Figs. 4-10 and 4-15. Figure 4-10a shows a wedge inserted between the lift and end vane. This warped the end vane in such a manner as to produce the desired hydrodynamic effect. Figure 4-10b shows a method of achieving the additional roll by means of a small auxiliary vane placed at the outboard end of the lower end vane. Figure 4-10c shows a model in which the trailing edges of the end vanes were equipped with a row of trim tabs which could be adjusted individually. In this manner the end vanes were made to produce a distribution of lift giving the desired roll. Figure 4-15 shows a 15-in. model in which the upper end vane was equipped with two adjustable vanes which may be used as trim surfaces.

The foregoing remarks provide a background for the following chronological description of towing tests of the biplane design. The transition from Plexiglas models in the flow channel to wood models in the towing tank immediately brought up the matter of weighting because of the greater reserve buoyancy of the wood. For stability around a horizontal axis, it is desirable to have the center of gravity below the center of buoyancy when the desired orientation exists. The flow channel tests had indicated the tip-rise effect and this suggested distributing the added mass so as to shift the center of gravity towards the outboard lift vane. The initial tank models were of the 5.5-in. size and in these the center of gravity was lowered by adding or inlaying sheet lead in the lift vanes and in the lower end vane. Models of negative, slightly negative, and approximately zero reserve buoyancy were obtained by adding varying amounts of weight. In all models the horizontal position of the center of gravity was made such that planes of the end vanes remained horizontal when the model was sinking freely.

At first some tests were conducted with the bridling system of the type evolved during the flow-channel tests. This system is shown in Fig. 4-10b and consisted of a single vertical line with adjustable horizontal position. However, the flexibility of the bridling line was undesirable at that phase of the test program and so the rigid system of Fig. 4-8 was developed. The model of Fig. 4-8 had lift vanes with an aspect ratio of one and a stagger of 45°. It also had a slightly negative resultant of weight and buoyancy with the center of buoyancy uppermost when the end vanes were horizontal. The tow cable was attached to a streamlined brass piece which could be clamped to the vertical rod at any height. The vertical rod was pivoted between the lower and upper end vanes so that it could rotate freely. The brass plates, in which the ends of the rod were pivoted, were slotted such that it was possible to adjust the horizontal position of the rod from front to back and from side to side. With this arrangement, the position of the bridling point could be determined and readily varied between tests. The resulting behavior of the paravane is described below.

The model of Fig. 4-8 was tested at various speeds in the range of 150 to 450 ft/min, the speed remaining constant in each test. At first the tip rise decreased the depth sufficiently so that the model broke the water surface at speeds considerably less than 450 ft/min. The wedge of Fig. 4-10a was added at this point in order to carry out the tests.

During tests at a speed of 150 ft/min it was noted that oscillations of the cable sweepback angle and the roll angle appeared when the bridling point was moved too far back from the leading edges of the end vanes. Photographs of the model disclosed that the oscillation was the result of a coupling between the sweepback angle and the angle of attack of the lift vanes, the latter angle reaching a value above the stalling point as the sweepback approach a minimum. The vertical position of the bridling point between the end vanes determined whether the paravane was stable, whether it rolled clockwise or counterclockwise, or whether it described a spiral with a large diameter and slow rotational motion. Moving the bridling point from side to side, that is, parallel to the leading edge of the end vanes, changed the moment of the hydrodynamic forces on the lift vanes, thereby causing a change in the angle of attack of these vanes until equilibrium was reached in a new orientation. The tests again brought out the tip-rise effect which now took on added significance since it indicated incipient instability.

The single-point bridling system imposed a severe restriction upon the pitch stability, i.e., recovery from disturbances which displace the angle of attack of the lift vanes, since it was relatively easy for disturbances to rotate the paravane about the vertical bar of the bridling system. In such a case, the recovery could only be obtained from the relative moments of the hydrodynamic forces upon the lift vanes and this factor caused the profile shape to be important in determining the equilibrium position. Thus,

the four different profiles shown in Fig. 4-11 were tried and some effects were observable. (Some of the various profiles in Fig. 4-12 were used later in the 15-in. biplane models.) However, as soon as the bridling system was changed to the four-point type shown in Figs. 4-7 and 4-9, the influence of the profile shape on recovery disappeared. The paravane could now be bridled so that a wider selection of orientations could be maintained while towing. Moreover, recovery from pitch disturbances was more positive.

Consideration was given to ways to overcome the tip rise and control the roll of the paravane. The 15-in. models were weighted so as to shift the center of gravity toward the outboard tip, but this measure can eliminate tip rise at only one speed and some hydrodynamic means is also required. The wedge of Fig. 4-10a could control the roll over a speed range of 3 to 1, but the sensitivity of the adjustment was too fine for this method to be useful. The auxiliary vane of Fig. 4-10 could be positioned as desired about a hinge axis passing through its hydrodynamic center and through the hydrodynamic center of the end vane. The effectiveness of this method was too small to be of practical value. Trim tabs were added to a 15-in. model in a manner similar to that of the 5.5-in. model of Fig. 4-10c. With only a small deflection of these tabs it was possible to obtain a relatively level orientation of the 15-in. model. This model operated satisfactorily within a speed range of 150 to 350 fpm. The fourth method of controlling roll by means of the adjustable vanes is shown in Fig. 4-15. Used as trim surfaces, these vanes could be set at the same angle of attack to compensate for any tendency of the paravane to rise. If oriented differentially, these surfaces could produce a roll moment.

In order to improve the lift-drag ratio obtained in model tests, two major steps were taken. One consisted of increasing the aspect ratio, which will increase the ratio of lift to induced drag. The other step was to increase the model size from 5.5 to 15 in. In the 5.5-in. models, the Reynolds number was so small that a large portion of the drag was due to this condition.

The improvement possible under the first step was limited by the fact that continued increase in aspect ratio eventually resulted in instability about a horizontal axis. Thus, for the models having an aspect ratio of two, it was found advantageous to lower the center of gravity of the lift vanes, as illustrated by the left-hand model of Fig. 4-13. In this manner, the resistance to roll was found to increase. It is observed that the lower center of gravity may therefore make it more difficult to vary the roll of the paravane if depth disturbances are to be countered in this manner. Fig. 4-14 shows a 15-in. biplane having an aspect ratio of two and a very low position of the center of gravity.

The following table presents the lift-drag ratios obtained with smooth models of the biplane design at a towing speed of 150 fpm.

Model Size	Aspect Ratio	Cable Sweepback Angle and (L/D)	Reynolds Number
5.5 in.	1	14° (4)	110,000
	2	10° (5.7)	110,000
15 in.	1	8° (7)	300,000
	2	5.7° (10)	300,000

For these small values of the cable sweepback angle, σ,

$$\sigma \cong \tan \sigma = D/L.$$

Thus, these results show that the percentage reduction of drag achieved by increasing the aspect ratio was the same (29%) for both model sizes. However, a much larger gain was obtained by increasing the Reynolds number from about 110,000 to 300,000. This step resulted in a 43% reduction of drag for both aspect ratios. These results verified the earlier decision to place emphasis on characteristics other than the lift-drag ratio when appraising performance of small models.

In addition to their potential usefulness as trim surfaces, the adjustable vanes of Fig. 4-15 may also be used as depth-control surfaces and, as such, are a possible form of manipulated element to be actuated by a depth-control mechanism. The adjustable vanes of Fig. 4-15 are equipped with small end plates to reduce their induced drag and to decrease the mutual interference between the flow over the control surfaces and that over the end vane at other points along its span. It might be advantageous to extend the effect of these end plates forward to the leading edge of the end vane by means of additional stationary plates. In this way, mutual interference might be further reduced by separating the stabilizer area of each control surface from the remainder of the end vane.

In deflecting the surfaces of Fig. 4-15 differentially, their effectiveness in producing roll depended, in part, upon the position of the center of gravity. For example, a model of aspect ratio one and similar to the largest of Fig. 4-7 was equipped with such control surfaces. By deflecting these surfaces the model could be rolled a considerable amount, and the depth was substantially affected. On the other hand, the depth of the aspect-ratio-two model of Fig. 4-14 was hardly affected by control surfaces of the same design. The latter model provided a greater roll-restoring moment due to the forces of weight and buoyancy, because the center of gravity was farther below the center of buoyancy and because the weight and displacement were greater. Deflection of the control surfaces also had the effect of increasing the drag of the upper end vane, causing the model to pitch backward and

bringing about an upward lift force on the end plates. This condition reduced the effectiveness of the surfaces when deflected in the direction to increase depth.

The experimental work in the towing tank was terminated at this stage. Thus far, it tended to verify the favorable results obtained with the biplane paravane in the flow channel, and it permitted some development of the design. The results gave promise that the biplane would be successful in a large-scale model, provided the desired equilibrium depth could be maintained. It remains to be determined whether this requirement can be met under full-scale conditions by means of adjustable bridling and trim surfaces to control roll and yaw, as was possible in model tests, and whether such a method will also be effective in maintaining the average roll and yaw at the desired values when realistic disturbances are present. These contingencies may require additional tests of trim surfaces. Experience with a large-scale model could also indicate a need for further investigation of control surfaces and a reappraisal of the method by which these elements produce the corrective influence to counter depth disturbances.

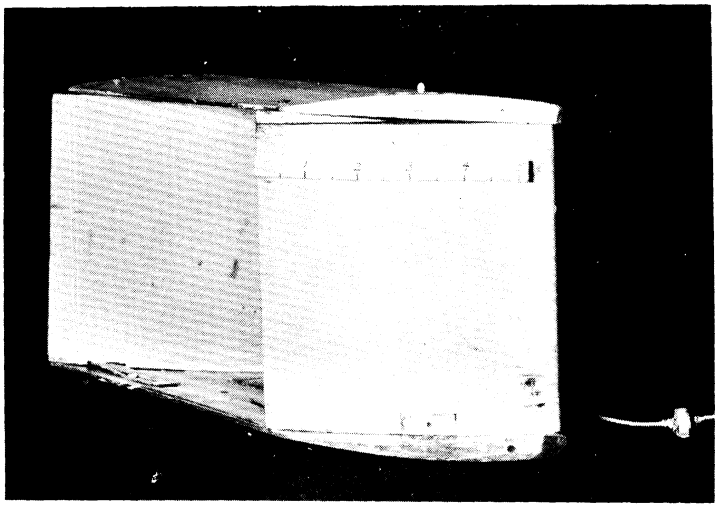

Fig. 4-10a.

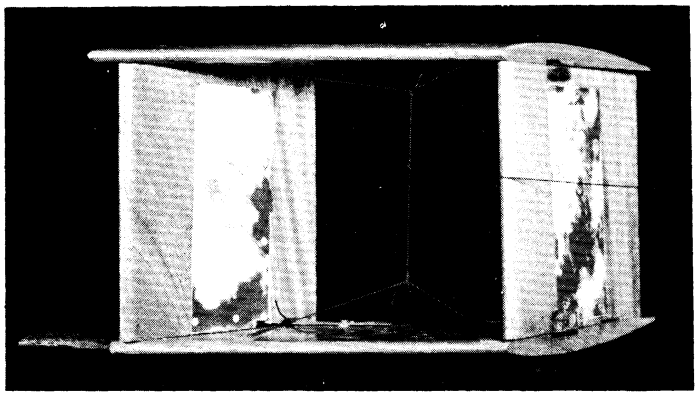

Fig. 4-10b.

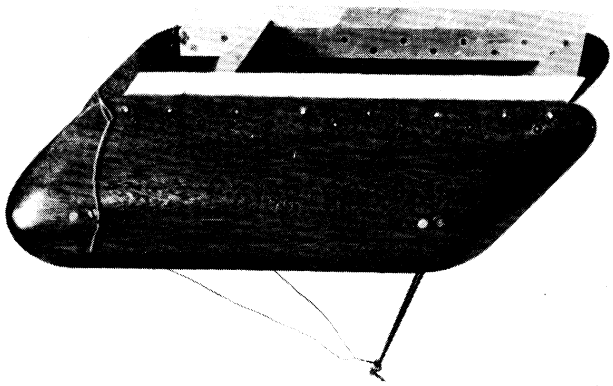

Fig. 4-10c.

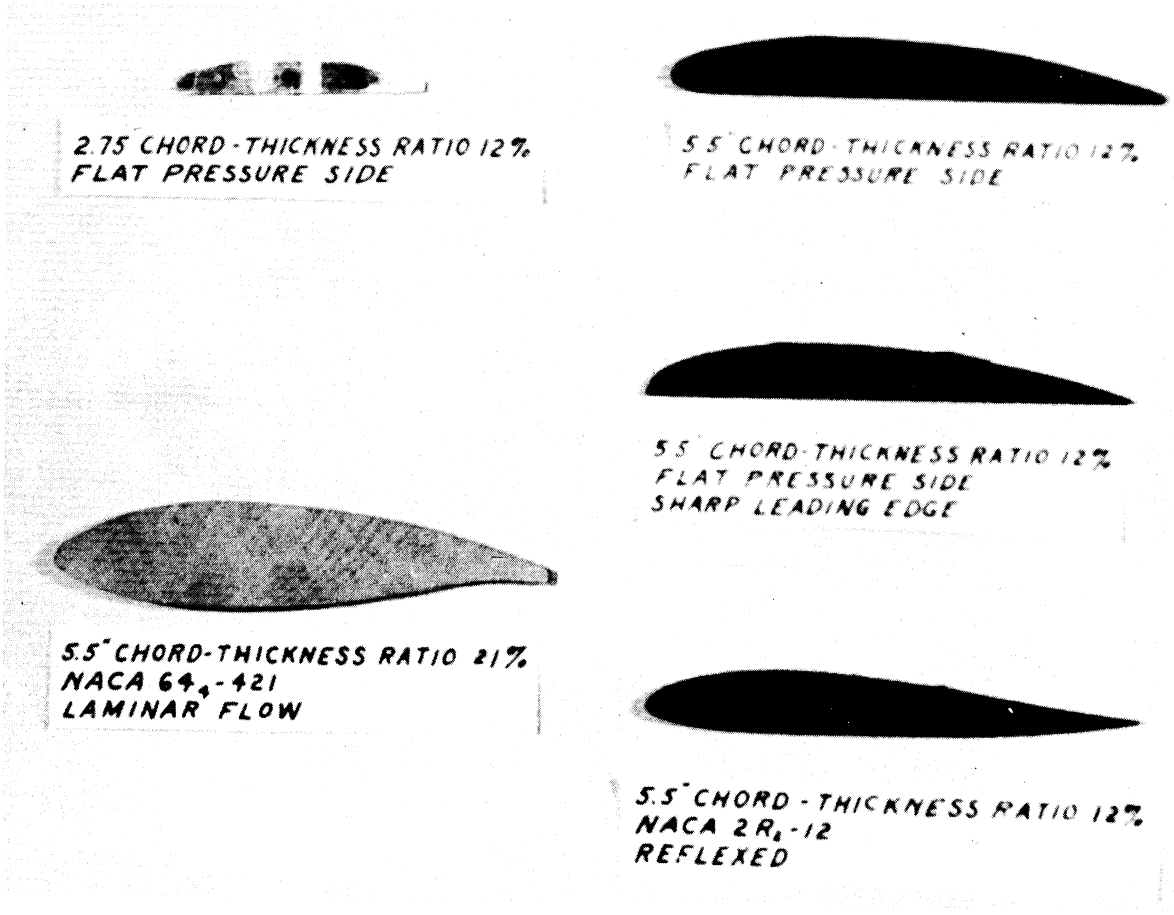

Fig. 4-11.

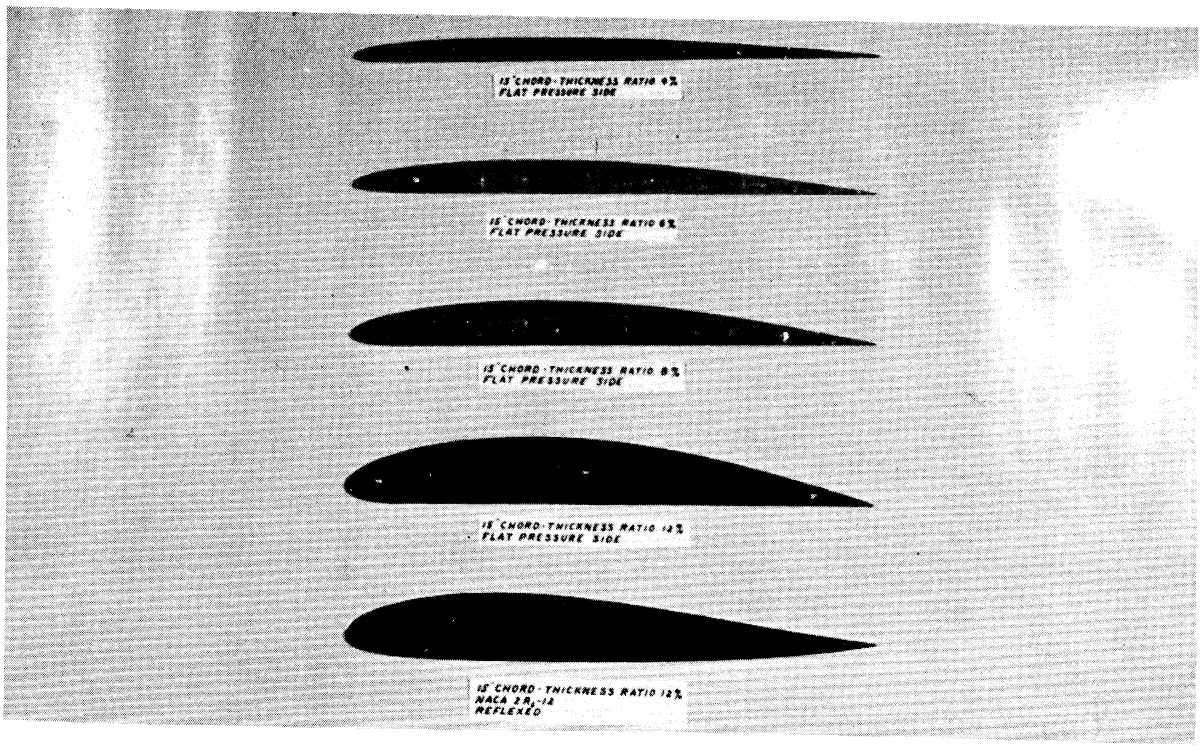

Fig. 4-12.

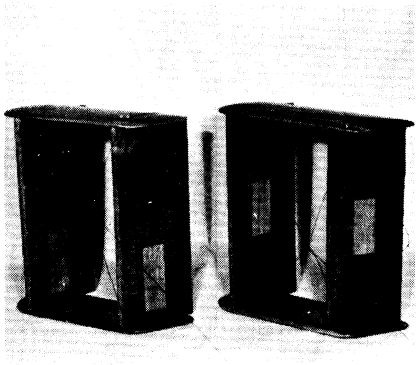

Fig. 4-13.

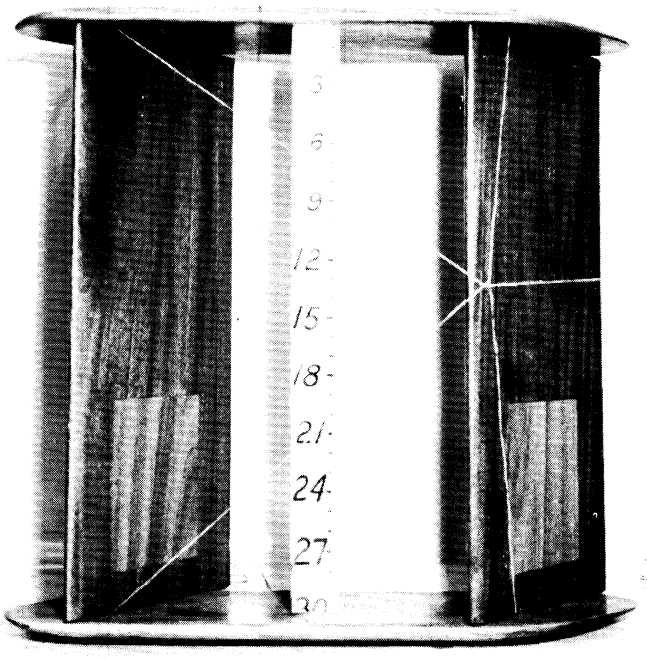

Fig. 4-14.

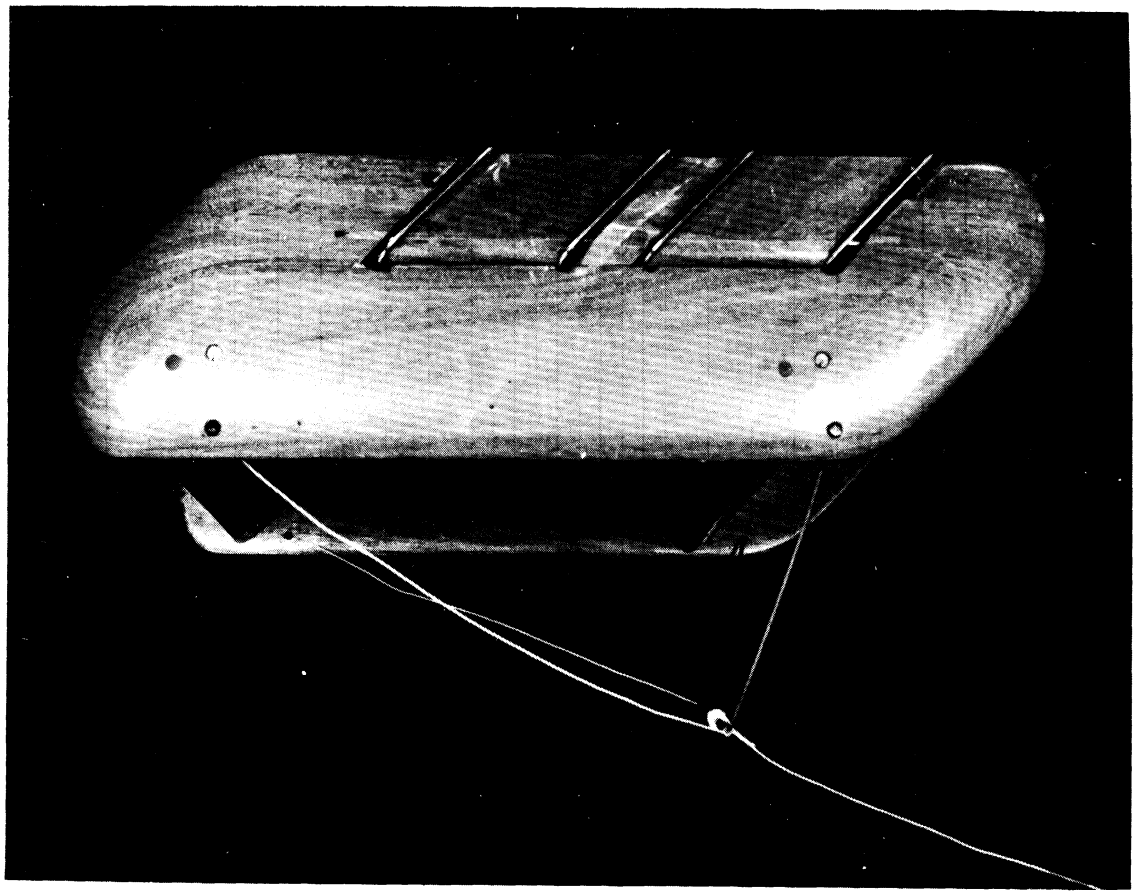

Fig. 4-15.

CHAPTER 5

DEPTH-CONTROL MECHANISMS

5.1 INTRODUCTION

This chapter is concerned with mechanisms to actuate the manipulated element, that is, the depth-influencing component of the hydrodynamic design which is intended to counter depth disturbances. The natural equilibrium depth of the paravane is assumed to be approximately equal to the desired depth. When the error in depth is excessive for any reason, the control action of the mechanism is required to actuate the manipulated element so as to insure that the paravane approaches the desired depth in an efficient manner. Thereafter, the control action must be such as to maintain the desired depth within allowable limits by countering unidirectional and oscillatory disturbances tending to create error. The depth was to be controlled within plus or minus 5 ft of the desired depth and the mechanism was to contain an adjustment so that the desired depth could be set at any point in the range of 30 to 50 ft below the surface of the water. Certain restrictions were placed on the type and design of mechanism which could be used. These items are described in section 2.3.

5.2 RESPONSE OF THE PARAVANE-CABLE SYSTEM TO DISTURBANCES

The variation of the depth of the paravane due to disturbances presents a dynamic problem. Depth variations of the oscillatory type will occur at low frequencies because the frequencies of significant disturbances prove to be small, as will be seen. Consequently, the damping and inertial forces which act laterally on the tow cable are small and it will be assumed that the cable remains straight during variation in depth.

The paravane orientation is assumed to remain constant. Under this condition, the cable sweepback angle, σ, is given by Equation (3.21) in which only the third term will vary with depth. Since the cable length, L_C, is now constant, this variation is due to the change of the outboard distance, L_{Cy}, with depth and will be small for normal vertical oscillations in the presence of depth control. It was specified that the force, D_B, exerted by the drag

body would, at all times, remain in the direction and sense shown in Fig. 3-1. As a consequence of these conditions, the system will be assumed to have but one degree of freedom which can be taken as the instantaneous depth, z, of the paravane below the tow point, or as the instantaneous value of the cable declination angle, θ. Changes in depth are then equivalent to a rotation of the paravane-cable system as a rigid body about the Q-axis of Fig. 3-1. It will be assumed also that the tow point is moving in a straight line and that the towing speed, while it may have any value in the range of 6 to 16 knots, remains constant during the depth variation being analyzed.

The desired depth below the tow point is denoted by z_d so that at any moment the error in depth is

$$e = z - z_d \quad . \tag{5.1}$$

The differential equation describing the motion of the system is obtained by summing moments about the Q-axis of Fig. 3-1 due to all the external forces on the paravane and cable. The tests of a paravane-cable system for response to a step disturbance in depth, described in Appendix D, showed the system to be quite linear. Therefore, the moments will be of the following types:

(a) Time-dependent moments due to depth disturbances or control surface action.

(b) Position-dependent moments which are functions of the angular position θ, or of z, the depth below the tow point.

(c) Velocity-dependent moments which are linear functions of the angular velocity, $\dot{\theta}$, or the vertical velocity, $\dot{z} = \dot{e}$.

(d) Acceleration-dependent moments which are linear functions of the angular acceleration, $\ddot{\theta}$, or the vertical acceleration, $\ddot{z} = \ddot{e}$.

(e) Constant moments which are independent of t, θ, $\dot{\theta}$, and $\ddot{\theta}$.

If a time-dependent vertical force on the paravane is denoted by f(t), its moment about the Q-axis is

$$M(t) = f(t)\,(L_C \cos \theta) \quad .$$

If f(t) is oscillating in harmonic motion, the above equation becomes

$$M(t) = F(\cos \omega t)(L_C \cos \theta) \quad , \tag{5.2}$$

where F is the amplitude and ω the circular frequency of f(t).

It was shown in section 3.5 that the vertical force required to maintain a given equilibrium depth is dependent on depth position and is

$$F_z = \frac{z}{L_{Cy}} L = \frac{z}{(L_C^2 - z^2)^{1/2}} \left(\frac{L}{\cos \sigma}\right) \tag{5.3}$$

A paravane of constant orientation will develop a vertical force which is independent of depth with the result that variations in depth will produce an imbalance of position-dependent forces. The net vertical force on the paravane will have a position-dependent moment about Q which, for small oscillations about the desired depth, may be written

$$M(z) = - \left[\frac{dF_z}{dz}\right]_{z = z_d} (z - z_d)(L_C \cos \theta_d) \quad , \tag{5.4}$$

or, by (5.1) and (5.3), this moment may be written

$$M(e) = - \frac{L_C^2}{(L_C^2 - z_d^2)^{3/2}} \left(\frac{L}{\cos \sigma}\right) (L_C \cos \theta_d)e \quad . \tag{5.5}$$

Letting

$z_d = 60$ ft $\qquad L/q = 27.6$ sq ft

$\sigma = 18.1°$

$L_C = 219$ ft $\qquad \theta_d = \sin^{-1} \frac{z_d}{L_C} \cong 16°$

yields

$$M(e) = - (29\ V^2)e \quad . \tag{5.6}$$

The vertical damping force on the tow cable will be ignored since it provides a velocity-dependent moment about the Q-axis which is extremely small relative to that of the vertical damping force on the end vanes of the paravane. In order to calculate the latter force and its moment, let α_a be the deviation of the absolute angle of attack of the pair of end vanes from that at which their resultant lift is zero, then in quiet water

$$\alpha_a = \tan^{-1}\left(-\frac{\dot{z}}{V}\right) \cong -\frac{\dot{z}}{V} = -\frac{\dot{e}}{V} \quad , \tag{5.7}$$

where α_a is measured in radians. The lift and drag coefficients of the end vanes may be represented in the form

$$C_L = k_1 \alpha_a \tag{5.8}$$

and

$$C_D = k_2 \ , \tag{5.9}$$

where k_1 and k_2 are constants determined from wind-tunnel data for the profile of the end vanes. Then utilizing (3.1), (3.2), (5.7), (5.8), and (5.9), the net vertical force on the end vanes is

$$F(\dot{e}) = - \rho(k_1 + k_2) S_{EV} V\dot{e} \ , \tag{5.10}$$

where S_{EV} is the reference area of one end vane. For end vanes of typical profile and an intermediate aspect ratio as used in biplane models, the following values are representative:

$$k_1 = \frac{\pi}{2}(AR) = 2.63 \text{ per radian}$$

$$AR = 1.67, \quad k_2 = .02, \quad \rho = 1.94 \text{ slugs/ft}^2 \ ,$$

where the expression for k_1 is valid [19] for $AR \cong 1.5$ and the value of 1.67 for AR was estimated from that of biplane models. With these values and Equation (5.10), the velocity-dependent moment is

$$M(\dot{e}) = F(\dot{e})(L_C \cos \theta_d) = - 640 S_{EV} V\dot{e} \ . \tag{5.11}$$

The acceleration-dependent moment about the Q-axis due to the paravane is the negative of the product of $\ddot{\theta}$ and the moment of inertia of the paravane with respect to Q. The moment for the cable is similarly obtained. Assuming a paravane weight of 1500 lb and a cable weight of about 400 lb,

$$M(\ddot{e}) = - 12{,}900 \ddot{e} \ . \tag{5.12}$$

In determining the total inertial moment of Equation (5.12), the virtual mass of any water accelerated is neglected. This step will result in relatively little error when the disturbing force is due to ocean waves.

The moments of the constant forces of weight and buoyancy are relatively small and will be ignored. For dynamic equilibrium in the absence of a time-dependent force, the moments of Equations (5.6), (5.11), and (5.12) must have a vanishing sum, that is,

$$-(12{,}900)\ddot{e} - (640\ S_{EV}\ V)\dot{e} - (29\ V^2)e = 0 \ , \qquad (5.13)$$

where each term represents a moment about the Q-axis. If each moment is divided by the moment arm, $L_C \cos\theta$, of an effective vertical force on the paravane, then (5.13) becomes

$$-(61)\ddot{e} - (3\ S_{EV}\ V)\dot{e} - (.14\ V^2)e = 0 \ , \qquad (5.14)$$

where V is in ft/sec and S_{EV} is in ft^2. Each term of (5.14) represents an effective force on the paravane. Dividing (5.14) by the coefficient of $\ddot{e}$ and multiplying by (-1),

$$\ddot{e} + (.049\ S_{EV}\ V)\dot{e} + (.0023\ V^2)e = 0 \ , \qquad (5.15)$$

which may be compared with the standard form of such an equation,

$$\ddot{e} + 2\xi\omega_N\dot{e} + \omega_N{}^2\, e = 0 \ , \qquad (5.16)$$

where the coefficients have the following values by comparison with (5.15):

$\omega_N = .048\ V$ (undamped natural circular frequency of the paravane-cable system)

$\xi = .51\ S_{EV}$ (ratio of the actual value of the damping constant of the paravane-cable system to its critical value).

At a speed of 6 knots, V equals 10 ft/sec and $\omega_N = .48$ radians/sec so that

$$T_N = 2\pi/\omega_N = 13 \text{ sec} \ , \qquad (5.17)$$

where T_N is the undamped natural period of oscillation of the system. At a speed of 16 knots, V equals 27 ft/sec and ω_N equals 1.3 radians/sec so that

$$T_N = 4.8 \text{ sec} \ . \qquad (5.18)$$

If S_{EV}, the area of a single end vane, is 33 ft^2, then the damping ratio is

$$\xi = 17 \ , \qquad (5.19)$$

which indicates that the damping constant [coefficient of $\dot{e}$ in (5.15)] is 17 times its critical value. The value given for S_{EV} in a full-scale paravane was estimated from the area of full-chord end vanes used in the later biplane models.

If, in quiet water, the towed paravane is displaced from its equilibrium depth by an amount e_o, it will return to equilibrium as shown in Fig. 5.1. This figure is a plot of the solution to (5.16) for such a displacement of the system which is referred to as a step disturbance. The high damping ratio of 17 is seen to indicate that the paravane will return slowly to the equilibrium depth and will not overshoot. Conversely, the large damping ratio indicates that the paravane will leave the equilibrium depth very slowly in response to a unidirectional external force such as that transmitted through the cable by roll or pitch of the ship. The large damping is seen to be due to the large lift-vane area.

When in quiet water an external time-dependent force acts on the paravane, the moment of (5.2) must be included in the summation, and the equation analagous to (5.14) is

$$-(61)\ddot{e} - (3\, S_{EV}\, V)\dot{e} - (.14\, V^2)e + f(t) = 0 \,, \qquad (5.20)$$

where each form represents an effective force on the paravane. Proceeding as before, (5.20) becomes

$$\ddot{e} + (.049\, S_{EV}\, V)\dot{e} + (.0023\, V^2)e = \left(\frac{1}{61}\right) F \cos \omega t \,. \qquad (5.21)$$

The corresponding standard form is

$$\ddot{e} + 2\xi\omega_N \dot{e} + \omega_N{}^2 e = \omega_N{}^2 E_o \cos \omega t \,, \qquad (5.22)$$

where E_o is the vertical displacement of the system from equilibrium which would be produced by a constant force equal to F, the amplitude of f(t). After any transient motions have decayed, the solution of (5.22) has the form

$$e = E \cos (\omega t + \phi) \,, \qquad (5.23)$$

where E is the amplitude of the oscillation in depth and ϕ is its phase angle with respect to a harmonically oscillating driving force, f(t). Values of E/E_o and ϕ may be determined by substituting (5.23) into (5.22). The result is plotted in Fig. 5-2 where it can be seen that, due to the high damping ratio, the paravane would oscillate at small amplitude and have a large lag behind the oscillating driving force. Since the parameters ω_N and ξ, of Fig. 5-2 play a similar role in Fig. 5-1, the response to an oscillatory disturbance may be determined from the response to a step disturbance. The latter was determined experimentally and gave values of ω_N and ξ of the same order as

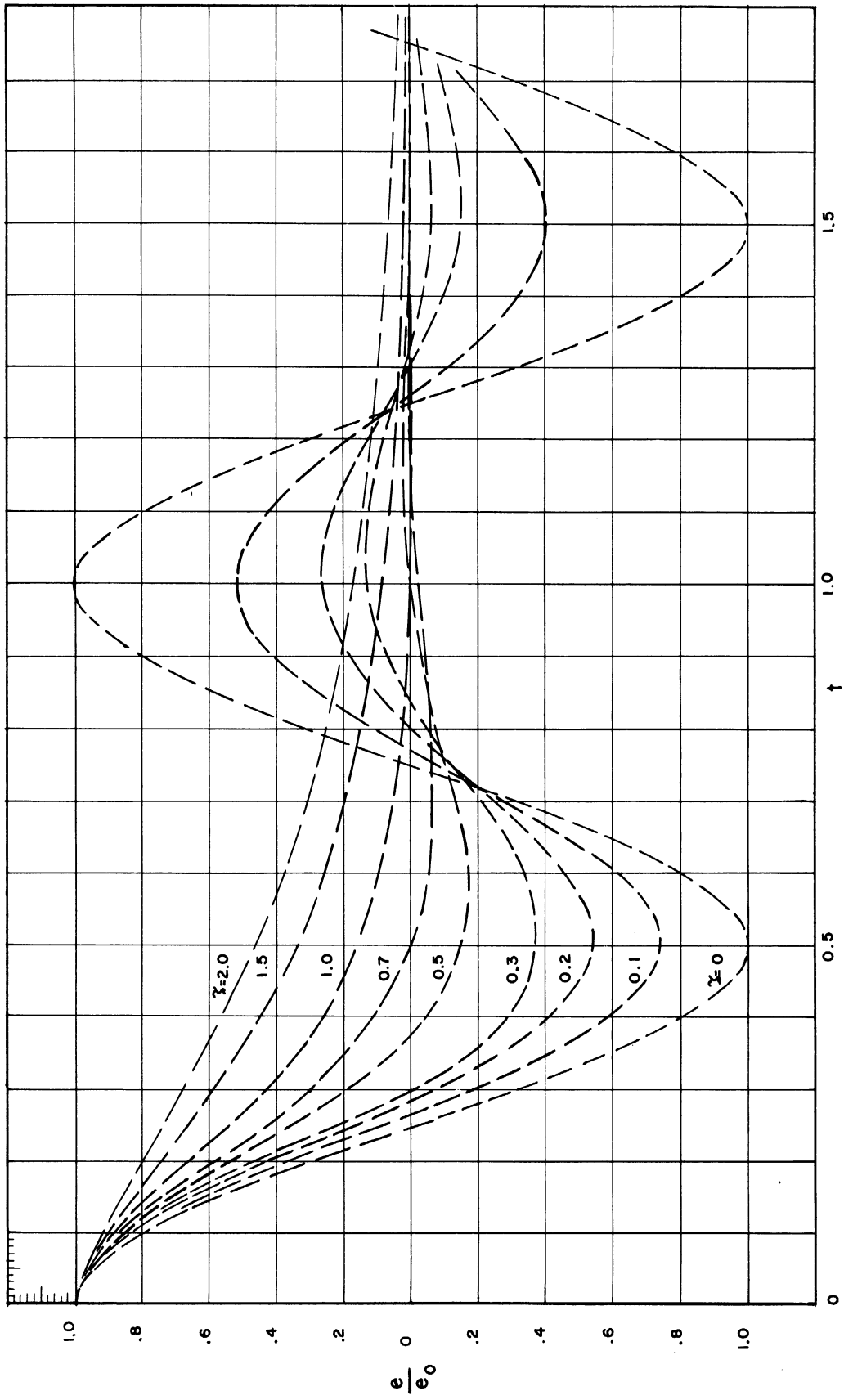

Fig. 5-1. Depth variation of paravane-cable system in response to a step disturbance.

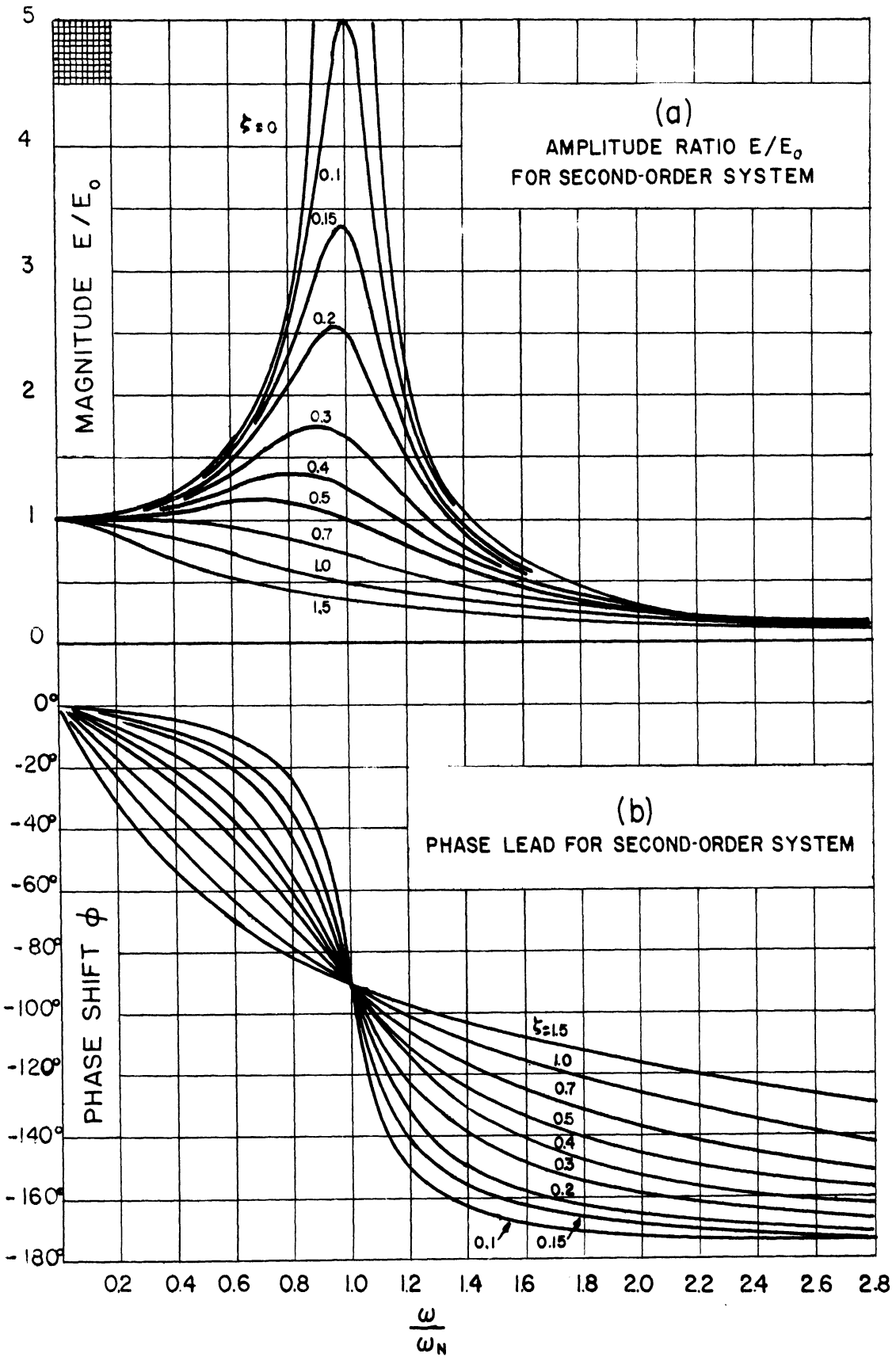

Fig. 5-2. Frequency response curves showing amplitude and phase angle of the depth oscillation of the paravane-cable system in response to an oscillating disturbance.

those obtained above by analytical means. The test set-up is described in Appendix D.

The foregoing development assumed quiet water. When waves are present, the vertical velocity $\dot{e}$ must be replaced by the quantity $(\dot{e} - v)$ where v is the instantaneous vertical velocity of the water at the depth in question. The velocity-dependent force, the second term of (5.20), is now the source of the disturbance and replaces f(t). Then (5.20) becomes, after dividing by 61,

$$\ddot{e} + (.0023\ V^2)e = (.049\ S_{EV}\ V)(v - \dot{e}) \quad . \tag{5.24}$$

Comparing (5.24) and (5.22), it is seen that the damping ratio, ξ, is now zero, that is, the paravane and cable behave as an undamped system because the velocity-dependent force has become the driving force. Referring to the curve for $\xi = 0$ in Fig. 5-2, it is seen that when ω, the circular frequency of the driving force of the waves is equal to ω_N, the depth oscillation will lag the driving force by 90° and the amplitude of depth displacement will become very large. Actually, the paravane amplitude will increase until its oscillatory velocity, $\dot{e}$, is in phase with and has the same amplitude as v, the velocity of the wave motion. The amplitude will then remain constant since the driving force on the right-hand side of (5.24) will approach zero, the difference $(v - \dot{e})$ remaining small and positive in order to drive the system against the neglected damping forces such as may result, for example, from the net effect of the vertical component of the wave motion on the tow cable.

The natural circular frequency and period of oscillation of the undamped system were found to be

$$\omega_N = .048\ V \tag{5.25}$$

$$T_N = 2\pi/\omega_N = 130/V \tag{5.26}$$

and are significant since they indicate the resonant frequency of the actual system when the disturbance is due to waves. In order to determine the likelihood of such resonance, it is necessary to determine the disturbance frequencies which can result from ocean waves having a significant amplitude at a depth of 30 ft.

5.3 WAVE DISTURBANCES

Important classes of periodic motion in the sea which may be of

interest include short and long surface waves, internal waves, and confused seas as found in deep water [20]. The principal interest in these motions will be to estimate the range of disturbance frequencies which they represent. For this purpose, consideration must be given to the wave period or frequency, the celerity of the wave, ship velocity, and ship direction relative to the wave fronts.

Surface waves are produced by the wind. Short waves are surface waves, the wave length of which is less than twice the ocean depth. They are fairly well described by classical hydrodynamic theory, according to which they are accompanied by an underwater motion which decreases exponentially with depth and which has the same period and celerity (velocity of progress) as that on the surface. An ocean region subjected to a constant wind velocity may reach a steady-state oscillation with a period corresponding to the wind speed. Fig. 5-3 shows observed values of the surface amplitude, wave height, and celerity as a function of the period for surface waves in a typical ocean region. The wave heights at all depths and the particle velocity at a depth of 30 ft were computed. Both the celerity and wave length are independent of depth. The wave height and particle velocity decrease exponentially with depth to a value of about one twenty-third that at the surface, for a depth of one-half wave length. Since wave lengths are large, appreciable motions can exist at paravane operating depths. The wave height is measured from trough to crest and is twice the amplitude.

Long waves are surface waves where the wave length is more than twice the ocean depth. The amplitude and particle velocity of long waves decrease linearly with depth. Since the maximum period of surface waves has been observed to be about 12 seconds, Fig. 5-3 indicates that long waves are unlikely at depths over 350 feet.

Confused seas can be the result of the interference of steady-state waves of the above types, waves undergoing forced growth, and waves in forced or free decay. Interference is of interest here primarily for the change it may cause in the range of important disturbance frequencies from that indicated by Fig. 5-3. Interferences where only one component wave has appreciable amplitude will be ignored. In general, wave interference produces an oscillatory surface motion of varying period which at a given time may range above and below the periods of the constituent waves. As a result there may exist, at small periods, waves of much greater amplitudes than those shown in Fig. 5-3 for steady-state surface waves of such periods. Similarly, there may be encountered waves of large period, corresponding to beat frequencies, which have sufficient amplitude to require attention but do not have the excessive heights shown in Fig. 5-3 for surface waves of such periods.

Internal waves are a phenomenon accompanying the variation of water density with depth. They exist primarily below the surface where their vertical amplitudes are much larger than at the surface. Their wave lengths

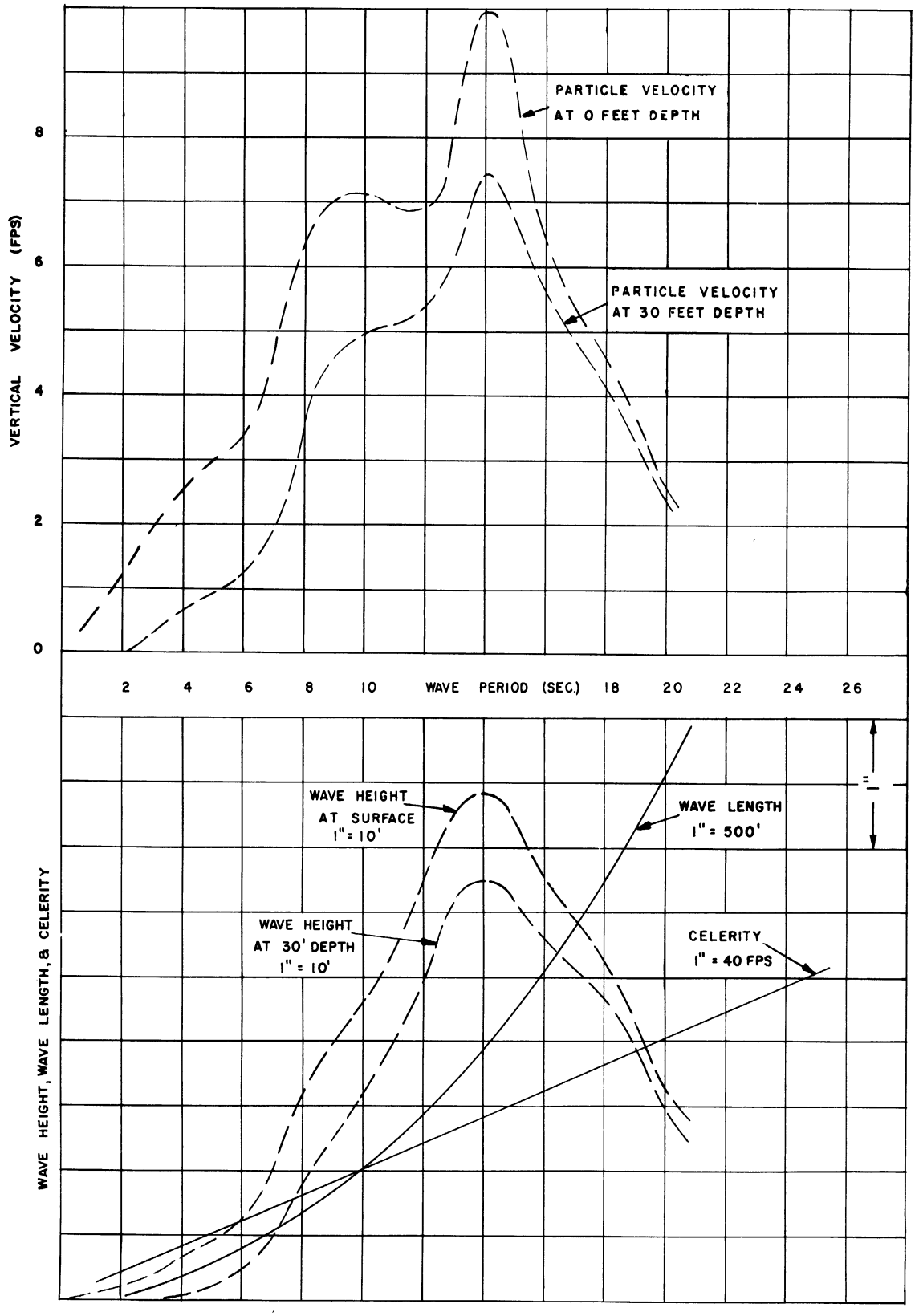

Fig. 5-3. Characteristics of steady-state, short-surface waves.

are shorter than those of tides and fall in the range of 17 to 63 km. or about 11 to 39 miles. The periods of such waves will generally be too long to be important to paravane operation.

Disturbance-Frequency Range.—In estimating the range of important disturbance frequencies relative to the paravane caused by waves, it appears sufficient from the foregoing discussion to consider only short surface waves and confused seas. Some theoretical analyses indicate that surface waves grow in length, and thus in celerity and period, after leaving a wind region in which they were produced. However, observations of waves with appreciable height seem rather to confirm the fact that the waves travel long distances at their original velocities. It will be assumed that confused seas of significantly large amplitudes are formed by the interference of pairs of short surface waves conforming to the steady-state pattern of Fig. 5-3. No attention will be paid to growth or decay, or to the effect of the variety of initial conditions which can precede a period of growth or decay due to wind shifts or the state of the waves when a wind rises. An estimate of significant wave periods must therefore be somewhat arbitrary.

Let the velocity of the ship and paravane have a range of 6 to 16 knots or about 10 to 27 fps. Based on Fig. 5-3, a period of 6 seconds may be selected as the minimum of importance when steady-state, short surface waves exist, since it corresponds to a wave amplitude of only 1.25 ft at a 30-ft depth. Similarly, a period of 9 seconds may be selected as a maximum on the basis that periods exceeding 12 seconds are rare and that amplitudes of 10 ft (wave heights of 20 ft) at the surface are the maximum for paravane operation. For steady-state waves of 6 to 9 seconds, the periods relative to the paravane fall in the range of about 3.24 to 61 seconds as shown in Fig. 5-4.

Due to the rapid change of amplitude and wave length with the period of short waves, beat waves produced by the interference of waves having periods of less than 9 seconds are either tantamount to the largest of the interfering waves or have beats of excessive wave length. Wave length is considered excessive if it is appreciably greater than a ship length of 500 ft, in which case the vessel tends to ride the waves and the paravane may be permitted to behave similarly. In addition to the beat wave produced, the resultant motion due to the interference of waves which travel in the same direction includes a component which has a wave length relatively near the average of the lengths of the interfering waves and also has approximately the average velocity. None of the cases in this paragraph therefore result in relative periods falling outside the range of 3.24 to 61 seconds.

However, in the case of interfering waves traveling in the opposite direction, the average wave-length component has a low velocity which results in a range of relative periods estimated to be about 6 to 53 seconds as shown in Fig. 5-5. This figure is based on the interference of single steady-state

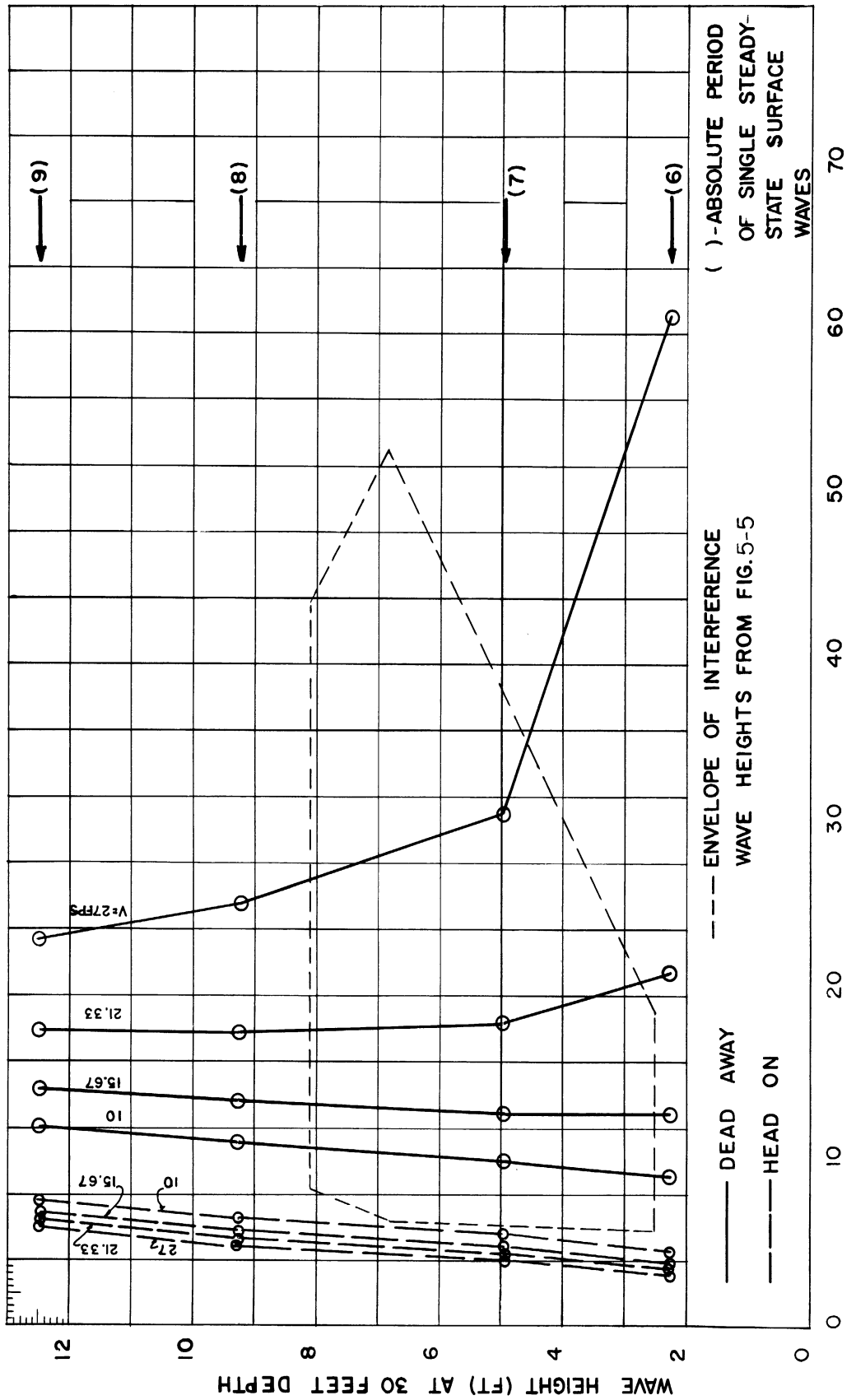

Fig. 5-4. Wave height vs relative period for single, steady-state surface waves having length and height within significant range.

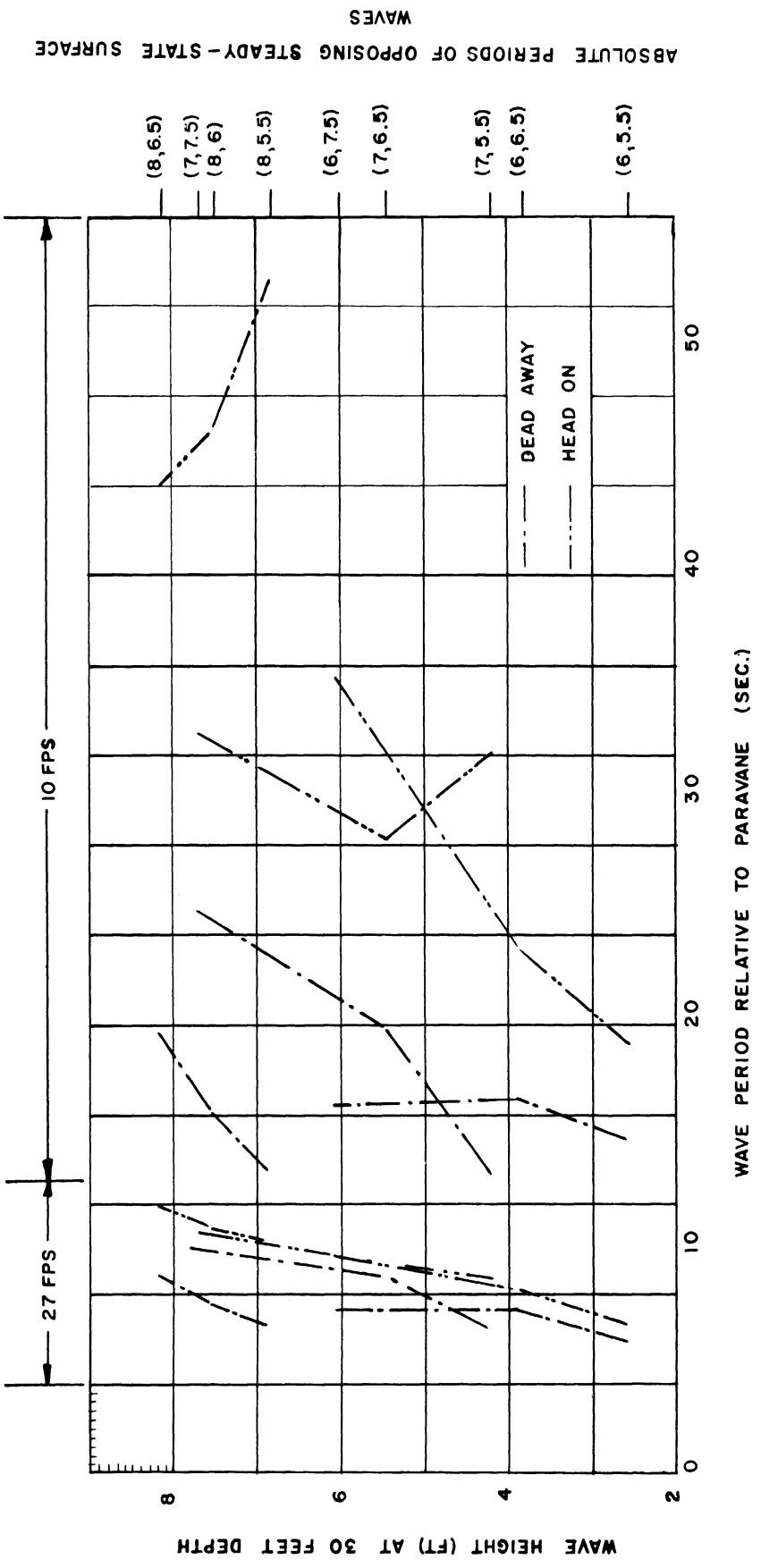

Fig. 5-5. Wave height vs relative period for the average-wave-length component resulting from the interference of two opposing steady-state surface waves (for the significant range of the height and length of the average-wave-length component).

waves of periods in the range of 5.5 to 8 seconds. The heights shown are the average heights of the beat wave. The range of 5.5 to 8 seconds is limited by the fact that interfering waves of smaller period have negligible amplitude at the depth of the paravane and waves of larger period would cause beat amplitudes at the surface which are excessive for paravane operation.

The envelope of Fig. 5-5 is superimposed on Fig. 5-4 showing that single, steady-state short waves determine the overall range of significant disturbance periods which will therefore be assumed to fall in a range of about 3 to 61 seconds. The range of the period and circular frequency of wave disturbances relative to the paravane then is

Wave Period (sec) Relative to Paravane	Circular Frequency of Wave Relative to Paravane (rad/sec)
$T_R = 3$	$\omega_R = 2.1$
$T_R = 61$	$\omega_R = .1$

The resonant period and circular frequency of the paravane-cable system were seen to lie in the following range:

$T_N = 4.8$	$\omega_N = 1.3$
$T_N = 13$	$\omega_N = .48$

resonance can therefore be expected. For waves of a given celerity and wave length, and for a given direction of tow, the disturbance frequency will vary as the towing speed, V. Since ω_N also varies as V, there will be for each direction of tow one wave pattern which will be in resonance with the paravane-cable system at all speeds. Then if that wave pattern has an absolute period in the range of 6 to 9 seconds, appreciable oscillations of depth may occur in the absence of depth control.

5.4 DESIGN OF THE CONTROL MECHANISM

The pressure-seismic, error-actuated mechanism was selected for the reasons given in section 2.3. The data of the preceding section permitted the derivation of an expression for the vertical velocity of the water and thus for the force on the end vanes due to the wave motion at a depth of 30 ft ($z_d = 60$). That is, relative to the paravane, the displacement of a wave may be closely represented by

$$z_\omega = Z_\omega \sin(\omega_R t) = Z_\omega \sin\left(\frac{2\pi}{T_R} t\right) ,$$

where z_ω is the amplitude at a depth of 30 ft and T_R the relative period of the wave. These quantities are evaluated in Fig. 5-4. Then the vertical velocity of the fluid due to wave motion is

$$v = \frac{2\pi}{T_R} z_\omega \cos\left(\frac{2\pi}{T_R} t\right) ,$$

which may be substituted for v in the right-hand side of (5.24), thus determining the disturbing force due to waves as a function of time. Full-scale control surfaces of the type of Fig. 4-15 were assumed, and their depth-corrective force was calculated as a function of their deflection, using average wind-tunnel data for surface of a hydrodynamically balanced type [16, 17]. The depth-corrective force was found as a function of time by an analysis of the control mechanism of Fig. 5-6. This expression was added to the right-hand side of Equation (5.24) since it also comprises a part of the external driving force on the paravane. The solution of the resulting differential equation provided the relation between the control-surface deflection, the wave period and height, and the towing speed which would minimize oscillations in depth. This relation then determined the size of the diaphragm, seismic system, and other components of the prototype depth-control mechanism shown in Appendix F.

The mechanism is shown schematically in Fig. 5-6 where the diaphragm is at A. The seismic masses are m_1 and m_2 and are counterpoised so as to avoid sensitivity to angular acceleration and retain sensitivity to vertical acceleration. The lengths r_g, r_m, and r_o are respectively the radius of the center of gravity, the radius of gyration, and the distance to outer end of a seismic mass from the axis of rotation. In the prototype design, m_1 and m_2 were equal and the spring k and the damping element C_2 were not used.

5.5 SERVOMECHANISM CONTROL EQUIPMENT

Automatic control equipment may be summarized as follows:

(a) Compensators.

(b) Feedback control equipment.
  (1) Error-driven control equipment.
  (2) Servomechanism control equipment.

In compensators, the corrective action of the control equipment is not influenced by a return signal to the equipment indicating the success of that action. In feedback control equipment, such information is returned and is termed the "feedback." The feedback is obtained from elements of the

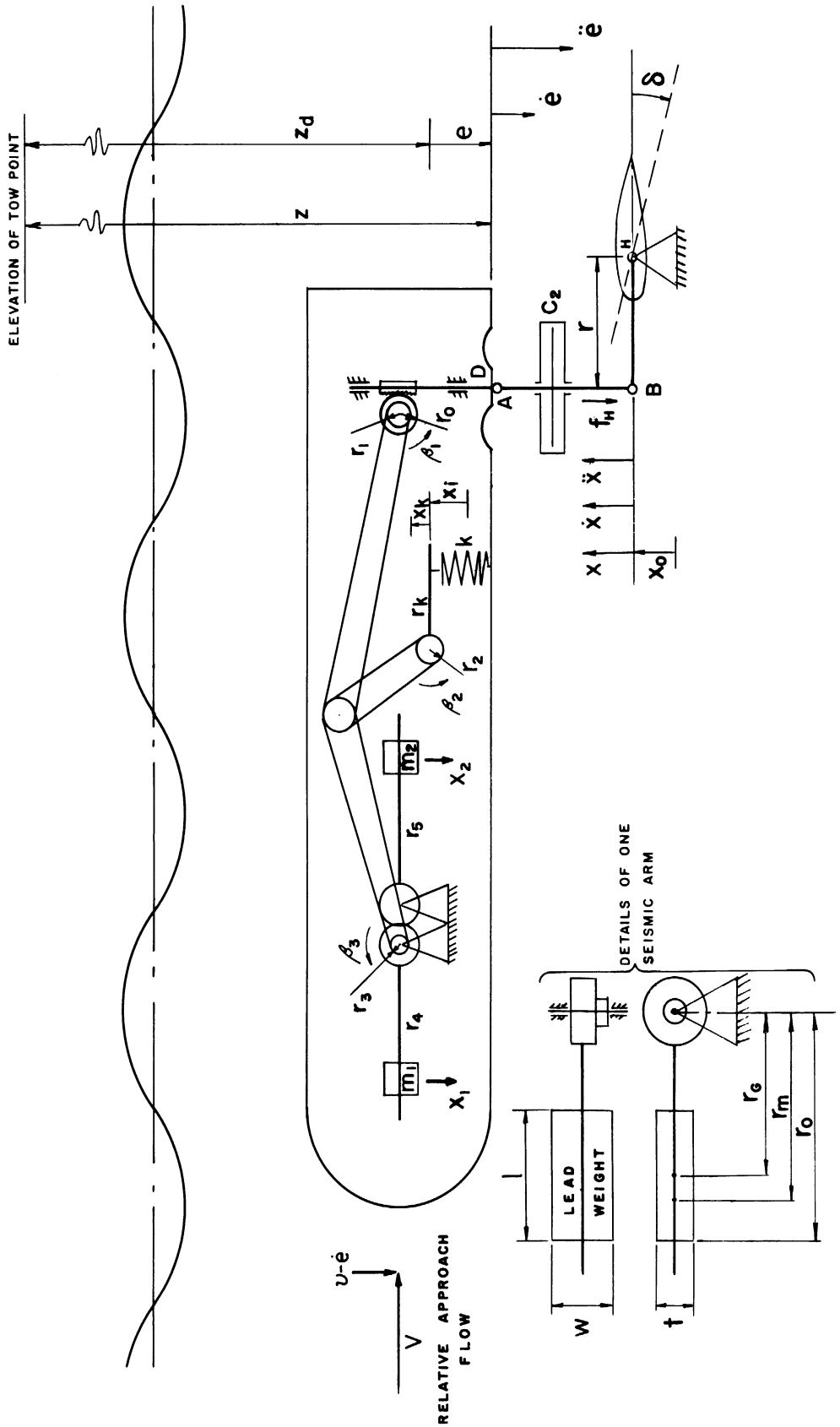

Fig. 5-6. Schematic diagram of pressure-seismic, error-actuated depth-control mechanism.

control equipment known as transducers which measure one or more of the system properties which are to be controlled, and convert them into a feedback signal which is transmitted to the control equipment.

The relation between the feedback and the resulting output of the control equipment is termed the control action. If the energy necessary for this action is taken from the feedback signal, the control equipment is of the error-actuated type. The prototype control of Appendix F, shown schematically in Fig. 5-6, falls in this category. If the feedback signal is required to supply only a negligible amount of energy and instead directs the flow of energy from an independent energy source, the control equipment is of the servomechanism type. The latter equipment is necessary where a complex control action is needed or where the energy requirements of the control action are large compared to the energy which can be obtained from the transducers.

If diaphragm and seismic elements such as those in Fig. 5-6 are required to drive only a small load and this action controls a slave mechanism which positively positions the control surface, the system is a servomechanism control. The servomechanism itself is the slave device. It requires an independent source of energy and has a feedback within itself. A common type is shown schematically in Fig. 5-7. The use of this principle for paravane depth control is illustrated in Fig. 5-8 where the stagnation pressure is used as the source of energy to the servomechanism. The load on the transducers is minimized by balancing pressures on the slide valve. The latter feature does not require close tolerances since some leakage is desirable. The various solid and liquid masses in the system can be arranged so as to aid the seismic masses.

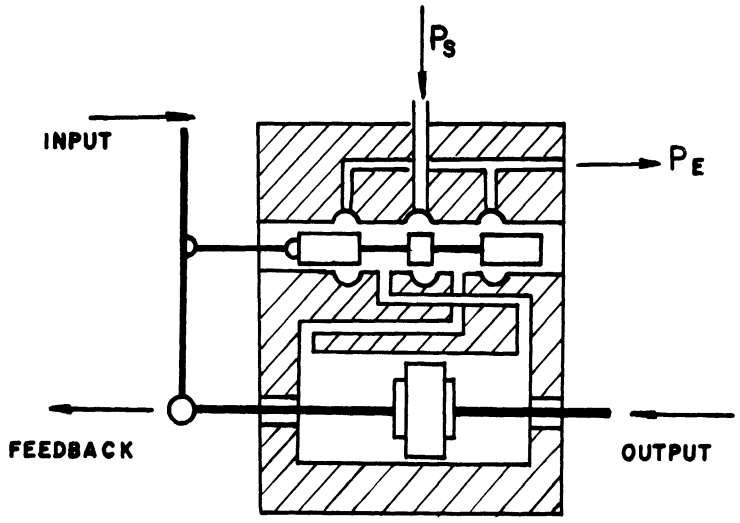

Fig. 5-7. Schematic diagram of typical servomechanism of the hydraulic-type (valve-controlled hydraulic ram with proportional feedback).

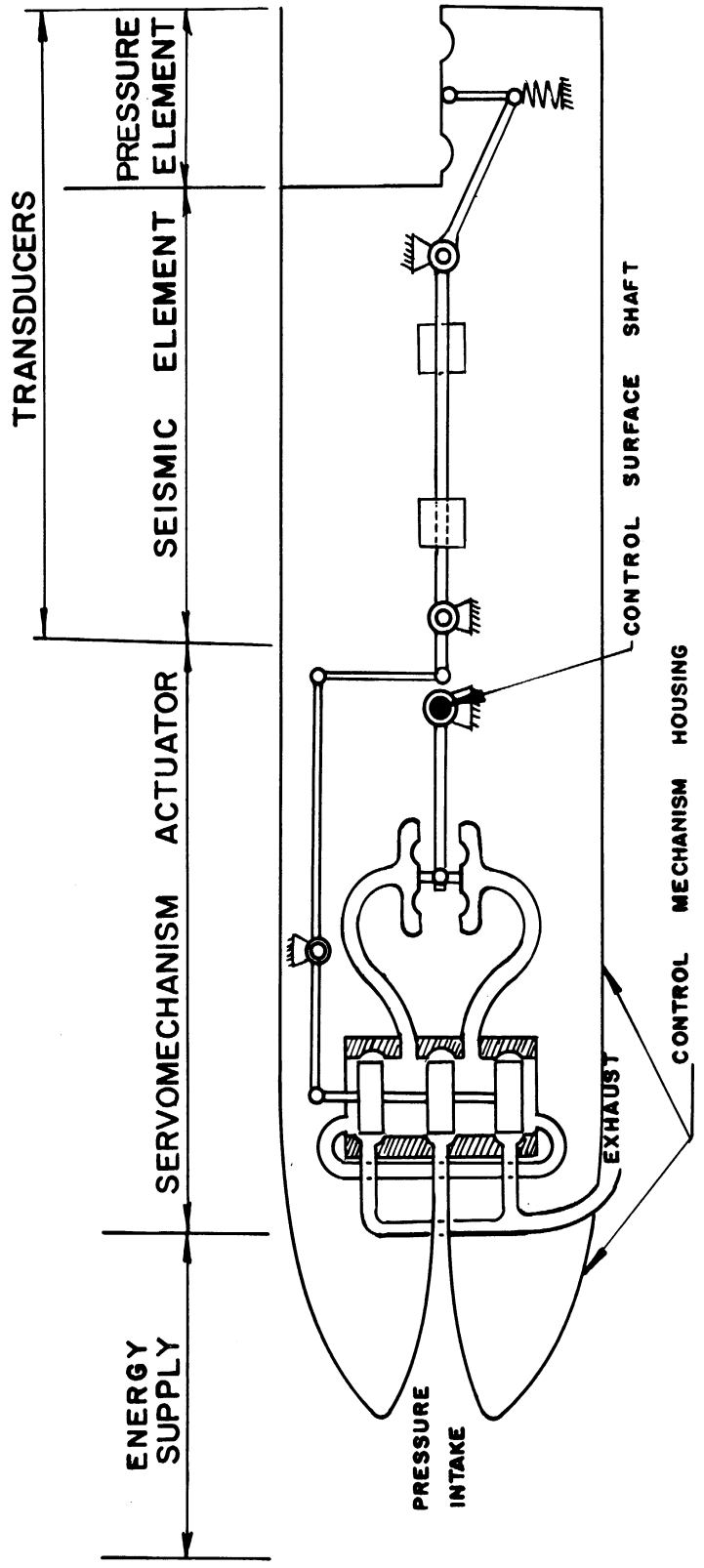

Fig. 5-8. The servomechanism principle illustrated for paravane depth control (servomechanism feedback not shown).

A substantial pressure differential could be maintained by proper design of the intake and of the exhaust port where an aspirator principle may be used to secure low pressure. Furthermore, large areas of the opposed diaphragms can be readily obtained. Nevertheless, the design of Fig. 5-8 is undesirable since it involves a flow of sea water through the slide valve and other parts of the circuit.

Figure 5-9 schematically illustrates a servomechanism in which the internal flow of sea water is avoided. In this case, the transducers have a large mechanical advantage for deflecting manipulated elements in the form of flow spoilers having a small hinge moment. A small pressure differential is sufficient and is developed almost instantly across the opposed diaphragms. The resulting motion of the diaphragms is in turn fed back to the manipulated elements. Thus the diaphragms exert on the control surface shaft whatever hinge moments are required at that instant to position the control surface in proportion to the input motion from the transducers. In this system, it is relatively easy to produce control action in which the control-surface deflection leads or lags an oscillation of depth, as desired. For convenience in illustrating the required feedback action, the spoilers in Fig. 5-9 are arbitrarily assumed to produce the output shown for the specified input.

While the mechanism of Fig. 5-9 would entail a certain amount of development work, it does offer a simple compact design in which a refined control action and positive positioning of control surfaces can be obtained. Of the various servomechanism controls conceived, Fig. 5-9 was the best which conformed to the restrictions described in section 2.3.

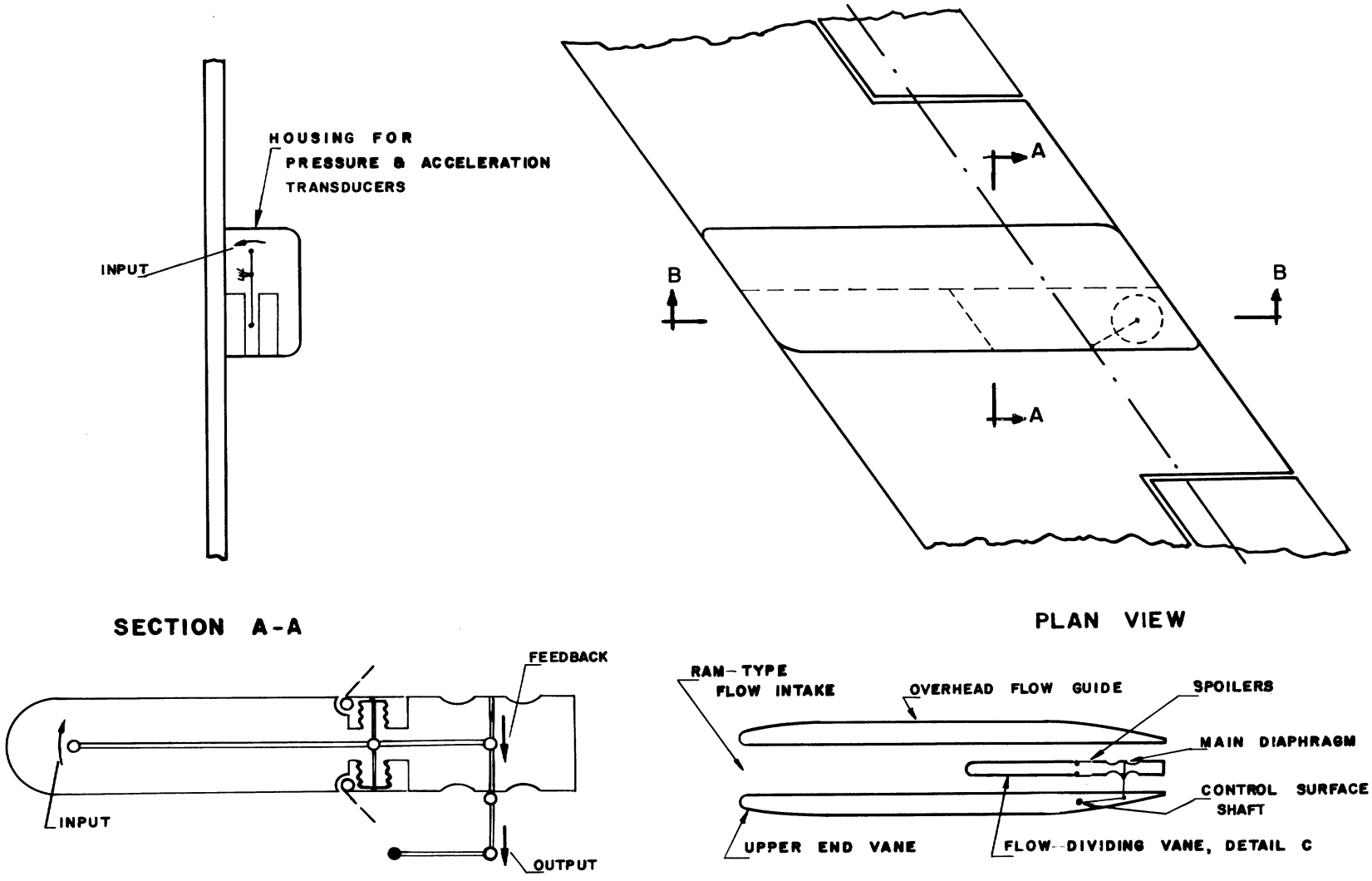

Fig. 5-9. Example of a servomechanism designed particularly for paravane depth control (spoilers arbitrarily assumed to produce the output shown for the specified input).

PART B

HIGH-LIFT PARAVANE

CHAPTER 6

PROTOTYPE DESIGN OF HIGH-LIFT PARAVANE

6.1 INTRODUCTION

The high-lift paravane, designed to operate in connection with a float, was required to develop a lift of 9,500 lb at 8 knots and to have its largest dimension less than 6 ft. No limit was placed on sweepback angle but it was considered desirable to keep the angle as small as practicable. The excess of weight over buoyancy was limited to 500 lb.

To meet the specified 9,500 lb at 8 knots, the lift per unit dynamic pressure is $L/q = 52.5 = C_L S$. For comparison the L/q for the high lift-drag ratio paravane was only 27.6. Thus in the high-lift design, noting also the difference in size, the lift coefficient must be four to five times as large, that is C_L is 2 to 3.

6.2 DESIGN OF PROTOTYPE

To obtain a high value of C_L the multi-slotted vane was adopted. As shown by the drawings in Appendix G, the final design is of the biplane type with each lifting surface made up of six identical elementary vanes. The decalage which was adopted was minus 10 degrees, with the chords of the lift vanes in the positions indicated by the drawing. Model tests at a speed of 2.5 ft/sec produced lift coefficients of 2.3 to 3.3. With the design which was finally adopted, the C_L must be 2.86. This should be easily realized by the prototype, considering the higher Reynolds number, the scale factor of 3.5, and the slight increase of aspect ratio of the prototype over the model.

Some characteristics of the prototype design follow.

Lift vane area	18.4 ft^2
span	4 ft - 4-1/2 in.
chord	2 ft - 2-1/4 in.
aspect ratio	2
gap, percent of chord, approx.	91%
Decalage of the lift vanes	minus 10°
Angle of stagger of the lift vanes	
aerodynamic angle of stagger, nominal	45°
geometric angle of stagger, approx.	50°
Approximate weight in aluminum alloy	400 lb

The model tests were made with profiled elementary vanes. The drawings show curved plates of uniform thickness with a semi-circular leading edge and an obliquely cut trailing edge. The trailing edge of the last elementary vane differs slightly from the others. For the prototype it would be appropriate if all leading edges and trailing edges were merely rounded. The position of the first elementary vane with relation to the last one should be carefully made as shown. It is likely that some adjustment of the position of the other vanes is permissible, but it seems just as well to maintain the positions which were successfully used during the towing tests. It appears that the end plates could be slightly reduced in overall length by using a little larger radius at the rearward acute angle.

The bridling system consists of four lines connected to the lift vanes and converging at the tow cable. In the towing tests the float was attached directly to the paravane. It should perform equally well with the float attached to the bridling point except that after a full stop the paravane might not return to its normal towing position. With this in mind it might be desirable, if it is practicable, to attach the float directly to the paravane. If it is decided to do this, suitable connections, not shown in the drawings, should be provided.

CHAPTER 7

DESIGN CONSIDERATIONS AND EXPERIMENTAL WORK

7.1 INTRODUCTION

The high-lift paravane having the characteristics described in section 6.1 was of interest for an application like that of the "O" type Multiplane Kite-Otter [mine-sweep size No. 1 (N)], BuShips Dwg. No. S 8101-1, 207, 904. The depth of the kite-otter is controlled by a float rather than by control surfaces. The depth of the high-lift paravane was to be controlled in a similar manner. The development of this paravane was authorized under the present project as a result of the excellent behavior of models of the high lift-drag paravane without control surfaces. The performance of these biplane models indicated to the Bureau of Ships representative that a tailless biplane design having high lift could be advantageous under certain conditions.

7.2 DESIGN IMPLICATIONS OF THE LIFT, WEIGHT, AND SIZE REQUIREMENTS. MULTI-SLOTTED VANES

The need to produce a lift force of 9500 lb at a towing speed of 8 knots requires that the lift per unit dynamic pressure be

$$\frac{L}{q} = 52.5$$

as determined from Fig. 3-4. The design requirement then is

$$C_L S = 52.5 \ .$$

A lift coefficient 0.5, such as considered for the high lift-drag ratio paravane, would require a total lift surface having an area of 105 ft^2. This area is about twice that of the high lift-drag ratio paravane and would be excessive for the high-lift paravane which was to be much smaller. The total single multi-vane lift surface of the size 1 kite-otter has an area requiring a lift coefficient of 2.98 to produce the specified lift. In order to obtain an even more compact design, a still higher lift coefficient and/or a greater number

of lift surfaces would be required.

The representative data of Fig. 3-6 indicated that a lift coefficient of 1.0 was about the maximum which could be expected from a conventional vane. Because of the large drag of the very long tow cable and other parts of the system, the drag of the high-lift paravane was of secondary importance and the latter required only a moderately high value of L/D. Thus, high-lift devices could be considered. The simplest of these consists of a lift vane containing slots which are arranged so as to delay the separation of the flow on the low-pressure side. Published data indicated that a C_L of 2 might be obtained by means of three slots [21]. However, this value was inadequate if the paravane were to be more compact than the kite-otter and have a weight which exceeded its buoyancy by a maximum of about 500 lb. However, since slots do increase the lift coefficient, an increase in their number could be expected to delay separation in vanes of greater camber successfully and lead to higher values of C_L. If so, an assembly of elemental vanes forming a single multislotted vane might provide the desired C_L [22]. The flow about various arrangements of elemental vanes was observed in the flow channel. The configuration selected was essentially that of Fig. 7-1 except that a sixth elementary vane was added in the prototype design. Fig. 7-1 also indicates the flow pattern.

The angle of attack of the multislotted vane is defined as the angle between its chord and the direction of the flow relative to the vane at a point considerably upstream. Even at the large angle of attack of Fig. 7-1, it is seen that the flow separated only a little and did so only near the last two elemental vanes. This condition indicated that a high lift coefficient could be obtained with the multislotted vane.

7.3 TOWING-TANK TESTS OF THE FLOAT-PARAVANE SYSTEM

The float used in the tank is shown in Fig. 7-2 and was a scale model of the Mark IV Float, BuShips Dwg. No. S 8108-1,207,907. In this float design the center of buoyancy, center of gravity, and tail vane are all aft of the towing bail. When towed in a fully submerged position, the tail of the float was above its nose. This negative angle of attack was necessary in order that the hydrodynamic forces on the body of the float and its tail vane might have large leveling moments about the shaft of the towing bail. The equilibrium orientation was reached when the sum of these moments and that of the weight was great enough to offset the large moment of buoyancy. The rise of the tail decreased as the towing speed was increased. At a towing speed of 80 ft/min, the angle of attack reached a moderately negative value which was about that estimated for the full-scale float at 8 knots.

Figure 7-3 is an end view of the multislotted lift vane used in high-lift models. The arrangement of the elemental vanes is visible. Also

shown is one of the two brass plates to which the ends of the elemental vanes were soldered to form the multislotted lift vane. The circular slot and the holes in the plates permitted attaching a pair of faired rectangular end vanes and fastening it in various orientations with respect to the chord of the multislotted vane. The span of the latter was 9.25 in. and its chord was 7.4 in.

The initial tests were conducted with a model having a single lift vane as shown in Fig. 7-4. The model was tested without the float. Although it was able to assume an outboard equilibrium position, its stability in pitch about a vertical axis was considered inadequate. Also, the lift force was too small to meet the specifications. Therefore, the biplane model of Fig. 7-5 was assembled. The design of the multislotted vane remained unchanged and faired end plates were again used.

When tested without the float, the biplane model exhibited the proper stability characteristics for this application. The model and float were tested together using separate pendants to connect them to the outboard end of the tow cable. With this arrangement, it was a problem to insure an orientation of the paravane which would provide a sufficient downward force to submerge the float. After some investigation, it was found advantageous to bridle the float to the upper end vane of the paravane. In this manner the end vanes could be tilted so that they produced the required downward force when towing. This arrangement also made it possible to control the orientation of the paravane when the towing operation was stopped and so insure that the system would return to the outboard equilibrium position when towing was resumed.

7.4 DESIGN DETAILS

In order to determine the extent to which the design could be varied for the purposes of structural strength and ease of manufacture of the full-scale paravane, the flow channel was used to investigate the importance of the thickness ratio and shape of the elemental vanes in obtaining a suitable pattern of flow.

For each thickness ratio over a wide range, it was possible to arrange the elemental vanes so as to maintain a desirable flow pattern. The extremes of thickness ratio which were tested are shown in Fig. 7-6 and Fig. 7-7, the latter containing elemental vanes having the relatively high thickness ratio of 0.25. The two figures reveal that the flow pattern is affected but little by variations of the thickness in the range tested. Thus, if necessary for structural strength, the elemental vanes may be made quite thick without substantial adverse effect on the lift coefficient.

The shapes of the leading and trailing edges are of interest from the standpoint of ease of manufacture. Figure 7-8a is a photograph of the

flow when each of the elemental vanes has a rounded leading edge and a 45° cut on the trailing edge. In Fig. 7-8b the leading edge is cut on a 45° angle and the trailing edge is rounded. Each of the elemental vanes of Fig. 7-8c has a 90° cut on both leading and trailing edge. It is observed that in all cases the general pattern of flow is quite good and no large localized disturbances are present. It was concluded that the shape of the edges was not a primary factor in the lift developed by the multislotted vane.

The equilibrium angle of attack of the float was considered briefly. A check was made of the applicability of the following expression for the lift coefficient of a vane of small aspect ratio [19] for determining the lift coefficient of the float body:

$$C_L = \frac{\pi}{2}(AR)\,\alpha_a + \pi(AR)^{1/3}\,\alpha_a^{5/3} \quad . \tag{7.1}$$

The float is a body of revolution and therefore its absolute angle of attack, α_a, is identical to its geometric angle of attack, α. In equation (7.1), α_a is measured in radians. The aspect ratio of the Mark IV float is 0.167. If the angle of attack has the arbitrary value of 7°, Equation (7.1) yields 0.082 for the value of C_L compared to the experimental value of 0.079 for a body of revolution similar to the float [15]. If the induced drag coefficient is approximately given by the following equation, first stated in Chapter 3,

$$C_{Di} = \frac{C_L^2}{\pi(AR)} \quad , \tag{7.2}$$

then this coefficient is equal to 0.013. The profile drag coefficient for a similar body of revolution [15] is 0.048, yielding a total drag coefficient of .061 compared to the experimental value of 0.068. It may be concluded that Equations (7.1) and (7.2), originally derived for vanes, will give values of the lift and drag of the float body which are of the correct order of magnitude. Similar estimates for the forces on the tail vane of the float are difficult since this vane lies in the wake of the float body, especially when the angle of attack of the float is negative.

If the tail-vane forces can be obtained, and if the centers of buoyancy and gravity of the float are known, the equilibrium angle of attack of the float could be estimated. In view of the circumstances, however, this probably should be done experimentally. With such information, the shaft of the towing bail could be relocated, if necessary, to insure a sufficiently small absolute value of the angle of attack of the float. The interest in this point stems from the fact that moderately large values of the angle of attack of the float appear to correspond to surprisingly large drag coeffi-

APPENDICES

APPENDIX A

INTRODUCTORY DETAILS

A.1 GLOSSARY

Hydrodynamic Terminology

A vane is a surface intended either to direct a flow or to receive a hydrodynamic force from a fluid in which it is immersed and with respect to which it has a relative velocity. In the latter case, the cross-section of the vane is usually profiled to obtain certain characteristics such as the relation of the lift and lift-drag ratio to the angle of attack.

The angle of attack or angle of incidence is the angle between the chord of a vane and the direction of flow relative to the vane. The latter direction is taken as that of the approach flow at points a long distance ahead of the vane. It is parallel to the direction of motion of the vane but is of opposite sense.

The absolute angle of attack of a vane is the difference between the existing angle of attack and the angle of attack at which the lift is zero.

Lift is the component of the hydrodynamic force on a vane which is perpendicular to the direction of the approach flow.

Drag is the component of the hydrodynamic force on a vane which is parallel to the direction of flow.

The chord of a vane is length of the profile view, usually taken as the length of the projection of the profile on a straight line from the leading to the trailing edge. For a profile with a flat high-pressure side, the chord lies in the plane of the flat side.

The hydrodynamic center of a vane is the point whose distance from the leading edge of the chord is one-quarter of the chord.

The center of pressure of a vane is the intersection of its chord with the line of action of the resultant lift.

The center of force of a vane is the point of application of the resultant hydrodynamic force on the vane.

The thickness of a vane is the dimension of the vane profile in a direction perpendicular to the chord.

The thickness ratio of a vane is the ratio of its maximum thickness to length of chord.

The span of a vane is its length from tip to tip as seen in the plan view of the vane. The span is measured in the chord plane.

The aspect ratio of a vane is the ratio of its span to its chord.

A lift vane of a paravane is a vane intended to supply the component of hydrodynamic force perpendicular to and away from the ship's course.

An end vane of a paravane is a vane mounted on the tip of a lift vane and usually perpendicular to the latter. Its purpose is to prevent flow across the tip of the lift vane from its high- to its low-pressure side. An end vane thus serves to reduce the vortex at the tips of a lift vane and thereby to reduce the portion of the drag caused by the vortex, the latter being called the induced drag.

The tow point is the point at which the tow cable is attached to the ship.

The junction point is the point at which the pendant of any towed body is connected to the tow cable.

The bridling point is the point at which the bridling lines of the paravane converge. It is the point at which the bridling system is connected to the outboard end of the tow cable.

The paravane pendant is the segment of the tow cable between the junction and bridling points.

The cable sweepback angle is the projection on a horizontal plane of the angle between the secant of the tow cable and a line through the tow point which is horizontal and normal to the ship's course. The secant is a straight line drawn from the tow point to the bridling point.

Depth-Control Terminology

Compensation is an operation which tends to reduce the difference between the actual state of a system and a desired state by employing means to offset the effects of disturbances without causal effect between the error in the state of the system and the action of the compensating means.

Feedback control is an operation which, in the presence of disturbing influences, tends to reduce the difference (error) between the actual state of a system and a constant or arbitrarily-varied, desired state and which does so on the basis of the difference.

The controlled variable is that quantity or condition of the controlled system which is controlled and, in feedback control, is also measured.

The desired value (set, point, or control point) is the desired condition of the controlled variable. It may be a constant or a function of time or of some other independent variable. The function may be continuous or discontinuous.

The error is the difference between the desired and actual values of the controlled variable. (Some error is essential to the operation of a feedback control by definition. Limits are usually set and comprise one of the major design criteria.)

A disturbance is a signal which, like the desired-value signal, tends to affect the value of the controlled variable.

Stability is the property of a control system in which the response of the controlled variable to a stimulus (the desired-value signal or a disturbance) decays if the stimulus dies. Or, if the stimulus reaches a steady-state and non-zero condition, the system may be (1) stable, if it reaches a steady-state condition of the controlled variable with any natural oscillations being transient, or (2) unstable, if it fails to reach a steady-state condition and grows progressively larger in a unidirectional or oscillatory manner, or a combination of both, or (3) marginally stable, if any initial oscillations persist but are of bounded amplitude.

A.2 NOMENCLATURE

Hydrodynamic Nomenclature

AR	Aspect ratio of a vane
b	Span of a vane (ft)

c	Chord of a vane (ft)
CB	Center of buoyancy
CG	Center of gravity
C_D	Drag coefficient of a vane
C_{DB}	Drag coefficient of an added drag body
C_{DO}	Profile drag coefficient of a vane
C_{Di}	Induced drag coefficient of a vane
$C_{D\pi}$	Parasite drag coefficient of a vane
C_L	Lift coefficient of a vane
C_{NC}	Coefficient of normal component of cable drag
C_R	Coefficient of resultant hydrodynamic force of a vane
d	Cable diameter (in.)
D	Drag of a vane or complete paravane (lb)
D_i	Induced drag of a vane (lb)
D_π	Parasite drag of a vane (lb)
F_Z	Vertical force of paravane on bridling point (lb)
F_N	Normal component of hydrodynamic drag on cable (lb)
g	Acceleration due to gravity (ft/sec^2)
h	Vertical distance (ft) between tow point and paravane (equilibrium value)
ℓ	Reference length (ft)
L_C	Length of tow cable (ft)
L_{Cy}	Paravane outboard distance measured at right angles (ft)
L_P	Length of paravane pendant (ft)

L	Lift of a vane or complete paravane (lb)
q	Dynamic pressure (lb/ft^2)
R	Resultant force of a lift vane or complete paravane (lb)
RN	Reynolds number
S	Reference area of lift vane (ft^2)
S_C	Reference area of tow cable (ft^2)
V	Velocity (ft/sec) of paravane or velocity of flow relative to paravane at a point considerably upstream from it
V_N	Velocity normal to cable (ft/sec)
W_C	Weight of cable (lb)
α	Angle of attack of a vane (degrees or radians)
α_a	Absolute angle of attack of a vane (degrees or radians)
γ	Glide angle of a vane or paravane ($\tan \gamma = D/L$)
γ_C	Specific weight of tow cable (lb/ft^3)
γ_ω	Specific weight of sea water (lb/ft^3)
ϵ	Angle (degrees) of roll of lift vane or paravane (equilibrium value)
θ	Angle (degrees) of declination of tow cable to horizontal (equilibrium value)
ν	Kinematic viscosity (ft^2/sec)
ρ	Mass density of sea water ($slugs/ft^3$)
ρ_C	Mass density of tow cable ($slugs/ft^3$)
σ	Cable sweepback angle (degrees) in horizontal plane (equilibrium value)
σ^*	Cable sweepback angle in oblique plane
ϕ	Angle (degrees) of inclination to vertical of projection of tow cable on y-z plane (equilibrium value)

Depth-Control Nomenclature

D_B	Extra drag due to drag body (lb)
e	Error (ft) in depth of paravane (instantaneous value)
e_o	Initial value of e (ft)
E	Amplitude of e (ft)
E_o	Displacement of depth of paravane due to a constant force (ft)
f	External driving force (lb)
F	Amplitude of f (lb)
M(e)	Depth position-dependent moment (lb-ft)
$M(\dot{e})$	Depth velocity-dependent moment (lb-ft)
$M(\ddot{e})$	Depth acceleration-dependent moment (lb-ft)
S_{EV}	Reference area of one end vane (ft^2)
T	Absolute period of a wave or other disturbance (sec)
T_N	Undamped natural period for depth oscillation of the paravane-cable system (sec)
T_R	Period of a wave or other disturbance relative to the paravane (sec)
v	Vertical velocity (ft/sec) of water due to waves (instantaneous value)
z	Instantaneous depth of paravane below tow point (ft)
z_d	Desired value of z (ft)
z_ω	Instantaneous displacement of a wave (ft)
Z_ω	Amplitude of z_ω (ft)
δ	Instantaneous deflection of control surface (degrees)
Δ	Amplitude of δ (degrees)
θ	Instantaneous declination (degrees) of tow cable to horizontal

θ_d	Desired value of θ
ξ	Damping ratio of paravane-cable system.
ϕ	Phase lead angle (radians) of the displacement of paravane depth with respect to the disturbing force
ω_R	Circular frequency of a wave or other disturbance relative to the paravane (sec)
ω	Absolute circular frequency of a wave or other disturbance (rad/sec)
ω_N	Natural circular frequency of undamped paravane-cable system (rad/sec)

APPENDIX B

REYNOLDS NUMBER. CAVITATION

B.1 REYNOLDS NUMBER EFFECTS

The Reynolds number of a vane is defined as

$$RN = \frac{Vc}{\nu} \tag{B-1}$$

and that of a tow cable as

$$RN = \frac{Vd}{\nu} \tag{B-2}$$

where V is the towing speed, ν the kinematic viscosity of water, c the chord of the lift vane, and d the diameter of the cable. The kinematic viscosity of water varies with temperature and salinity as shown in Fig. B-1.

If ℓ represents the magnitude of the characteristic dimension, such as chord or diameter, we may plot a universal Reynolds number curve, RN/ℓ vs V, for any size vane or cable in sea water. This plot is contained in Fig. B-2 with the temperature of the water as a parameter. Figure B-3 gives the Reynolds number directly for vanes having chord sizes in the range of interest here. Figure B-4 performs a similar function with respect to cables.

Assuming that the lift-vane chord will lie in the range of 3 to 5 ft and the cable diameter between 1 and 2 in., and considering the temperature extremes to be 45°F and 85°F, the maximum variation of the Reynolds number for a velocity range of 6 to 16 knots is as follows:

Item	Min. RN	Max. RN
Lift Vane	1.8×10^6	14.6×10^6
Cable	$.5 \times 10^5$	4.8×10^5

The minimum temperature encountered may be somewhat less than 45°F, resulting in slightly lower minimums for RN. This possibility is not important for present purposes.

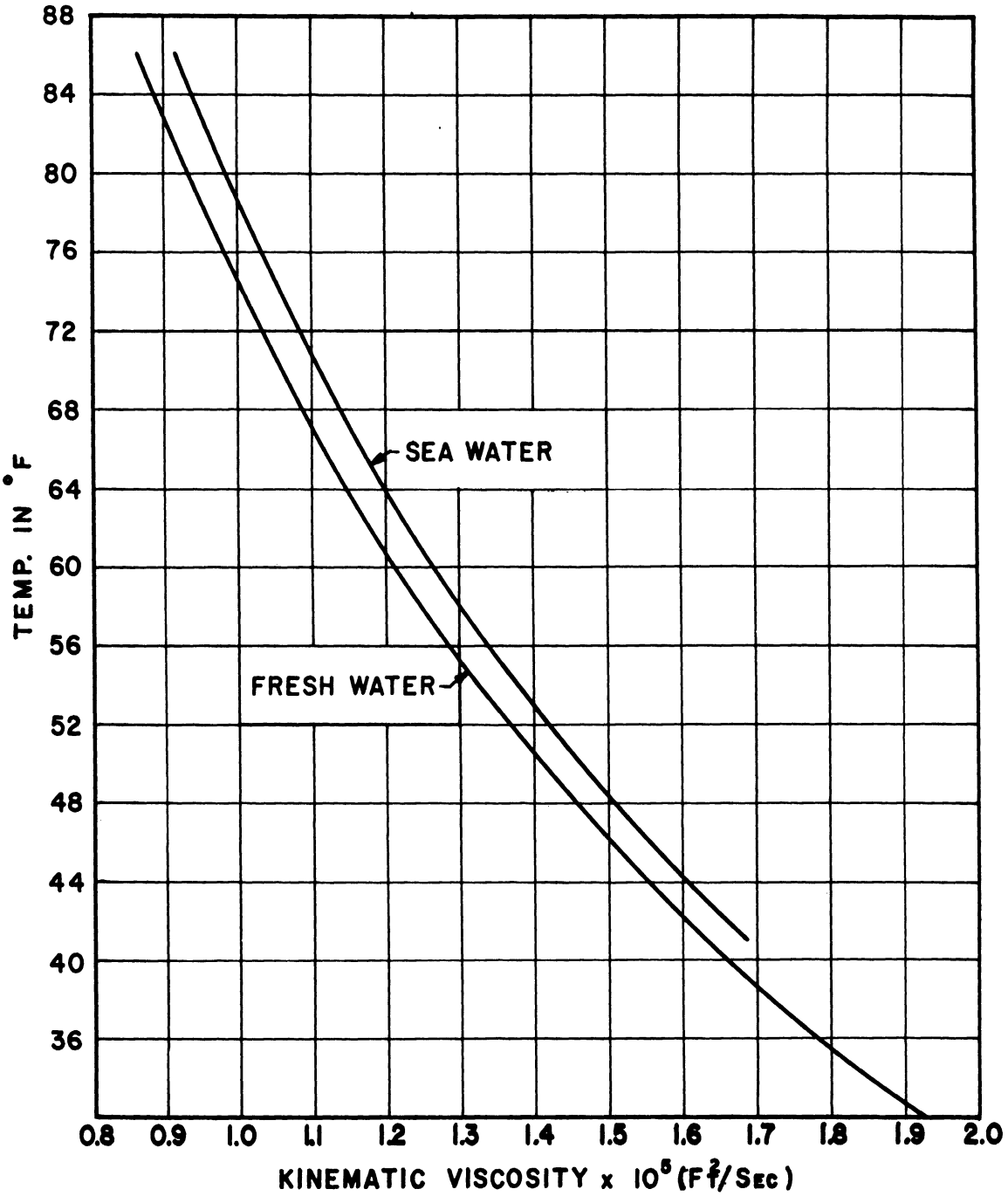
88
84
80
76
72
68
64
60
56
52
48
44
40
36
TEMP. IN °F
SEA WATER
FRESH WATER
0.8
0.9
1.0
1.1
1.2
1.3
1.4
1.5
1.6
1.7
1.8
1.9
2.0
KINEMATIC VISCOSITY x 10⁵ (Ft²/Sec)

Fig. B-1.

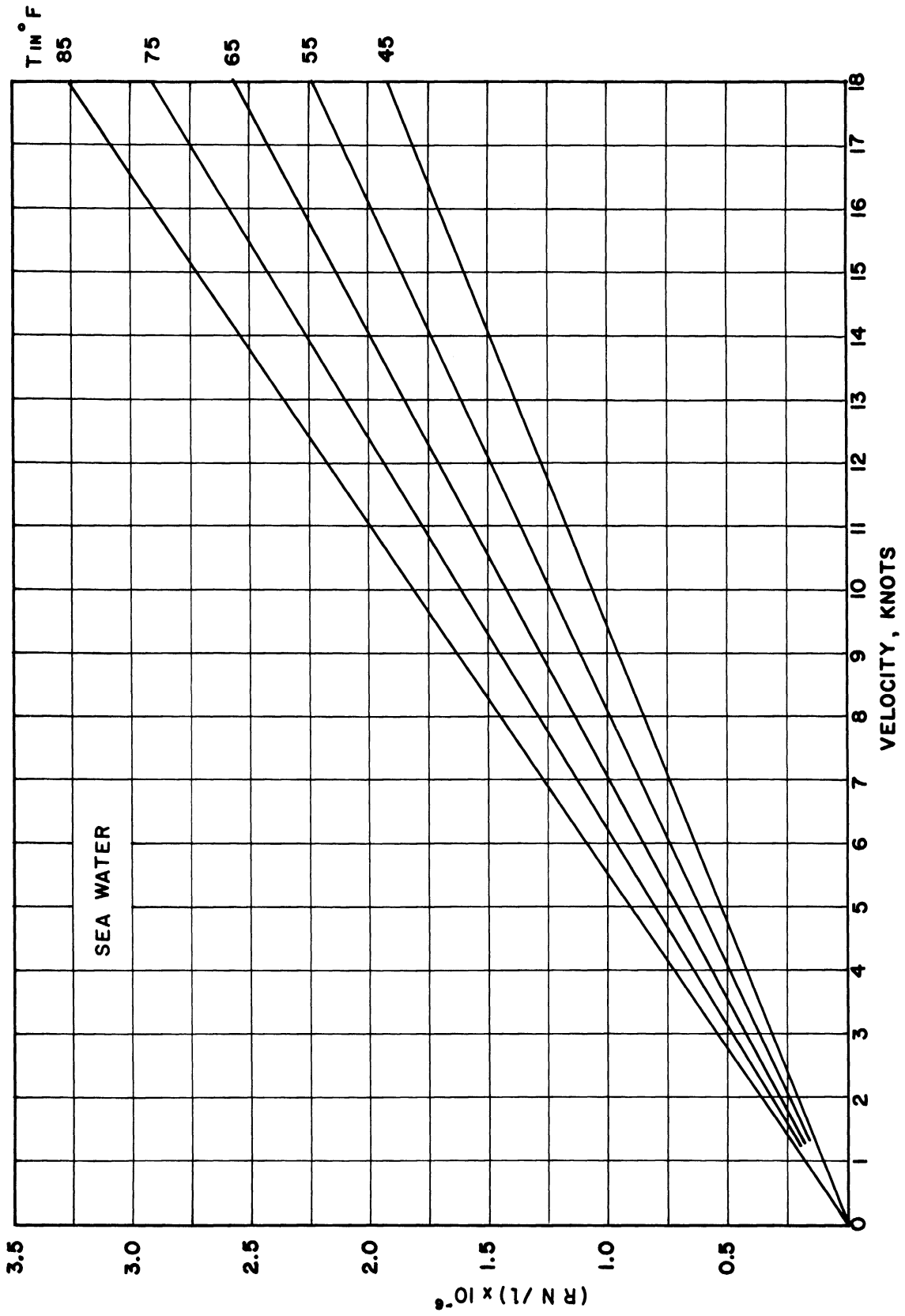
T IN °F
85
75
65
55
45
SEA WATER
VELOCITY, KNOTS
0
1
2
3
4
5
6
7
8
9
10
11
12
13
14
15
16
17
18
3.5
3.0
2.5
2.0
1.5
1.0
0.5
(R N /L) x 10⁻⁶

Fig. B-2.

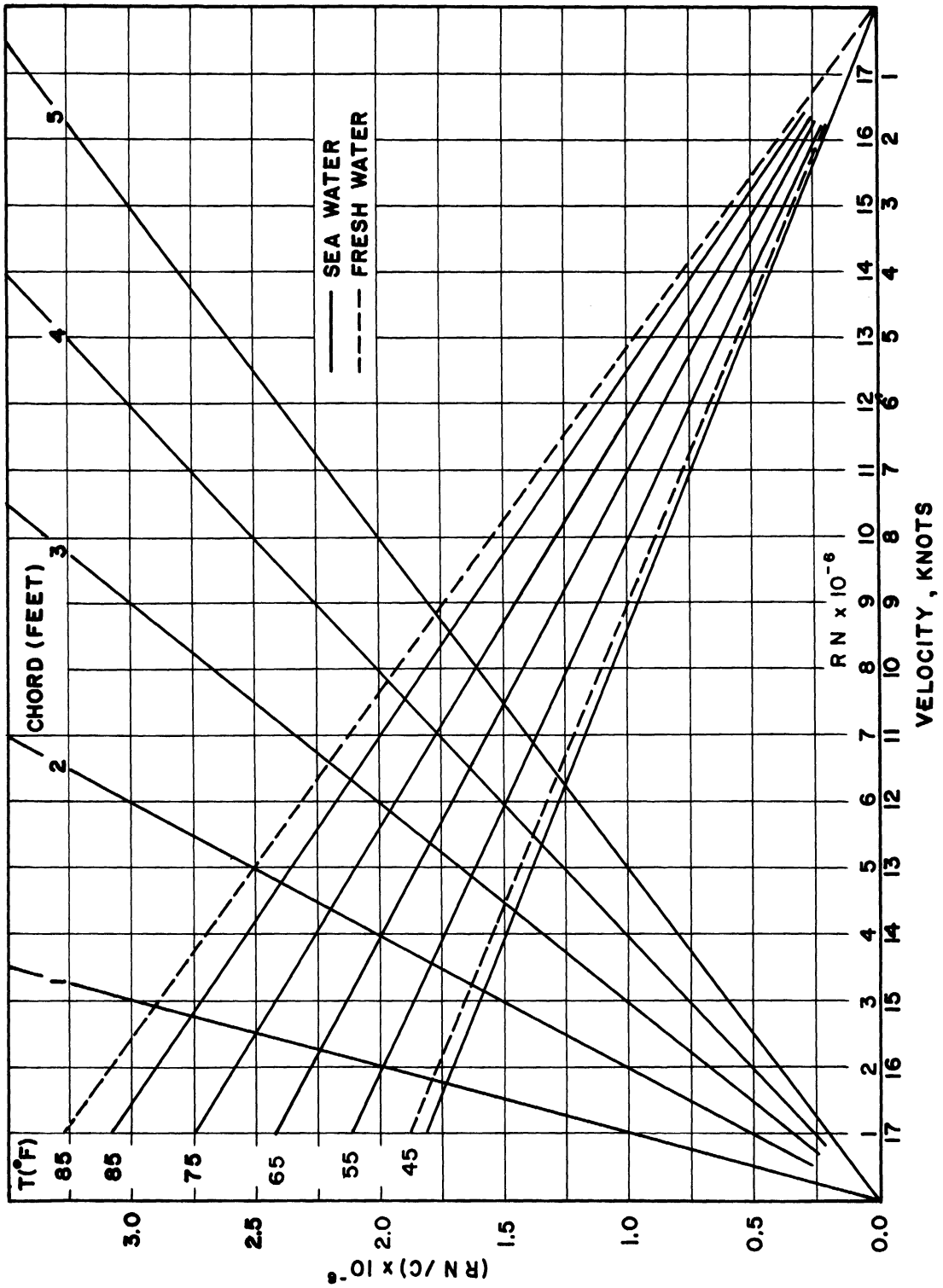
SEA WATER
FRESH WATER
CHORD (FEET)
T(°F)
85
85
75
65
55
45
(R N /C) x 10⁻⁶
3.0
2.5
2.0
1.5
1.0
0.5
0.0
R N x 10⁻⁶
VELOCITY, KNOTS

Fig. B-3.

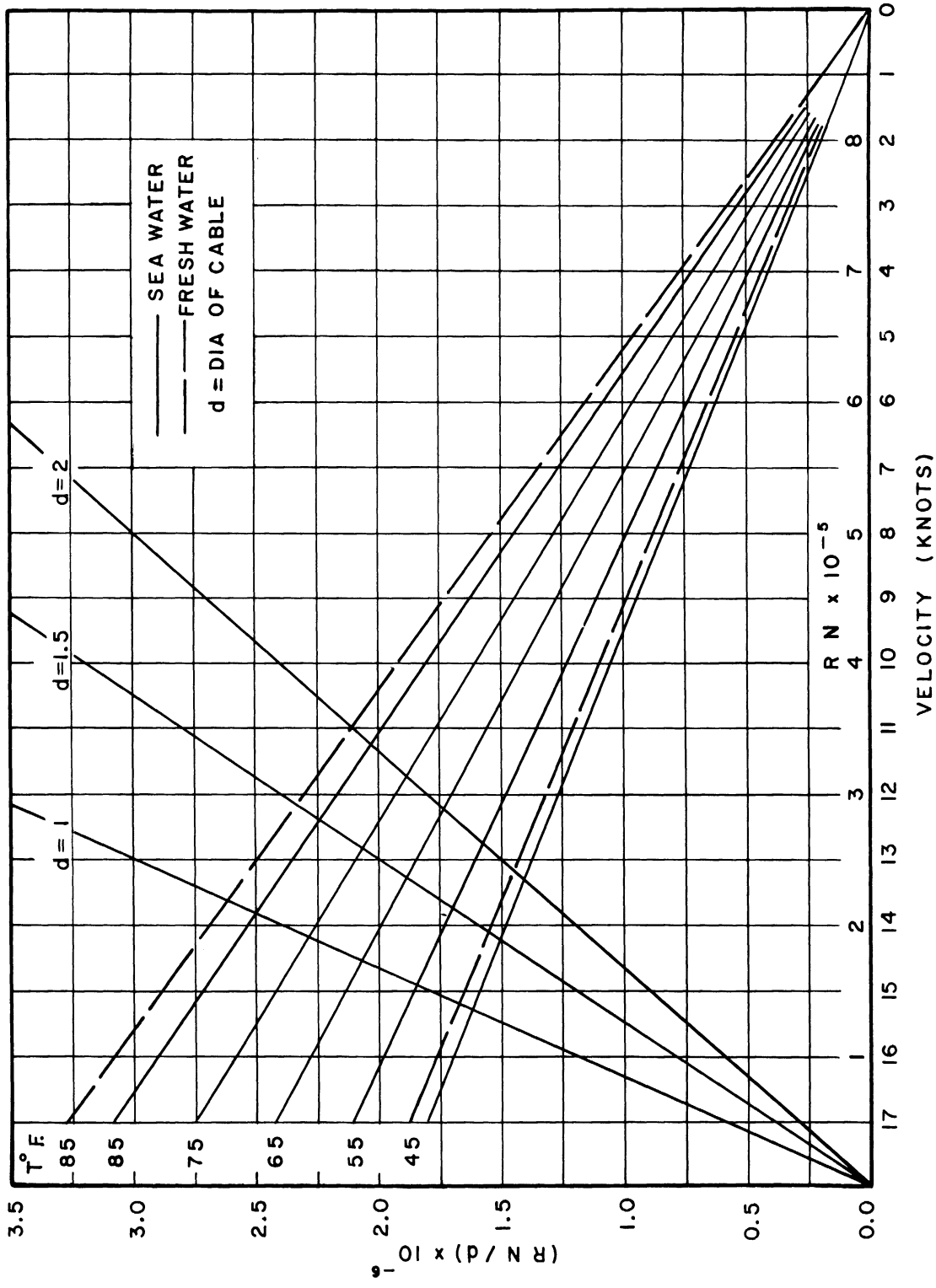
SEA WATER
FRESH WATER
d = DIA OF CABLE
d = 2
d = 1.5
d = 1
T° F.
85
85
75
65
55
45
3.5
3.0
2.5
2.0
1.5
1.0
0.5
0.0
(R N / d) x 10⁻⁶
R N x 10⁻⁵
0
1
2
3
4
5
6
7
8
9
10
11
12
13
14
15
16
17
VELOCITY (KNOTS)

Fig. B-4.

Reynolds Number Effects for Lift Vanes.—The following general statements can be made for conventional vanes [1, 2, 3]*:

(a) Increasing the Reynolds number usually increases the maximum value approached by the lift coefficient as the angle of attack increases to that corresponding to stall. At normal (smaller) angles of attack the lift coefficient is relatively unaffected.

(b) The slope of the curve of lift coefficient vs angle of attack is independent of Reynolds number.

(c) The coefficient of the moment of the resultant hydrodynamic force about the aerodynamic center of an airfoil or hydrodynamic center of a vane increases with the Reynolds number in the range of 200,000 to 1.3×10^6, beyond which the moment coefficient is relatively constant.

(d) The section drag (profile drag) coefficient diminishes markedly with increase of the Reynolds number from about 170,000 to 350,000. The coefficient changes less rapidly with further increase in RN.

The latter three statements assume a normal angle of attack below the stall point.

Reynolds Number Effects for Cables.—When the flow is reasonably close to being perpendicular to the cable, the drag on the cable may be computed accurately by considering only the component of flow, V_N, normal to the cable and the cable drag coefficient, C_{NC}, as determined experimentally with normal flow [4]. That is, the tangential component of the drag is negligible and, in fact, proves to be of the order of 1% of the normal drag in the present problem where the small cable sweepback angle causes the flow tangential to the cable to be very small.

Hoerner [5] seems to indicate that C_{NC} is about the same for stranded cables and circular cylinders. This statement agrees fairly well with data from the David Taylor Model Basin [6, 7] and will be accepted here.

Curves of C_{NC} vs RN for cylinders [8, 9, 10] are decidedly different for various roughnesses. In general, for RN in the interval of 100,000 to 300,000 the curves dip (C_{NC} decreases) due to the transition from laminar to turbulent boundary-layer flow. If the cylinder is rough, the dip is less pronounced.

Conclusions.—It is seen that in the present problem the operating values of the Reynolds number for lift vanes are above the range in which the

*Numbers in brackets refer to the bibliography at the end of this report.

hydrodynamic characteristics vary significantly with RN. Standard wind-tunnel data at low Mach numbers and tank data are customarily obtained at high RN and may therefore be used in selecting a vane design.

The operating range of RN for cables is seen to straddle the range in which the normal drag coefficient varies. In conservative estimates of cable drag, it will therefore be necessary to adopt a value of C_{NC} outside the dip, e.g., a value in the neighborhood of unity or, more conservatively, a value of 1.4. For a faired cable, C_{NC} will be assumed to be 0.4. Some instability of the cable may be expected when the Reynolds number lies in the transition region.

Other Considerations.—In the above discussion, no consideration has been given to the effect of the varied turbulence of ocean water. The latter property can shift the range of RN in which the hydrodynamic coefficients vary, as compared to the range determined under laboratory test conditions. However, the general trends will remain as stated above. No detailed consideration has been given to profiled cables since the available unclassified literature sheds little light on the subject other than suggesting the tendency of a profiled cable oblique to the flow to rise and to be unstable.

The effect of variation of the Reynolds number on the performance of control surfaces can be much more complex than that indicated above for simple vanes. While the static hydrodynamic properties of control surfaces can be summarized in a manner similar to that for simple vanes, the dynamic properties can be evaluated reliably only by full-scale tests under operating conditions.

Since in this work the model paravanes were tested at Reynolds numbers falling in and below the transition range for the profile drag coefficient of the lift vanes, the lift-drag ratio of the paravane proper should improve in full-scale tests. This effect will offset to some extent the reduction in lift-drag ratio due to the added drag caused by the depth-control housing, control surfaces (especially when deflected), and other new factors arising due to the increase to full scale and the advent of realistic operating conditions.

B.2. CAVITATION

A sufficient condition for the inception of cavitation is that the pressure at some point in the water fall to the value of the vapor pressure [11]. As the velocity of the approaching stream is increased, this condition would be expected to occur first at the point where the fluid velocity reaches a maximum as it passes near the tow cable or a lift vane.

The relation between towing speed and the minimum pressure may be calculated by means of Bernoulli's equation and published data as to the maximum velocity reached in the free stream as it flows around cylinders and vanes. The vapor pressure may be determined approximately from available data which takes into account the salinity and temperature of the water. Appraisals of the likelihood of cavitation made on this basis were merely estimates since the pressure may be lower than that calculated at the centers of eddies generated in the flow as it passes the cable or vane. Furthermore, the vapor pressure is also a function of the air content of the water which was not considered. However, the calculations were useful when they indicated that the cavitation conditions were far removed from those to be encountered.

Vanes.—It has been verified that wind-tunnel data as to the distribution of velocity about an airfoil section may be used to determine the velocity distribution about a hydrofoil having the same profile [12]. The velocities near vanes having a representative variety of NACA profiles and thicknesses were determined relative to the free-stream velocity and for various values of the lift coefficient. The calculation was made by means of the NACA approximate method of superimposing theoretical values of the following three velocity distributions: that over the basic thickness form of the profile at zero angle of attack, that corresponding to the design load distribution of the mean line of the profile, and that corresponding to the additional load distribution associated with angle of attack [13, p. 11-13]. The relation between the lift coefficient and angle of attack is then given by the wind-tunnel data for the profile. For a broad range of the lift coefficient above and below 0.5, and a minimum depth of 30 ft, most of the profiles required a speed considerably in excess of 16 knots for inception of cavitation at the chordwise position corresponding to maximum velocity. At 16 knots, cavitation was likely for only a few profiles which were of the symmetrical type. In these cases, the desired value of the lift coefficient (selected as 0.5 in Chapter 3) corresponded to a high angle of attack which was too close to the stalling point. All of the profiles approached cavitation at 16 knots if the angle of attack, α, was sufficiently large in the positive direction or was sufficiently small or negative. Thus, the criterion for avoiding cavitation placed upon the characteristics of the profile, and upon α, requirements which were similar to those discussed in Chapter 3 for avoiding stall and lift-reversal.

Cables.—The situation as to cavitation is somewhat different with regard to the tow cable when the latter is only partially submerged. Calculations indicated that, at a speed of 16 knots, cavitation is likely in a region adjacent to the cable and extending from the water surface down to a depth of several feet. Due to the inclination of the cable which is dictated by the specifications of the present problem, a depth of several feet corresponds to an appreciable fraction of the submerged part of the cable. The upper portion of this region will likely be a pocket open to the atmosphere. It is known that the pocket may sometimes become enclosed under the water as the speed increases and that this can occur at speeds of less than 16 knots.

Since the design of the cable was beyond the scope of the project, this matter was not considered further. It is likely that the conditions described will cause estimates of the cable drag, and thus of the equilibrium value of the cable sweepback angle, to be somewhat inaccurate.

APPENDIX C

HIGH LIFT-DRAG RATIO PARAVANE. FURTHER EXPERIMENTAL WORK IN THE TOWING TANK

C.1 THE FACILITIES FOR TOWING TESTS

Figure C-1 is a general view of the University of Michigan towing tank which is 360 ft long, 22 ft wide, and 10 ft deep. The photograph shows the rear of the electrically driven rail car as well as a paravane in the towing position. Towing speeds up to about 15 ft/sec are available. The two parallel platforms below the deck of the car, which extend from the front to a point several feet behind the rear edge of the car, were used to launch and manipulate the paravane during towing tests. Not shown in the photograph is the false bottom of the tank which occupies the middle third of the towing tank length and can be raised to simulate shallow water conditions.

Figure C-2 shows a front view of the towing tank, including the spray device to produce turbulence. The influence of the latter upon the performance of the paravane was negligible, hence the device was not used.

Figure C-3 shows the general view of the paravane towing set-up. The tow cable runs from the bridling point of the paravane to the tow point which is to the left and slightly ahead of the paravane. A reference line through the tow point was stretched from side to side at right angles to the direction of motion in order to permit measurement of the cable sweepback angle. The paravane position, especially as to depth, was determined by the device shown in Fig. C-4. It consists of a dolly which traverses the width of the tank on rails. These rails in turn can be moved backward and forward by virtue of a second set of rails running parallel to the motion of the car. Scales along the tracks and a graduated vertical pointer permitted a complete determination of the paravane position.

C.2 FURTHER TOWING TESTS OF BIPLANE MODELS

The results obtained with the model of Fig. 4-8, as described in section 4.3, warranted additional investigation of the biplane to determine

the importance of design details. Some of these further tests have been described in section 4.3 and included investigations of bridling, the fairing of the end vanes, the length of end-vane chord, the stagger of the lift vanes, the trim surfaces, the magnitude and distribution of weight, the aspect ratio, the Reynolds-number effect on models, and the depth-control surfaces. Other tests of design details were conducted. These are described below and included investigations with a drag body attached to the tow cable. The effects of waves were also observed. Bridling and aspect ratio were investigated further, and tests were run with variations in the profile and thickness ratio of the lift vanes. Some tests were conducted to determine the behavior of the paravane during a large forward sweep toward the equilibrium position.

The model of Fig. 4-8 was also tested with both stable and oscillating drag bodies. These bodies had a small, downward resultant of weight and buoyancy, and were attached to the tow cable at a junction point slightly inboard from the bridling point. In comparison with the straightness and sweepback angle of the tow cable when no extra drag was present, the addition of a drag body produced a bend at the junction point, the sweepback angle of the inboard segment increasing and that of the outboard segment being unchanged. The stability and other aspects of the performance of the paravane were unimpaired, even for large oscillations of the unstable drag body.

Tests of the biplane in the presence of waves produced some steady-state oscillation, but no instability was observable for the wave conditions obtainable in the tank.

After the evolution of the bridling to a system of four converging flexible lines, as described in section 4.3, a variation of the latter arrangement was tested. It consisted of a semi-rigid system in which the two inboard bridling lines were replaced by rigid members as shown in Figs. C-5 and 4-10c. As a result of the change, the inboard lines could exert a force, and thus a control on the paravane, while under compression. This characteristic was advantageous during the deceleration of the paravane at the end of a forward sweep where the rigid members were effective in limiting the angle of attack of the lift vanes.

The range of aspect ratio which was investigated is shown in Fig. C-6. From left to right, the models in this figure have lift vanes of the following aspect ratios: 0.5, 1, 1.5, 2, 2.5, and 3. Increases of aspect ratio in the range of one to three were of greatest interest and resulted in some increase in lift-drag ratio as illustrated by the data tabulated in section 4.3. However, as this gain was realized, the paravane developed a pronounced instability with respect to a horizontal axis.

Figure 4-11 shows some variations of the lift-vane profile. These profiles were tested in a 5.5-in. model designed for good stability, that is, one having the four-line bridling, moderate aspect ratio for stability in roll

and yaw, and 45° stagger for stability in pitch when using end vanes of full chord. Under these conditions, the lift-drag ratio of the paravane was relatively unaffected by variation of profile among a group having suitable wind-tunnel data. The profile having a flat high-pressure side with rounded leading edge had the advantage of ease of construction in full-scale size. This profile was selected for the variation of thickness ratio in 15-in. models. Lift vanes having the reflexed profile were also constructed in the 15-in. size, but in only one thickness. These 15-in. vanes are shown in Fig. 4-12. It was concluded that the thickness may be varied to meet the requirements of weight, buoyancy, and structural strength. For these profiles, thicknesses in the lower portion of the range are preferable hydrodynamically.

A 15-in. biplane model with the flexible four-line bridling, lift vanes having an aspect ratio of one and a stagger angle of 45°, and full-chord end vanes was used to study the behavior of the paravane during a large forward sweep from an initial cable sweepback angle of 90° and with a constant length of tow cable. This model is shown in Fig. C-7. The end vanes were reinforced at the bridle attachment points in order to withstand large forces during the sweep. Tests were conducted from two initial attitudes, that is, two initial orientations of the model with respect to its pitch axis. In one orientation, the leading edges of the end vanes were initially at 90° to the direction of towing, so that the lift vanes had an angle of attack which was about 45° larger than that existing in outboard equilibrium. In the other initial orientation, the leading edges were at 180° to the direction of motion so that the angle of attack was about 135° larger than normally.

For both initial attitudes the paravane swept forward about the tow point in a circular path and attained the equilibrium sweepback angle. For both initial attitudes the paravane reached nearly identical orientations after a very small portion of the sweep was completed, as shown in Figs. C-8a and C-9a for the 90° and 180° initial attitudes, respectively. When the sweep was somewhat over 50% complete (Figs. C-8b and C-9b), the cable tension reached a maximum of about 10 times its value in the final equilibrium position. Following this point, the system decelerated and the paravane underwent a rapid variation in pitch (Fig. C-10). It then overshot the equilibrium position by a small amount (Fig. C-11a), fell back to a sweepback angle slightly greater than that of equilibrium (Fig. C-11b) and, after one more forward swing (Fig. C-11c), it reached equilibrium (Fig. C-11d). This behavior strongly indicates that the system is less than critically damped as might be expected since the cable was relatively thin and short, and the paravane was developed for low drag in order to obtain a high lift-drag ratio.

The large forward sweep from the initial attitude of 90° is approximately representative of the effect of turning the ship away from the paravane. In fact, this test represents an idealized extreme where the ship suddenly turns away from the paravane through an angle equal to the complement of the equilibrium sweepback angle of the tow cable. The initiation of the

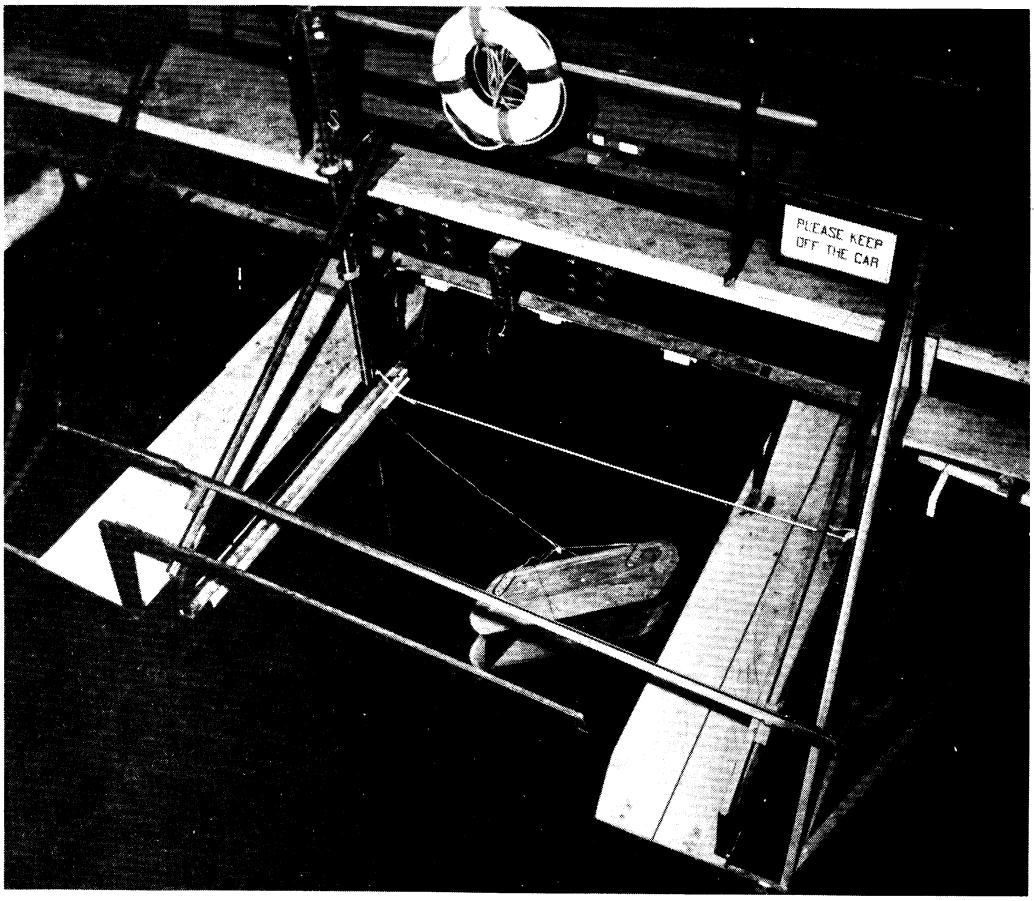

Fig. C-3.

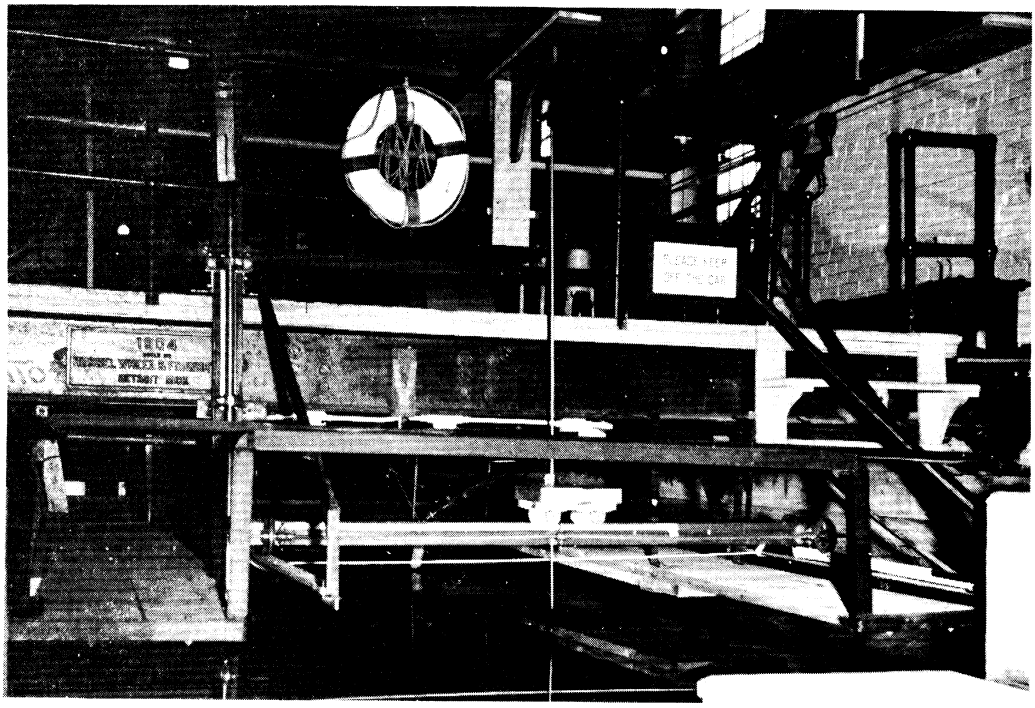

Fig. C-4.

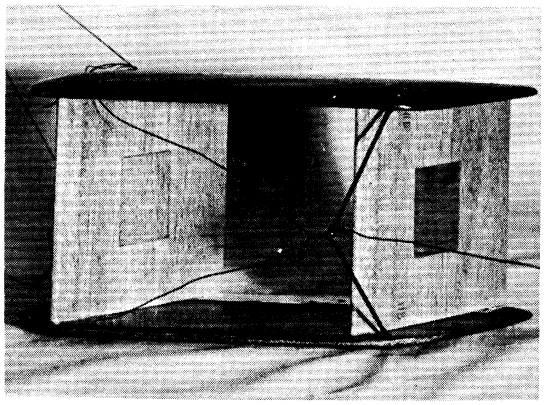

Fig. C-5.

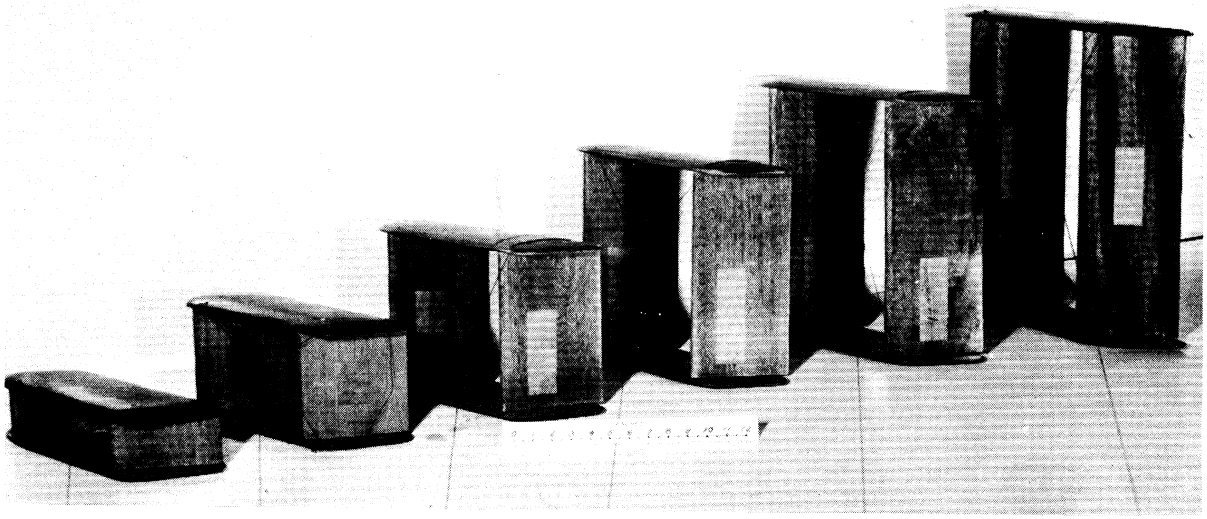

Fig. C-6.

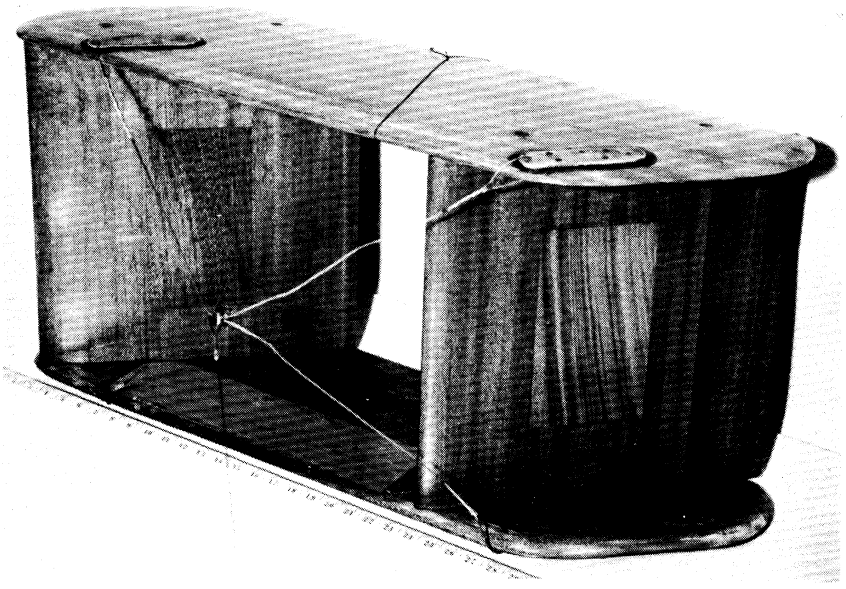

Fig. C-7.

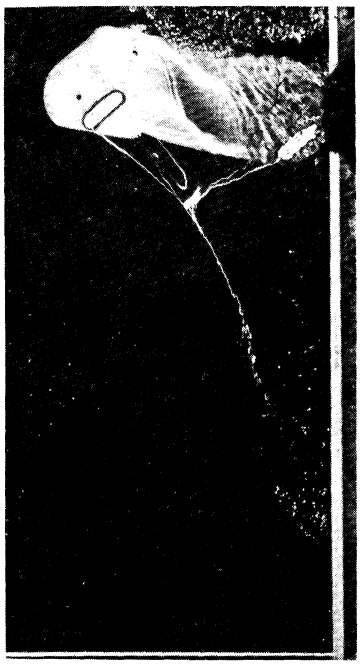

Fig. C-8a.

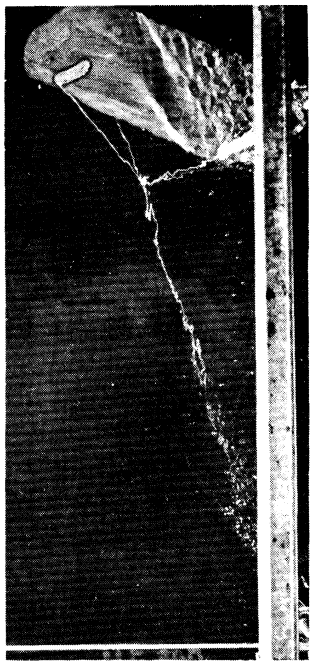

Fig. C-9a.

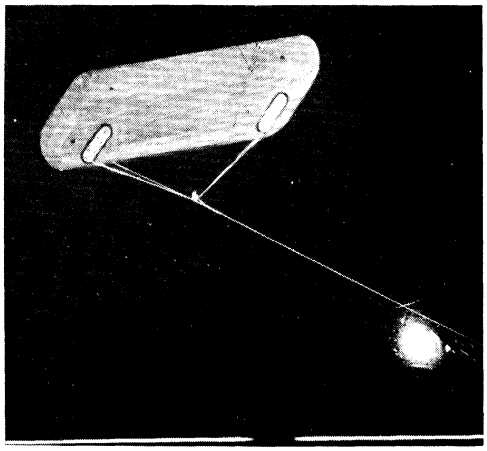

Fig. C-8b.

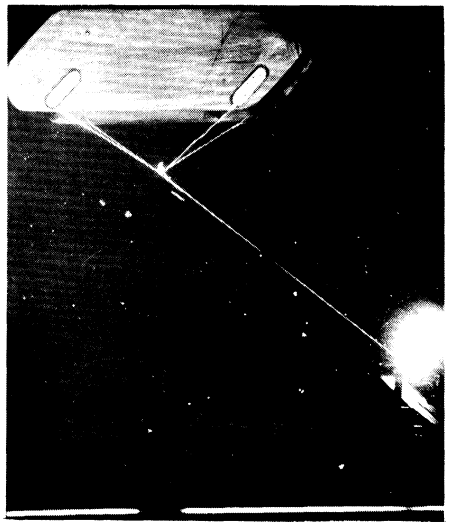

Fig. C-9b.

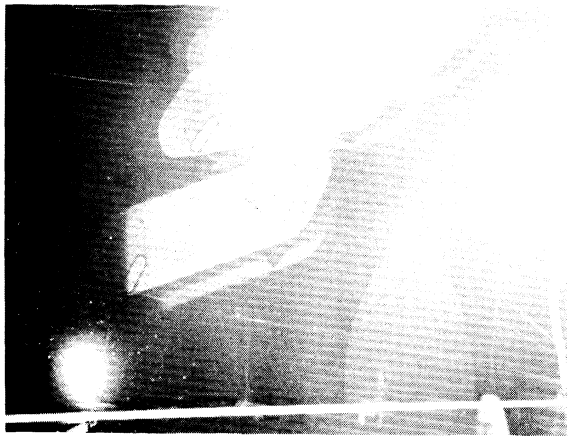

Fig. C-10.

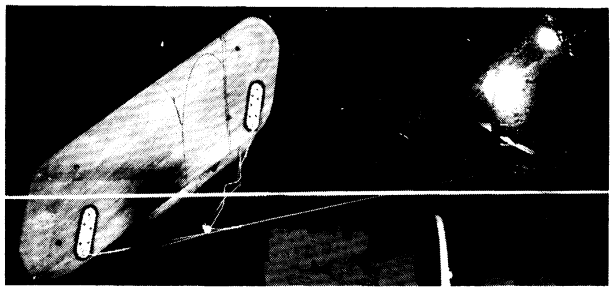

Fig. C-11a.

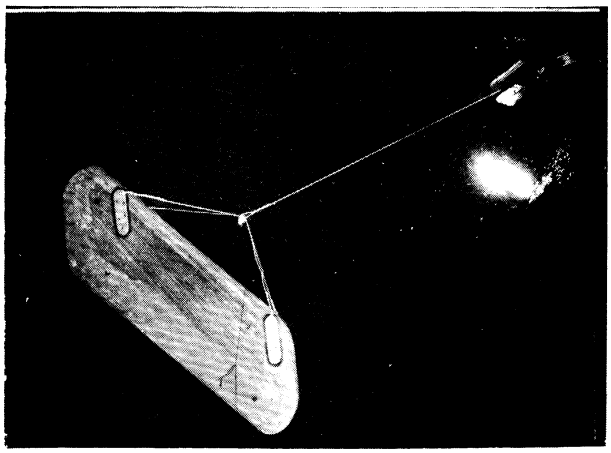

Fig. C-11b.

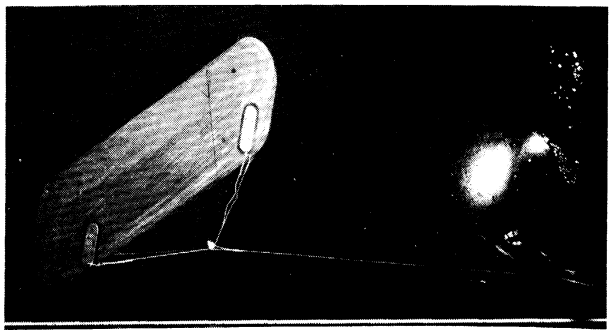

Fig. C-11c.

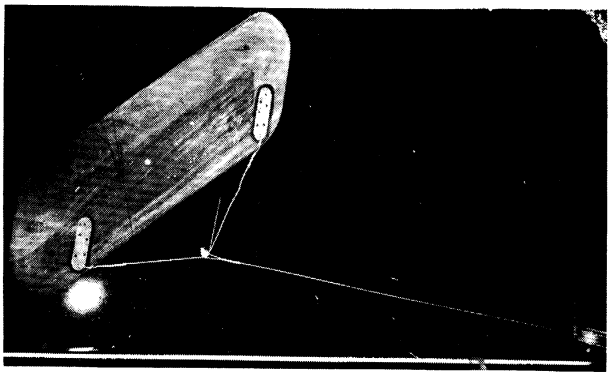

Fig. C-11d.

APPENDIX D

TESTS OF A HIGH-LIFT DRAG RATIO PARAVANE SYSTEM FOR DEPTH CONTROL CHARACTERISTICS

The following pages contain photographs and diagrams of the apparatus used in determining the step-function response of the paravane-cable system. Their description follows.

FIGURE D-1

This picture is an oblique view of the rear of the naval-tank tow car equipped for the step-function tests. The tow cable can be seen running to the left from the submerged paravane. A test line runs 9 ft vertically upward from the upper end vane, forward over two pulleys, and down behind the tall plank supporting the forward pulley. The test line served the dual purpose of providing a step-function disturbance to the paravane and continuously indicating the depth during the resulting response of the system. The rear pulley and vertical plank are supported by the triangular truss which is clamped to the large I-beam supporting the rear of the tow car. The trailing edges of the horizontal end vanes of the paravane were equipped with adjustable trim tabs, those on the upper end vane being visible in the picture.

FIGURE D-2

This photograph is a view from directly behind the tow car. The submerged paravane appears at the bottom of the picture. The details of the rear-pulley support are seen to consist of an oblique cross member attached to a boom extending aft of the truss. This arrangement permits positioning of the rear pulley directly above the towed paravane at various speeds.

FIGURE D-3

This view, looking aft from a point on the tow car, shows the remainder of the test line and the electric timer with a large sweep second

hand. The depth scale moves with the test line past a horizontal reference bar at the point of depth indication. In this way, full-scale continuous recordings of depth and time could be made by a motion-picture camera in horizontal alignment with the scale reading. A weight on the test line caused the towed paravane to ride at less than the natural depth for the existing speed. The step-type disturbance was then achieved by suddenly removing the weight. The resulting response was recorded.

FIGURE D-4

This front view of the paravane model used in step-function tests shows the four-point bridling and relatively large stranded tow cable of 1/4-in. diameter. Two upwardly deflected trim tabs on the lower end vane are visible near the outboard lift vane. These proved the most effective, in adjusting the paravane depth, of all tabs on either end vane. This paravane model was suitable for step-function tests since it possessed a representative lift force and end-vane shape, the latter two characteristics being the primary factors in the response to depth disturbances.

FIGURE D-5

This figure shows schematically the functional details of the setup in the towing tank.

FIGURE D-6

This figure is a plan view of the upper end vane showing the position of the center of gravity of the paravane and the axes for describing the location of the point at which the test line (Fig. D-5) was attached to the upper end vane.

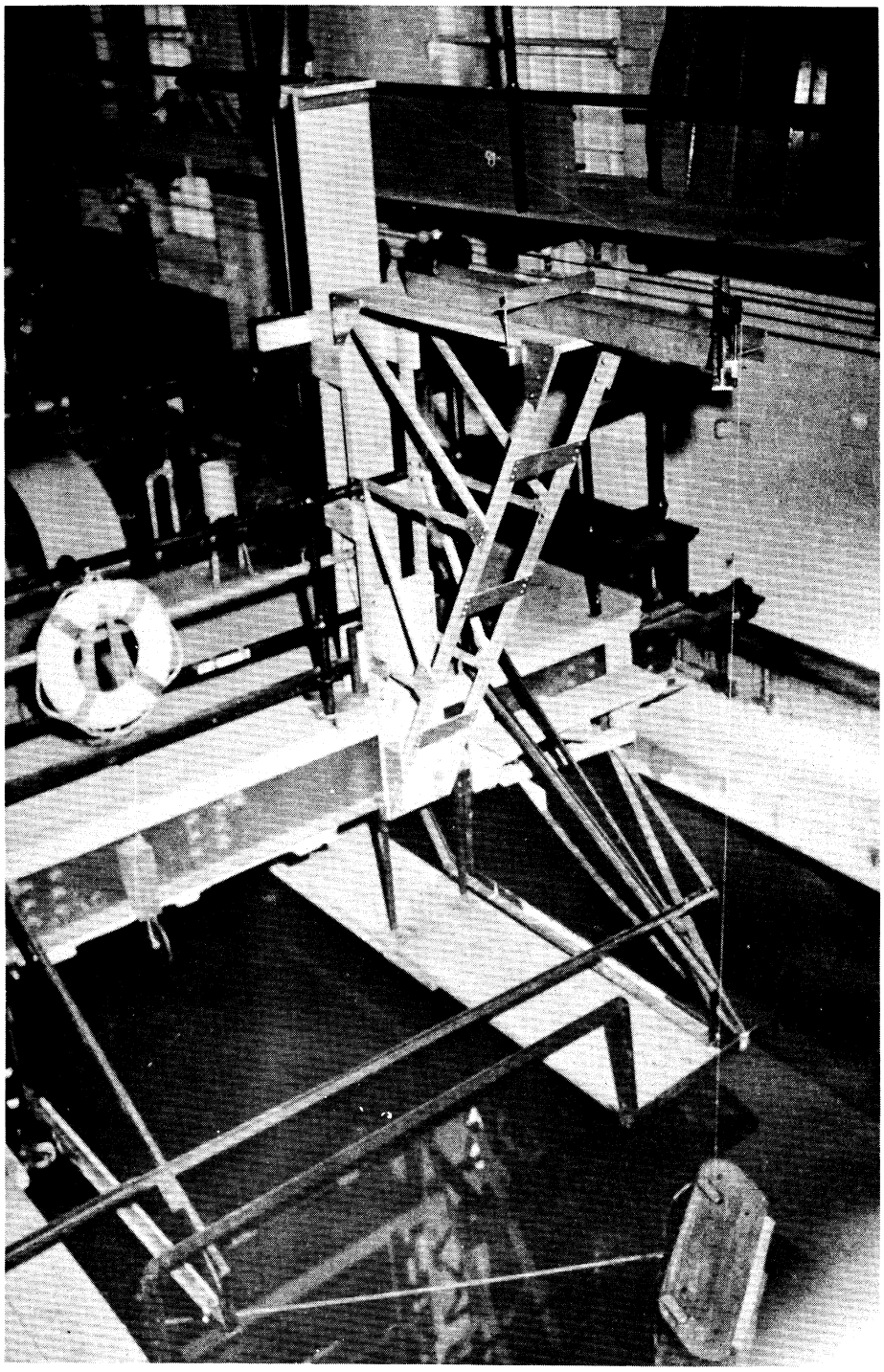

Fig. D-1.

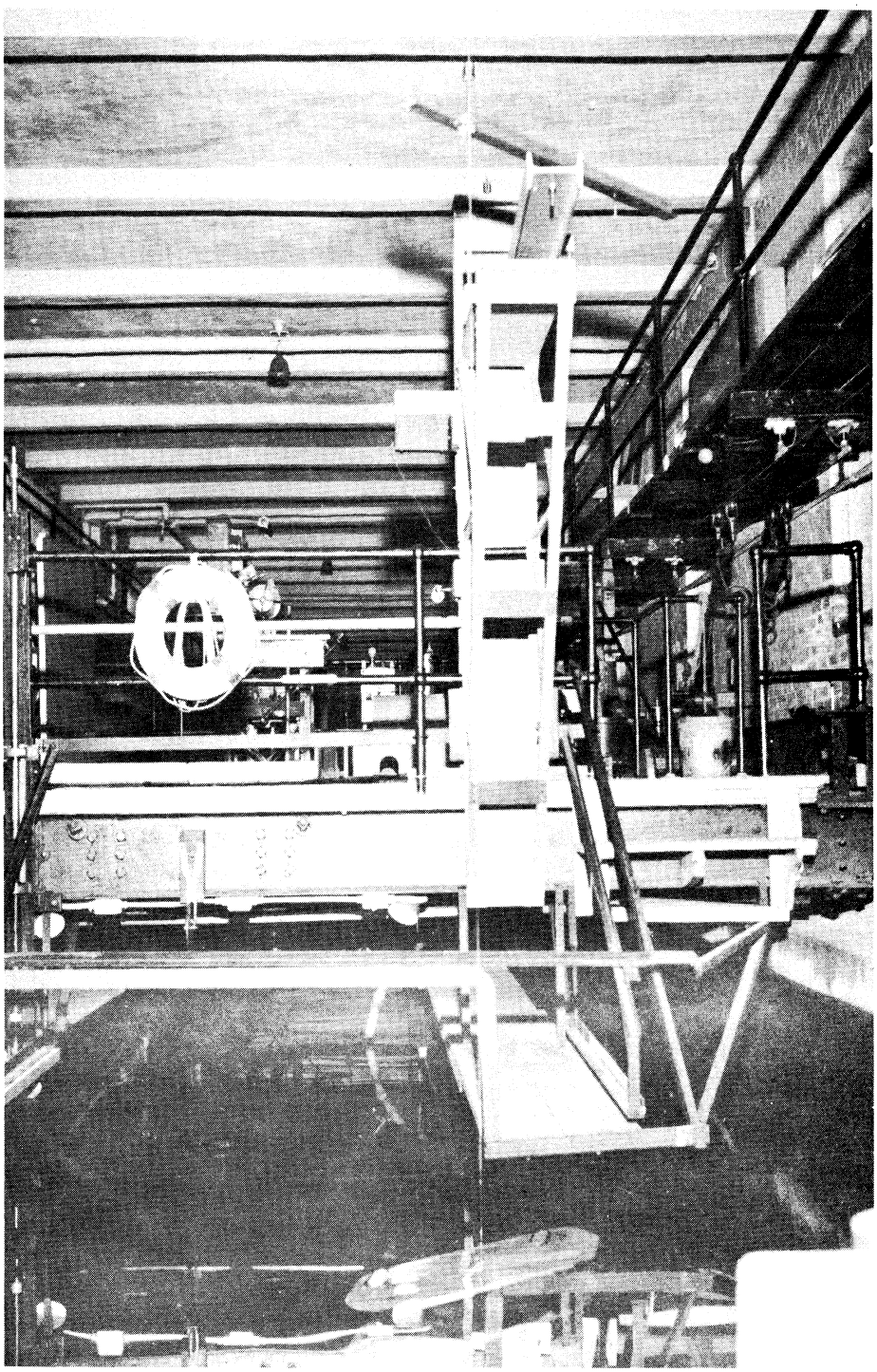

Fig. D-2.

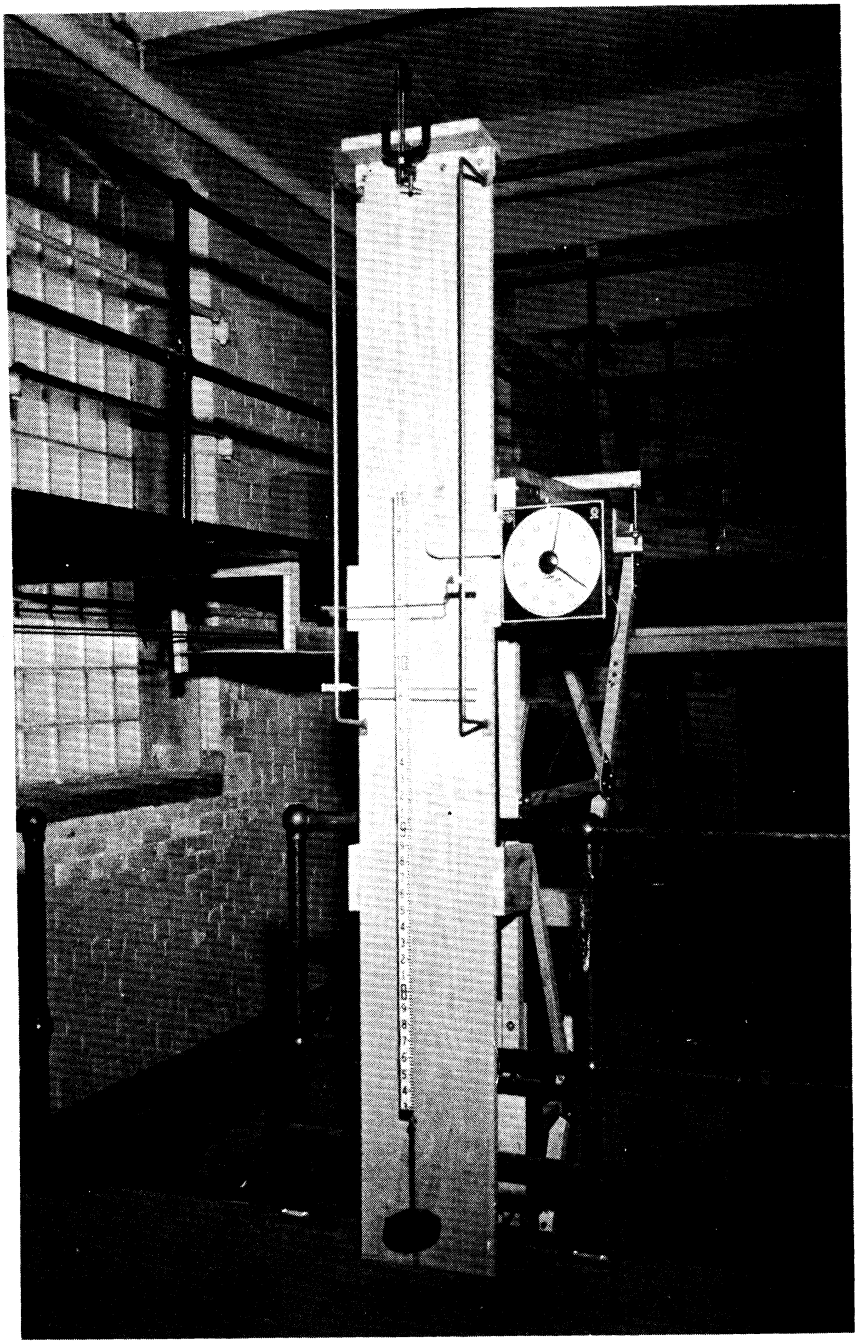

Fig. D-3.

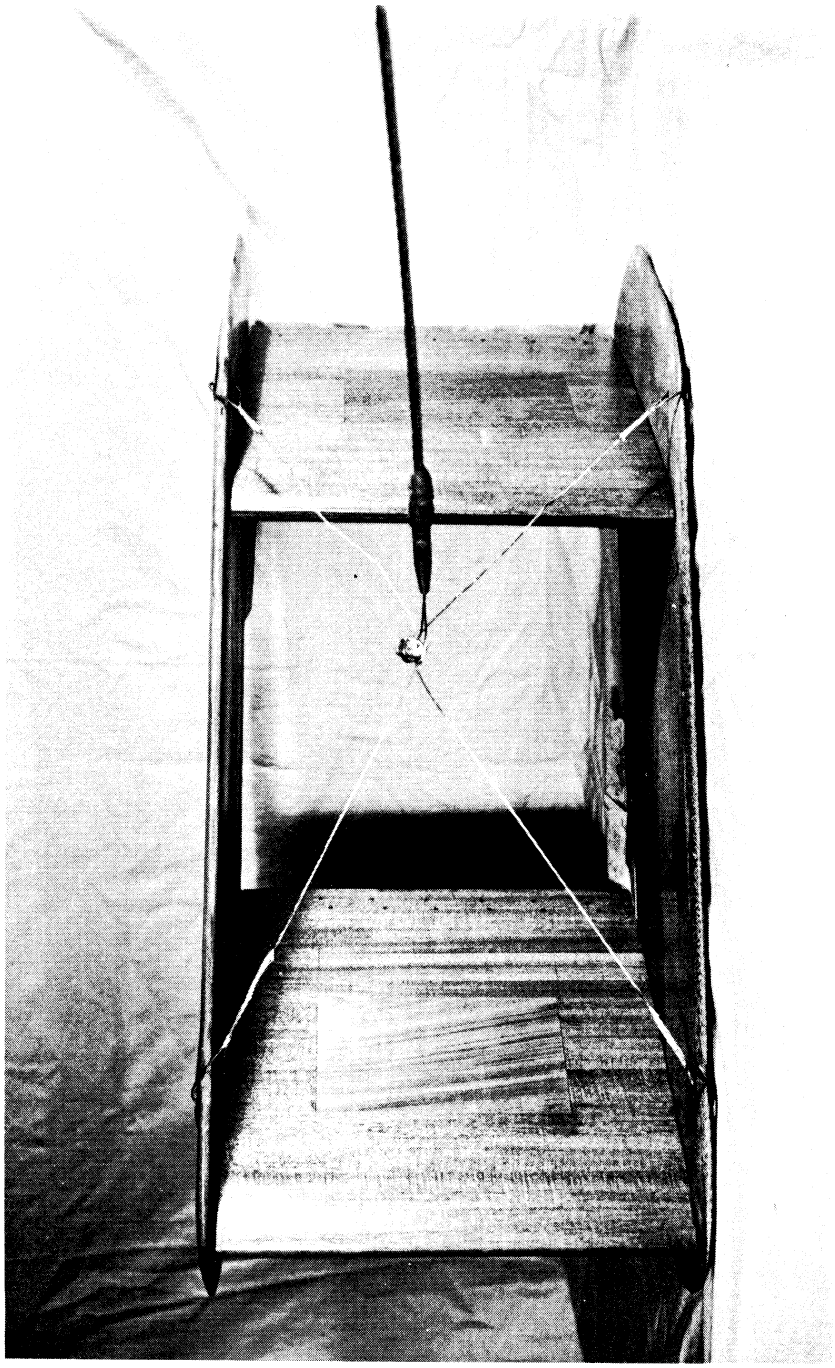

Fig. D-4.

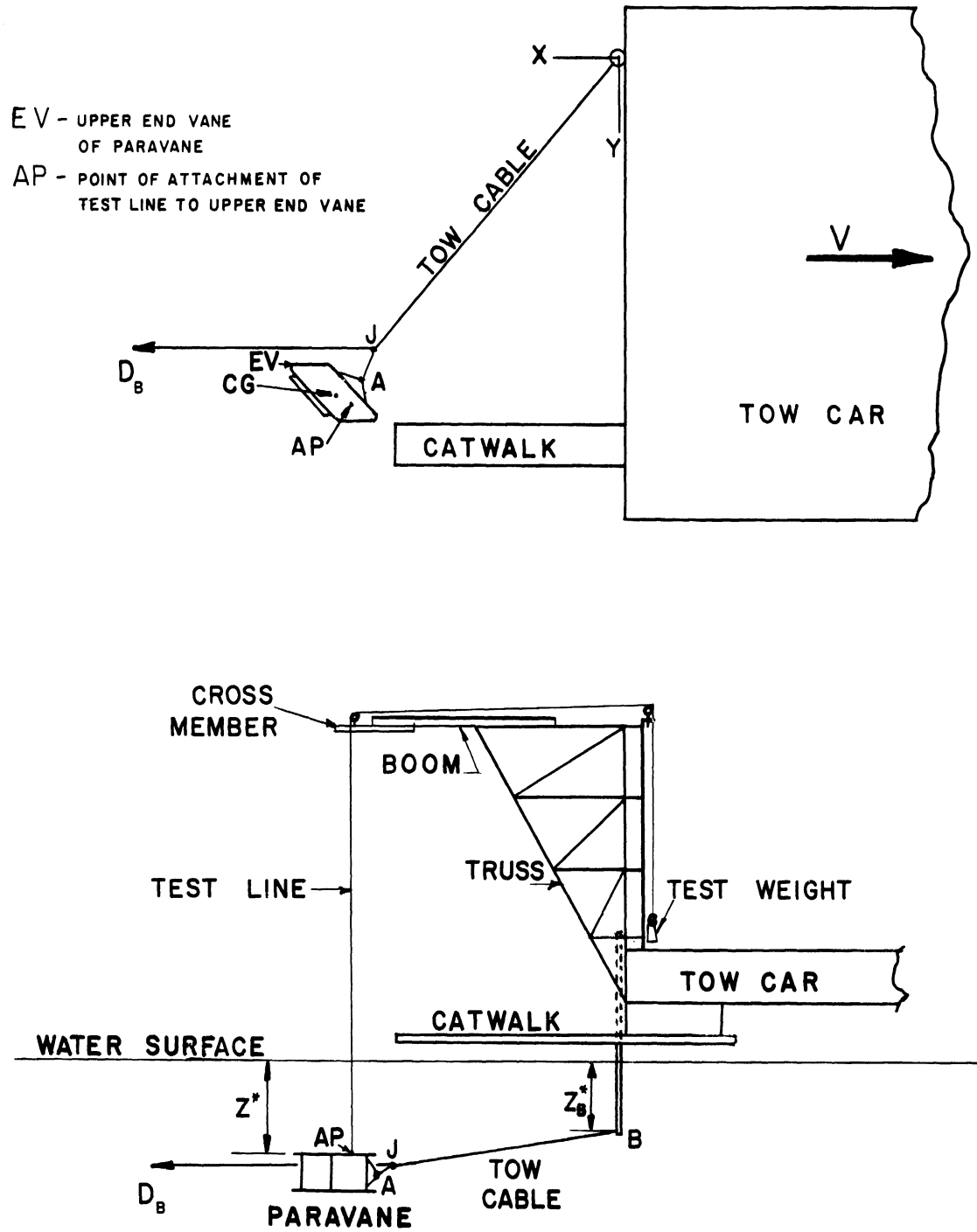

Fig. D-5. Setup in towing tank for testing response of paravane-cable system to a step disturbance.

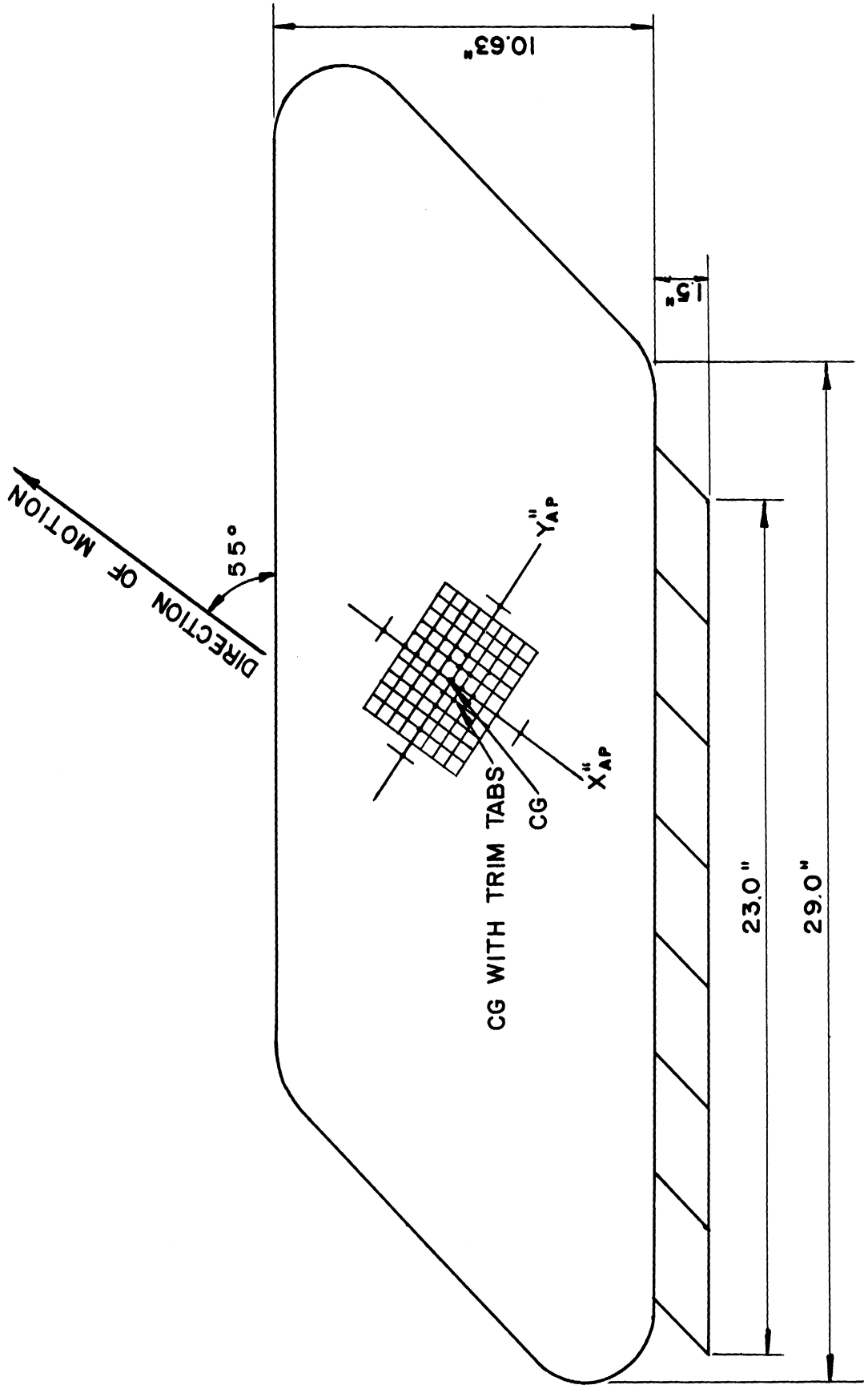

Fig. D-6. Upper end vane and axes for describing the location of the attachment point.

APPENDIX E

PRELIMINARY STUDY OF STABILITY CONTROL FOR HIGH LIFT-DRAG RATIO PARAVANE

A preliminary theoretical study was conducted to determine the extent to which the motion of the paravane in a vertical plane could be controlled by means of an internal mechanical oscillator. The oscillator was to act as a dynamic absorber and thus absorb energy which would otherwise appear as an oscillation of the paravane. Since the paravane oscillation to be damped in this fashion may be the result of a disturbance as well as instability, the mechanism would perform some of the functions of a depth control. In order to determine the potential effectiveness of the device, the paravane was idealized to a horizontal surface and an internal mass-spring-damper mechanism as shown in Fig. E-1. In an actual design, the internal mechanism might be located inside a vertical rather than a horizontal vane of the paravane in order to allow appreciable vertical motion of the internal mass relative to the paravane. The paravane was assumed to have an average velocity, V, which was constant and horizontal. The forces on the paravane due to the cable and the lift vanes were ignored in this preliminary study.

The system composed of the paravane and oscillator was assumed to have three degrees of freedom, namely, vertical translation, x_1, of the paravane center of gravity, angular displacement, θ_1, of the paravane about a horizontal axis through the center of gravity and normal to the direction of motion, and vertical translation, x_2, of the mass located in the oscillator. Assuming that the angular displacement is small, the equations of motion may be linearized. Corresponding to the above degrees of freedom, these equations are respectively as follows:

$$m_1\ddot{x}_1 = -k(x_1 + \theta_1 b - x_2) - c(\dot{x}_1 + \dot{\theta}_1 b - \dot{x}_2) + R$$

$$m_2\ddot{x}_2 = -k(x_2 - x_1 - \theta_1 b) - c(\dot{x}_2 - \dot{x}_1 - \dot{\theta}_1 b)$$

$$I_1\ddot{\theta} + I_o\omega\dot{\theta}_1 = -k(x_1 + \theta_1 b - x_2)b - c(\dot{x}_1 + \dot{\theta}_1 b - \dot{x}_2)b + Ra$$

The term $I_o\omega\dot{\theta}_1$ represents the virtual mass effect during angular displacement due to the fact that, in addition to the mass of the paravane, some mass of water must be accelerated during an angular acceleration of the

paravane. The circular frequency of oscillation, ω, is included in the term so that the effect of the virtual moment of inertia, I_o, will depend on the frequency. The virtual mass effect during vertical acceleration of the paravane was neglected as indicated by the fact that only the mass, m_1, of the paravane appears on the left-hand side of the first equation. The quantities appearing in these equations are as follows:

x_1 Vertical displacement of the paravane center of gravity (CG)

x_2 Vertical displacement of the mass in the oscillator

θ_1 Angular displacement of the paravane from horizontal

m_1 Mass of paravane without oscillator

m_2 Mass located in the oscillator

I_1 Moment of inertia of the paravane about its CG

I_o Virtual moment of inertia

R Resultant hydrodynamic force on the paravane

k Spring rate of oscillator

c Damping constant of oscillator

a Horizontal distance by which the CG of the paravane lies ahead of the center of force of the horizontal vane constituting the idealized paravane

b Horizontal distance by which the CG of the paravane lies ahead of the point of attachment of the oscillator to the paravane

The equations of motion were solved for a steady-state oscillation of x_1, x_2, and θ_1 in response to a periodic disturbance due to waves having a displacement x_o and a celerity relative to the paravane which was equal to the towing speed. The steady-state solution also assumed that

$$\xi = c/(4\ km)^{1/2} = 0 \quad \text{(zero damping)}$$

$$\gamma = I_o/I_1 = 0 \quad \text{(zero virtual moment of inertia)}$$

Figure E-1 is a plot of the solution for the cases

$$\beta = m_2/m_1 = 1/5 \text{ and}$$

$$\beta = 1/2 .$$

Also, the quantity b was taken as equal to (-1/2) i where i is the radius of gyration of the paravane about its CG that is,

$$I_1 = m_1 i^2 \quad .$$

In Fig. E-1 the quantities A_0, A_1, A_2, and θ_i are respectively the amplitudes of x_0, x_1, x_2, and θ_1. A large value of m_2 (equal to one-fifth of m_1) is seen to be required to reduce the amplitude of the spring to about four-tenths of the amplitude of the wave. Furthermore, it is necessary to provide a means of automatically varying the term $(k/m_2)^{1/2}$, the undamped natural frequency of the oscillator, so that the ratio, α, of the disturbing frequency to the natural frequency remains in the vicinity of 0.8. Under these conditions the paravane CG will have half the amplitude of the wave. The amplitude of the CG is zero when α equals about 1.04, but this point corresponds to excessive excursion of the oscillator spring. The decrease in amplitude is obtained by varying θ_1 so that the resultant flow has a minimum attack on the horizontal surface.

The problem was analyzed with the oscillator attached to the paravane at its CG (b = 0) and at a point behind the center of force, [b = +(1/2)i]. These cases gave much larger amplitudes of the spring and CG than those in Fig. E-1. Of the three locations of the oscillator, the third, [b = +(1/2)i], provided the least amplitude of angular oscillation of the paravane.

The study indicated that the internal oscillator could produce the desired effect. A practical design would require a study of modifications of the oscillator in order to reduce the amplitude of the spring excursion. In an actual design, the oscillating mass may be liquid rather than solid. The fact that the device is entirely internal makes it a very desirable method of controlling the oscillations of a high lift-drag ratio paravane.

The motion of the internal mass is a potential source of energy for other purposes. However, the energy would have to be converted into another form required by the consuming device, such as a depth control. In view of the undesirability of electrical apparatus, the conversion equipment would probably be too bulky to be accomodated on a high lift-drag ratio paravane.

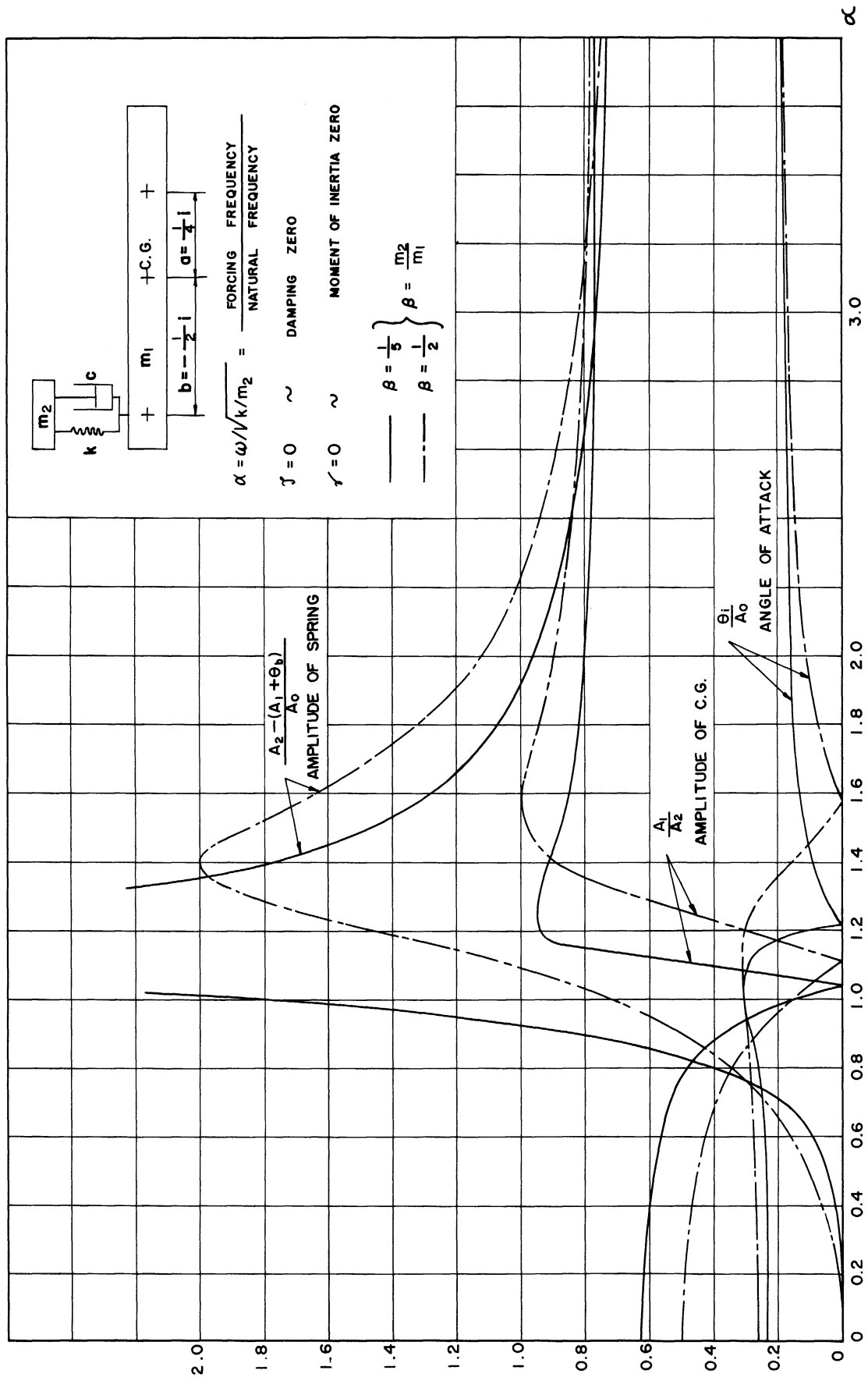
α
3.0
2.0
1.8
1.6
1.4
1.2
1.0
0.8
0.6
0.4
0.2
0
m2
c
k
m1
+C.G.
b=-1/2 l
a=1/4 l
α = ω/√(k/m2) = FORCING FREQUENCY / NATURAL FREQUENCY
γ = 0 ~ DAMPING ZERO
γ = 0 ~ MOMENT OF INERTIA ZERO
β = 1/5
β = 1/2
β = m2/m1
(A2 − (A1 + θb)) / A0 AMPLITUDE OF SPRING
A1/A2 AMPLITUDE OF C.G.
θi/A0 ANGLE OF ATTACK

Fig. E-1.

APPENDIX F

DRAWINGS OF PROTOTYPE HIGH LIFT-DRAG RATIO PARAVANE

APPENDIX G

DRAWING OF PROTOTYPE HIGH-LIFT PARAVANE

BIBLIOGRAPHY

Specific References

1. Jacobs, E. N., and A. Sherman, Airfoil Section Characteristics as Affected by Variation of the Reynolds Number, NACA TR 586 (1937).

2. Loftin, L. K., Jr., and W. J. Bursnall, The Effects of Variations in Reynolds Number Between 3.0 x 10^6 and 25.0 x 10^6 upon the Aerodynamic Characteristics of a Number of NACA 6-Series Airfoil Sections, NACA TR 964 (1950).

3. Fitzpatrick, J. E., and W. C. Schneider, Effects of Mach Number Variation Between 0.07 and 0.34 and Reynolds Number Variation Between 0.97 x 10^6 and 8.10 x 10^6 on the Maximum Lift Coefficient of a Wing of NACA 64-210 Airfoil Section, NACA TN 2753 (August 1952).

4. Kuethe, A. M., "Some Aspects of Boundary-Layer Transition and Flow Seperation on Cylinders in Yaw," Proc., 1st Midw. Conf. Fluid Dyn., 1950, pp. 44-55.

5. Hoerner, S. F., Aerodynamic Drag. Dayton, Ohio: Published by the Author, 1951, p. 138.

6. Thews, J. G., and L. Landweber, The Tension in a Loop of Cable Towed Through a Fluid, David W. Taylor Model Basin Report 422 (June 1936) p. 32.

7. Landweber, L., Hydrodynamic Forces on an Anchor Cable, November 1947. BTR-OTS-USDOC, PB 92298.

8. Fage, A., and J. H. Warsap, The Effects of Turbulence and Surface Roughness on the Drag of a Circular Cylinder, Great Britain, ARC R and M 1283 (October 1929).

9. Fage, A., and V. M. Falkner, Further Experiments on the Flow Around a Circular Cylinder, Great Britain, ARC R and M 1369 (February 1931).

10. Fage, A., Drag of Circular Cylinders and Spheres, Great Britain, ARC R and M 1370 (May 1930).

11. Kempf, G., and E. Foerster, Hydromechanische Probleme des Schiffsantriebs, Hamburg: Hamburgische Schiffbau-Versuchsanstalt e.v., 1932, pp. 227-343.

12. Daily, J. W., "Cavitation Characteristics and Infinite Aspect-Ratio Characteristics of a Hydrofoil Section," ASME Trans., vol. 71, No. 3 (April 1949).

13. Abbott, I., A. E. Von Doenhoff, and L. S. Stiver, Jr., Summary of Airfoil Data, NACA TR 824 (1945).

14. Glauert, H., Elements of Aerofoil and Airscrew Theory. 2nd Ed. Cambridge: Cambridge Univ. Press, 1947, pp. 146-7.

15. Prandtl, L., and A. Betz, Ergebnisse der Aerodynamischen Versuchsanstalt zu Göttingen. München and Berlin: R. Oldenbourg. vols. 1 and 2, 1923 (Prandtl). vol. 3, 1927, and vol. 4, 1932, (Prandtl and Betz).

16. Nagel, F. von, "Flügel mit seitlichen Schieben," Vorläufige Mitteilungen der Aerodynamischen Versuchsanstalt zu Göttingen, vol. 2, July 1924.

17. Gothert, R., and G. Giese, A Catalogue of Tail Unit Measurements of the German Aircraft Industry, FB 1305 (November 1940). Translation: R and T 416 (British Ministry of Supply). Catalogued by CADO as ASTIA No. 66257.

18. Gothert, R., and G. Giese, A Catalogue of Some Improved Elevator Qualities, FB 1305/2 (October 1942). Translation: R and T 417 (British Ministry of Supply). Catalogued by CADO as ASTIA No. 66257.

19. Lawrence, H. H., "The Lift Distribution on Low Aspect-Ratio Wings at Subsonic Speeds," J. Aer. Sc., vol. 18, No. 10 (October 1951).

20. Sverdrup, H. U., M. W. Johnson, and R. H. Fleming, The Oceans. New York: Prentice-Hall, Inc., 1942.

21. Lachmann, G., Results of Experiments with Slotted Wings, NACA TM 282 (October 1924).

22. Frey, Kurt, and H. Söhle, "Modellversuche an Scherbretten verschiedener Form," Schiffbau, Schiffahrt und Hafenbau, vol. 35, No. 4 (February 1934), pp. 49-53.

General References

AIRFOILS, HYDROFOILS, VANES, AND HIGH-LIFT DEVICES

Aerodynamic Characteristics of Aerofoils, NACA TR 93 (May 1921).

Aerodynamic Characteristics of Aerofoils II, NACA TR 124 (December 1921).

Aerodynamic Characteristics of Aerofoils III, NACA TR 182 (October 1923).

Pinkerton, R. M., Calculated and Measured Pressure Distribution over the Mid-span Section of the NACA 4412 Airfoil, NACA TR 563 (1936).

Theodorsen, T., and I. Naiman, Pressure Distributions for Representative Airfoils and Related Profiles, NACA TN 1016 (February 1946).

Jones, R. T., Effects of Sweepback on Boundary Layer and Separation, NACA TN 1402 (July 1947).

Jacobs, E. N., K. E. Ward, and R. M. Pinkerton, The Characteristics of 78 Related Airfoil Sections from Tests in the Variable-Density Wind Tunnel, NACA TR 460 (1948).

Loftin, L. K., Jr., and H. A. Smith, Aerodynamic Characteristics of 15 Airfoils, NACA TN 1945 (October 1949).

Ward, K. E., and N. S. Land, Preliminary Tests in the NACA Tank to Investigate the Fundamental Characteristics of Hydrofoils, NACA WR L-766 (September 1940).

Frey, Kurt, "Verminderung des Strömungswiderstandes von Körpern durch Leitflächen," Forschung a. d. Geb. d. Ing., vol. 4 (1933), pp. 67-74.

Frey, Kurt, "Verminderung des Strömungsverlustes in Kanälen durch Leitflächen," Forschung a. d. Geb. d. Ing., vol. 5 (1934), pp. 105-117.

Frey, Kurt, Experiments with Rotating Cylinders in Combination with Airfoils, NACA TM 382 (September 1926).

CABLES

Thews, J. G., and L. Landweber, The Tension in a Loop of Cable Towed Through a Fluid, David W. Taylor Model Basin Report 422 (June 1936), p. 33.

Eggink, H., "Form und Widerstand angeströmter Seile," Aerodynamisches Institut der Technischen Hochschule Aachen. Deutsche Luftfahrtforschung FB 1504 (November 1941). BTR-OTS-USDOC: PB 36435.

Mustert, R., Auftrieb und Widerstand von schräg angeströmten zylindrischen Körpern, Aerodynamische Versuchsanstalt zu Göttingen, Deutsche Luftfahrtforschung FB 1690 (October 1942). BTR-OTS-USDOC: PB 37164.

Camp, G. D., The Shape of a Flexible Rope Towing a Submerged Body, Univ. of Calif. DWR Rpt. M5 (November 1942). BTR-OTS-USDOC: PB 37083.

Landweber, L., and M. H. Protter, The Shape and Tension of a Light Flexible Cable in a Uniform Current, David W. Taylor Model Basin Report 533 (October 1944).

Landweber, L., Hydrodynamic Forces on an Anchor Cable, David W. Taylor Model Basin Report R-317 (November 1947).

Pode, L., Tables for Computing the Equilibrium Configuration of a Flexible Cable in a Uniform Stream, David W. Taylor Model Basin Report 687 (March 1951).

Bursnall, W. V., and L. K. Loftin, Jr., Experimental Investigation of the Pressure Distribution about a Yawed Circular Cylinder in the Critical Reynolds Number Range, NACA TN 2463 (September 1951).

Gowen, F. E., and E. W. Perkins, Drag of Circular Cylinders for a Wide Range of Reynolds Numbers and Mach Numbers, NACA TN 2960 (June 1953).

CAVITATION

Rouse, H., and J. S. McNown, Cavitation and Pressure Distribution on Head Forms at Zero Angle of Yaw, Iowa Studies in Engineering Bulletin 32 (1948).

OCEANOGRAPHY

Krummel, O., Handbuch der Oceanographie. Stuttgart: J. Engelhorn. vol. 1, 1907; vol. 2, 1911.

CONTROL THEORY

Lauer, H., R. Lesnick, and L. E. Matson, Servomechanism Fundamentals. New York: McGraw-Hill Book Co., Inc., 1947. (Theory and Devices).

Brown, G. S., and D. P. Campbell, Principles of Servomechanisms. New York: John Wiley and Sons, Inc., 1948. Chapters 7 and 8 (Synthesis).

Ahrendt, W. R., and J. F. Taplin, Automatic Feedback Control. New York: McGraw-Hill Book Co., Inc., 1951. (Introduction and Theory).

MacMillan, R. H., The Theory of Control in Mechanical Engineering. Cambridge: Cambridge Univ. Press, 1951. (Theory and Devices).

Perkins, C. D., and R. E. Hage, Airplane Performance, Stability and Control. New York: John Wiley and Sons, Inc., 1949.

Jones, A. J., and B. R. Briggs, Survey of Stability Analysis Techniques for Automatically Controlled Aircraft, NACA TN 2275 (January 1951).

DEPTH DISTURBANCES

Cornish, V., Waves of the Sea and Other Water Waves. Chicago: The Open Court Publishing Co., 1912.

Sewall, H. R., Investigations of Underwater Pressure Records and Simultaneous Sea Surface Patterns, Contrib. No. 386, Woods Hole Oceanographic Inst. Trans., Am. Geophysical Union, vol. 18, No. 5 (1937).

Sverdrup, H. U., and E. W. Munk, Wind, Sea, and Swell: Theory of Relations for Forecasting. H. O. Publications No. 601 (Scripps Inst. of Oceanography for Hydrographic Office, U. S. Navy) (May 1947).

Folsom, R. G., "Subsurface Pressures Due to Oscillatory Waves," Trans., Am. Geophysical Union, vol. 28, No. 6 (December 1947).

Barber, T. F., and F. Ursell, "Generation and Propagation of Ocean Waves and Velocities," Royal Society (London) Philosophical Trans., February 24, 1948, pp. 527-60.

Barnaby, K. C., Basic Naval Architecture. London: Hutchinson's Scientific and Technical Publications, 1949.

Mewes, E., Wave Dimensions in North and Baltic Seas, U. S. Army Corps of Engineers, Beach Erosion Board Bulletins, vol. 4, No. 2 (April 1950).

U. S. Navy Department, Techniques for Forecasting, Wind Waves and Swells, Pub. No. 604, U. S. Navy Hydrographic Office (1951).

Russell, R. C. H., and D. H. Macmillan, Waves and Tides. London: Hutchinson's Scientific and Technical Publications, 1952.

DEPTH CONTROL, EXISTING EQUIPMENT

Low, A. M., Mine and Countermine. New York: Sheridan House, 1940.

Allen, W. M., Remote Control for Torpedo Depth Setting, AAF, Eng. Div., Report M-53-556-494 (1943). BTR-OTS-USDOC: PB 6773.

Healey, J. F., Remote Control for Torpedo Depth Setting, AAF, Eng. Div., Reports M-53-556-452, 527 (1942, 43). BTR-OTS-USDOC: PB 6772, 6774.

Hoch, H., Dämpfung der Schwingungen bei der Tiefensteuerung des Torpedos, April 1943. BTR-OTS-USDOC: PB 56640.

Hoch, H., Die Kurs und Tiefensteuerung des Torpedos bei Berücksichtigung des Schiebens, July 1943. BTR-OTS-USDOC: PB 56437.

Hoch, H., Der Einfluss der Schräg-lage des Pendels auf die Stabilität der Tiefensteuerung des Torpedos, September 1943. BTR-OTS-USDOC: PB 56650.

U. S. Naval Torpedo Station, Electric Depth and Gyro Angle Setting Device from German Aircraft Torpedo, Interim Report No. 6, U. S. Naval Torpedo Station, Newport, R. I. (July 1945). BTR-OTS-USDOC: PB L 81725.

Planungsamt des Reichsforschungsrates, (Osenburg), Hannover. FIAT Microfilm Reel CC153, Frames 1-880 (1931-45). BTR-OTS-USDOC: PB L 73379. (Torpedo).

Meyer, Dr., Beschreibung der U-Boots-Tiefensteuerung 7502-S615-4001, August 1949. BTR-OTS-USDOC: PB 99048.

DEPTH CONTROL, POTENTIAL COMPONENTS

Kirk, D. B., The Effect of Transmission Distance on the Stability of Flow-Control Processes. Bulletin of Moore Products Co., Philadelphia, Pa.

Landis and Gyr, Inc., Sealed Miniature Ball Bearings. Catalog 8. New York: L and G, Inc.

Moore, C. B., "The Solution of Instrumentation Problems on the Pneumatic Null Balance Method," Instruments Magazine, September 1945.

Moore, C. B., "The Inverse Derivative-A New Mode of Automatic Control," Instruments Magazine, March 1949.

Moore Products Co., Nozzle Flow Characteristics in Pneumatic Force-Balance Circuits. Philadelphia: Moore Products Co., Bulletin (1946).

Moore Products Co., Nullmatic Differential Pressure Transmitters. Philadelphia: Moore Products Co., Bulletin 102 (1948).

Moore Products Co., Built-In Valve Positioners. Philadelphia: Moore Products Co., Bulletin 704 (1949).

Robinson Aviation, Inc., Unit Mountings for Vibration Control and Shock Protection. Tereboro, N. J.: Robinson Aviation, Inc., Technical Bulletin 700 (1953).

Research Controls, Mini-Flow Valves. Tulsa: Research Controls, Inc., Bulletin.

Thompson Industries, Inc., Ball Bushings. Manhasset, New York: Thompson Industries, Inc., Bulletin.

Titeflex, Inc., Titeflex Expansion-Type Bellows. Newark, New Jersey: Titeflex, Inc., Bulletin No. 300. (1953).

United States Rubber Co., Flexible Connectors. New York: U. S. R. Co., Mech. Goods Div., Aircraft Catalog.

Vickers, Inc., Oil Hydraulic Pumps and Controls. Detroit: Vickers, Inc., Catalog No. 5001.

DEPTH CONTROL, POTENTIAL METHODS AND EQUIPMENT

Hale, W. E., Barometric Altitude Control for B-29 No. 45-21795, for the Mogul Project (Project 188-5) AAF, AMC, Eng. Div. Memo Rpt. TSEPE-673-133 (June 1946). BTR-OTS-USDOC PB L 78679.

Phillips, W. H., Theoretical Study of Some Methods for Increasing the Smoothness of Flight Through Rough Air, NACA TN 2416 (July 1951).

U. S. Office of Scientific Research and Development, Natl. Defense Res. Comm., Basic Methods for the Calibration of Sonar Equipment, Summary Technical Report, vol. 10 (1946).

DEPTH CONTROL, PRESSURE MEASUREMENT

Bear, R, M., Differential Pressures on a Pitot-Venturi and Pitot-Static Nozzle over 360° Pitch and Yaw, NACA TR 264 (1927).

Kiel, G., Flugmessungen zur Bestimmung der günstigsten Anbringung von Staugeräten an Flugzeugen, ZWB Forschungsbericht 62 (March 1934). BTR-OTS-USDOC: PB 38492.

Kiel, G., Total-Head Meter with Small Sensitivity to Yaw, NACA TM 775 (August 1935).

Krisam, F., Speed and Pressure Recording in Three-Dimensional Flow, NACA TN 688 (August 1935).

Spaulding, E. R., and K. G. Merriam, Comparative Tests of Pitot-Static Tubes, NACA TN 546 (November 1935).

Platt, R. C., Turbulence Factors of NACA Wind Tunnels as Determined by Sphere Tests, NACA TR 558 (1936).

Kiel, G., Measurement of the True Dynamic and Static Pressures in Flight, NACA TM 913 (October 1939).

Wildhack, W. A., and V. H. Goerke, Corrugated Metal Diaphragms for Aircraft Pressure Measuring Instruments, NACA TN 738 (November 1939).

Letko, W., Investigation of the Fuselage Interference on a Pitot-Static Tube Extending Forward from the Nose of the Fuselage, NACA TN 1496 (December 1947).

Gracey, W., and E. F. Scheithauer, Flight Investigation of the Variation of Static Pressure Error of a Static Pressure Tube with Distance Ahead of a Wing and a Fuselage, NACA TN 2311 (March 1951).

Schulze, W. M., C. C. Ashby, Jr., and J. R. Erwin, Several Combination Probes for Surveying Static and Total Pressure and Flow Direction, NACA TN 2830 (November 1952).

Prandtl, L., Essentials of Fluid Dynamics. Glasgow: Blackie and Son Ltd., 1952. pp. 54, 252.